



HAL
open science

Phox2b+ interneurons of the hindbrain : a developmental, anatomical and functional study

Selvee Sungeelee

► **To cite this version:**

Selvee Sungeelee. Phox2b+ interneurons of the hindbrain : a developmental, anatomical and functional study. Development Biology. Université Paris-Saclay, 2022. English. NNT : 2022UPASL077 . tel-04478293

HAL Id: tel-04478293

<https://theses.hal.science/tel-04478293>

Submitted on 26 Feb 2024

HAL is a multi-disciplinary open access archive for the deposit and dissemination of scientific research documents, whether they are published or not. The documents may come from teaching and research institutions in France or abroad, or from public or private research centers.

L'archive ouverte pluridisciplinaire **HAL**, est destinée au dépôt et à la diffusion de documents scientifiques de niveau recherche, publiés ou non, émanant des établissements d'enseignement et de recherche français ou étrangers, des laboratoires publics ou privés.

Phox2b+ interneurons of the hindbrain: a developmental, anatomical and functional study

Etude développementale, anatomique et fonctionnelle d'interneurones exprimant le facteur de transcription Phox2b dans le tronc cérébral

Thèse de doctorat de l'université Paris-Saclay

École doctorale n° 568, signalisations et réseaux intégratifs en biologie
Spécialité de doctorat : Sciences de la vie et de la santé
Graduate School : Life Sciences and health
Réfèrent : Faculté de médecine

Thèse préparée dans l'unité de recherche: : Institut de Biologie de l'École Normale Supérieure (CNRS, Inserm), sous la direction de **Jean-François BRUNET** et de **Gilles FORTIN**, Directeurs de recherche, Ecole normale supérieure,

Thèse soutenue à Paris-Saclay, le 06 décembre 2022, par

Selvee SUNGEELEE

Composition du Jury

Micaela GALANTE PU, Université Paris-Saclay	Présidente
Filippo RIJLI PU, Friedrich Miescher Institute for Biomedical Research	Rapporteur & Examineur
Niccolò ZAMPIERI CR, Max-Delbrück-Centrum für Molekulare Medizin	Rapporteur & Examineur
Julien BOUVIER DR, Université Paris-Saclay	Examineur
Muriel THOBY-BRISSON DR, Université de Bordeaux	Examinatrice

Titre : Etude développementale, anatomique et fonctionnelle d'interneurons exprimant le facteur de transcription *Phox2b* dans le tronc cérébral

Mots clés : Développement, Premoteurs, Tronc cérébral, Formation réticulée, Orofaciale, Physiologie

Résumé : La formation réticulée du pont et du tronc cérébral contiennent des neurones impliqués dans des processus homéostatiques vitaux tels que l'alimentation, la thermorégulation ainsi que le contrôle cardiovasculaire et respiratoire. Malgré les caractérisations fonctionnelles de cette région, celle-ci demeure mal caractérisée en termes de types neuronaux génétiquement définis. Notre étude se focalise sur trois noyaux pré-ormoteurs génétiquement identifiés - l'IRT^{*Phox2b*}, le Peri5^{*Atoh1*} et le Sup5^{*Phox2b*} - susceptibles de coordonner soit l'ingestion de liquides (dans le cas de l'IRT^{*Phox2b*} et le Peri5^{*Atoh1*}) ou la fermeture de la mâchoire lors de la mastication (dans le cas du Sup5^{*Phox2b*}) chez la souris. Ils sont caractérisés par leur expression du gène à homéoboîte *Phox2b* qui régit le développement du système nerveux autonome chez les vertébrés mais aussi chez les invertébrés.

Un traçage rétrograde à partir de muscles spécifiques de la face identifie l'IRT^{*Phox2b*} comme étant pré-moteurs aux muscles qui ouvrent la mâchoire et élèvent la langue. Une stimulation brève de l'IRT^{*Phox2b*} ou celle du Peri5^{*Atoh1*} chez l'animal vigile déclenche l'ouverture de la mâchoire, tandis que celle de l'IRT^{*Phox2b*} provoque aussi la protrusion de la langue. La stimulation du Sup5^{*Phox2b*} quant à elle induit la fermeture de la mâchoire. De plus, la stimulation non-rythmique de IRT^{*Phox2b*} induit une alternance rythmique de la protraction et de la rétraction de la langue, en synchronisme avec l'ouverture et la fermeture de la mâchoire. Enfin, des enregistrements calciques par photométrie montrent que l'IRT^{*Phox2b*} et le Sup5^{*Phox2b*} sont actifs pendant le léchage et la mastication respectivement, et représentent ainsi des substrats sous-corticaux sous-tendant deux comportements alimentaires stéréotypés.

Title : *Phox2b*+ interneurons of the hindbrain: a developmental, anatomical and functional study

Keywords : Development, Premotorneurons, Medulla, Reticular formation, Orofacial, Physiology

Abstract : The reticular formation of the pons and medulla is known to contain neurons that participate in vital homeostatic functions such as feeding, thermoregulatory as well as cardiovascular and respiratory control. Despite these broad functional attributes, it remains poorly characterized in terms of genetically defined neuronal types. Here, we uncover three genetically-identified and behaviorally-relevant pre-ormotor nuclei - IRT^{*Phox2b*}, Peri5^{*Atoh1*}, and Sup5^{*Phox2b*} - that can organize fluid intake (for the first two) and biting (for the latter) in mice and are characterized by the expression of the pan-autonomic homeobox gene *Phox2b*.

They are located, respectively, in the intermediate reticular formation of the medulla and around the motor nucleus of the trigeminal nerve. Retrograde tracing from dedicated muscles identified them as premotor to jaw-opening and tongue-protruding muscles (IRT^{*Phox2b*} and Peri5^{*Atoh1*}) and to jaw-closing muscles (Sup5^{*Phox2b*}). Stimulation of either IRT^{*Phox2b*} or Peri5^{*Atoh1*} in awake animals opens the jaw, while IRT^{*Phox2b*} alone protracts the tongue. Stimulation of Sup5^{*Phox2b*} induced jaw closure. Moreover, non-rhythmic stimulation of IRT^{*Phox2b*} induces a rhythmic alternation of tongue protraction and retraction, synchronized with jaw opening and closing. Finally, fiber photometry recordings showed that IRT^{*Phox2b*} and Sup5^{*Phox2b*} are active during lapping and chewing respectively, thus identifying subcortical substrates underlying two stereotyped feeding behaviors.

ACKNOWLEDGEMENTS

I would like to thank the members of the jury, particularly Dr Niccolò Zampieri and Dr Filippo Rijli for agreeing to evaluate this Ph.D. thesis, Dr Muriel Thoby-Brisson and Dr Julien Bouvier for acting as examiners and Dr Micaela Galante for presiding over the jury.

My most profound appreciation goes to my Ph.D. supervisor, Dr Jean-François Brunet for his time, guidance, and unwavering support throughout my Ph.D.

I would like to give special thanks to Bowen Dempsey for his invaluable advice, support, and assistance throughout the whole project.

Last but not least, I am very grateful to all IBENS staff who provided technical assistance for my project, especially Caroline Mailhes-Hamon, Astou Tangara, Fatima Melouki, Bilel Mokhtari, and Zoubida Chettouh. I am also indebted to the IBENS animal core facility, particularly to Gwendoline Firmin, Eléonore Touzalin, and Amandine Delecourt.

Table of Contents

INTRODUCTION	1
MAMMALIAN OROFACIAL MOVEMENTS.....	3
1.1. <i>TYPES OF OROFACIAL MOVEMENTS</i>	3
1.2. <i>THE MOTOR PLANT FOR FEEDING MOVEMENTS.....</i>	6
1.3. <i>BRAINSTEM MOTOR CONTROL OF FEEDING.....</i>	9
1.3.1. Cranial motor nuclei for ingestive orofacial movements	9
1.3.2. Motor nucleus of the trigeminal nerve (Mo5)	9
1.3.3. Motor nucleus of the facial nerve (Mo7)	10
1.3.4. Relationship of the accessory nuclei of the trigeminal and facial nerves (Acc5 and Acc7).....	10
1.3.5. Motor nuclei for the hypobranchial muscles (tongue muscles and infrahyoids)	15
1.4. <i>BRAINSTEM SENSORY CONTROL OF FEEDING.....</i>	18
1.4.1. First order sensory neurons for ingestive orofacial movements	18
1.4.2. Second order sensory neurons for ingestive orofacial movements	25
1.5. <i>REGULATION OF OROFACIAL BEHAVIORS BY HIGHER-ORDER BRAIN CENTERS ..</i>	29
1.5.1. Cortical control	29
1.5.2. Superior colliculus	30
1.5.3. Cerebellar control.....	31
1.5.4. Basal ganglia	32
1.6. <i>INTERNEURONS OF THE RETICULAR FORMATION</i>	34
1.6.1. The reticular formation	34
1.6.2. Regions of the reticular formation and the slow birth of the IRt.....	34
1.7. <i>PREMOTOR NEURONS.....</i>	40
1.7.1. Central rhythm/pattern generators	41
1.7.2. General considerations on the architecture of rhythmic centers in vertebrates	42
1.8. <i>COORDINATION BETWEEN RHYTHMIC OROFACIAL ACTIONS.....</i>	47
1.9. <i>Phox2b, A MASTER REGULATOR OF AUTONOMIC REFLEX CIRCUITS.....</i>	48
RESULTS 1: A MEDULLARY CENTER FOR LAPPING IN MICE	51
RESULTS 2: A PONTINE CENTER FOR CHEWING.....	52
<i>ABSTRACT.....</i>	53
<i>INTRODUCTION.....</i>	53
<i>RESULTS</i>	54
Ontogeny and topology of Sup5 ^{Phox2b}	54
Connectivity of Sup5 ^{Phox2b}	56
Sup5 ^{Phox2b} stimulation triggers jaw closure.....	58
Sup5 ^{Phox2b} is active during ingestive orofacial movements.....	59

<i>METHODS</i>	68
Mouse strain, sex, and age	68
Animal husbandry	68
Viral vectors for tracing, optogenetic, and fiber photometry experiments	68
Surgical procedures.....	69
Histology	70
Behavioral experiments	71
Automated markless pose estimation	74
Data analysis	75
DISCUSSION	76
<i>IS IRt^{Phox2b} REQUIRED FOR LAPPING?</i>	76
<i>IS IRt^{Phox2b} A LAPPING CPG?</i>	76
<i>WIDER INTEGRATIVE ROLES FOR IRt^{Phox2b}</i>	80
<i>INTEGRATIVE ROLE OF Sup5^{Phox2b}</i>	80
<i>Phox2b AS A MASTER GENE FOR INGESTIVE BEHAVIORS</i>	83
<i>Mes5 AS ORGANIZING CENTER FOR Sup5^{Phox2b}</i>	85
REFERENCES	86
PUBLIC SUMMARY	107

Phox2b+ interneurons of the hindbrain:
a developmental, anatomical and functional study

INTRODUCTION

For a long time and to this day, neurons have been studied based on their position in stereotaxic terms: focal lesions, stimulations, injection of dyes, and of course electrical recordings. However, in certain regions of the brain, these approaches fail to define physiologically coherent neuronal ensembles, because of the intermingling of different cell types with radically different roles. A case in point is the finding that permanently silencing supratrigeminal nucleus (Sup5) neurons (without cell-type definition) or optogenetically exciting them has the same effect on jaw closing muscle activity (**Stanek et al., 2016**). Neurotransmitter expression is often used to define neural types, but while the neurotransmitter that a neuron expresses is a major characterizing feature of that neuron, it does not uniquely identify it. This is reflected in the contradictory roles which have been ascribed to populations of neurons in certain brain regions: e.g., it has been shown that SNL (lateral substantia nigra)-projecting neurons of the (largely gabaergic) CeA regulate both appetitive and aversive learning in mice (**Robinson et al., 2014; Steinberg et al., 2020**) and manipulating either glutamatergic or gabaergic neurons in the ventrolateral periaqueductal gray (vlPAG) elicits antinociceptive and defensive responses (**N. E. Taylor et al., 2019**). A recent study has shown that even amongst glutamatergic vlPAG neurons, different subsets of neurons might mediate different components of the defensive response in mice (**Tovote et al., 2016**).

The existence of functional heterogeneity in circuits compounded by a lack of specific cellular markers has hampered precise functional manipulations and delineation of such circuits in mammals (e.g., using virally-mediated optogenetic perturbation experiments). Indeed, the PreBötC rhythmogenic kernel is still inaccessible 30 years after its discovery since the developmentally-expressed *Dbx1* transcription factor in this region characterizes functionally heterogeneous neurons generating sigh (**Lieske et al., 2000**), the eupneic rhythm (**Bouvier et al., 2010**) and rapid breathing associated with arousal states (**Yackle et al., 2017**). This is in sharp contrast with invertebrate pacemakers for which every constituent cell has been identified, and their functional connectivity determined in vitro (**Silverston & Miller, 1980**).

A current revolution in neurosciences has been the import of genetic and developmental criteria to define neural types (**Zeng & Sanes, 2017**). These purely molecular criteria have rarely failed to corroborate neuron types previously recognized on morphological and electrophysiological grounds, and

often added many more. More recently technologies based on viruses have added projection patterns as defining criteria (**Ferreira-Pinto et al., 2021; Han et al., 2017a; Ruder et al., 2021; Tovote et al., 2016; Usseglio et al., 2020**). Current data point to combinations of transcription factors as the best (i.e. most parsimonious) descriptors of neuron types in vertebrates as well as invertebrates, (**Arendt et al., 2019; Hobert, 2021; Jessell, 2000**), and, in combination with Cre and Flp mice (and of course stereotaxic position), these genetic signatures enable unprecedented precision and reproducibility in the recording and manipulations of neuronal ensembles. This type of approach is particularly welcome for the hindbrain in whose "reticular formation" many neuron types are intermingled on a small scale, without clear cytoarchitectonic boundaries.

During my PhD, I studied three novel populations of reticular neurons in the mouse, named IRt^{Phox2b} , $Peri5^{Atoh1}$ and $Sup5^{Phox2b}$, endowed with a genetic signature that makes them unambiguously defined neuroanatomical objects. This genetic signature includes the transcription factor *Phox2b*, previously linked, in my host lab, with the development of the autonomic nervous system and of many oropharyngeal motoneurons (**Dauger et al., 2003; Pattyn et al., 1999; Pattyn et al., 2000**). The latter, belonging to the class of "special visceral motoneurons", can be included in a broader definition of the visceral nervous system, in line with their physiological functions, which ancestrally were purely homeostatic: for feeding and breathing. Remarkably, the three novel interneuron classes that I studied belong to this extended version of the visceral nervous system, not only through their ontogeny, but their physiological role: they are premotor to oropharyngeal motoneurons and involved in feeding behaviors.

In the introduction, I will provide a general background for the neural control of feeding behaviors, followed by a brief presentation of the homeodomain protein *Phox2b*. The results section will be devoted to the description and discussion of the developmental and physiological characterization of IRt^{Phox2b} , $Peri5^{Atoh1}$ and $Sup5^{Phox2b}$, which are the subject of two papers (one published, and the other in preparation).

MAMMALIAN OROFACIAL MOVEMENTS

1.1. TYPES OF OROFACIAL MOVEMENTS

The bones and muscles of the head execute movements that subserve many behaviors, important for both homeostasis and interaction with the environment (**Kurnikova et al., 2017; Moore et al., 2014**): they participate in breathing (critical to maintain CO₂/pH levels), in feeding (suckling in newborn mammals, chewing, licking, and lapping in terrestrial vertebrates for intraoral transport of nutrients and water), in sampling and exploring the surroundings (whisking — a vibrissa-based form of touch, particularly in rodents —, sniffing — which facilitates olfaction—, non-nutritive licking/chewing — which enable taste (**Moore et al., 2014**)). More sophisticated orofacial movements are involved in vocal communication (speech in humans) and they share behavioral features and sensory requirements with non-vocal oromotor behaviors (**Wilson et al., 2008**)

Like most bodily movements, orofacial ones fall under several types:

- i) They can be voluntary (e.g., speech production), or reflex (e.g., the jaw jerk reflex), some involving both volitional and reflex regulation (e.g., swallowing);
- ii) Some are rhythmic (e.g., jaw opening and closing during chewing);
- iii) They range from 'simple' motor acts involving a small subset of muscles —as in jaw opening — to more integrated motor "behaviors" such as chewing and swallowing during feeding;
- iv) They may be learned (e.g., speech production) or innate (e.g., licking), and some innate movements may undergo postnatal maturation (e.g., changes in chewing patterns (**Westneat & Hal, 1992**)).

One way in which orofacial behaviors stand out among bodily movements is the sheer number of muscles (of the face, jaw, tongue, palate, pharynx and larynx) that they mobilize in highly coordinated fashion. Up to 30 to 40 muscle pairs and several cranial nerves participate in swallowing in mammals (**Jones, 2003**) and greater than 50 individual muscles are involved in whisking (Dörfl, 1982). Moreover, the very same orofacial muscle can be recruited in different behaviors, e.g., *musculus nasolabialis*, an extrinsic vibrissa muscle, dilates the nostrils during sniffing and retracts the whisker pad

during whisking (**Berg & Kleinfeld, 2003; Hill et al., 2008**); and different orofacial behaviors exploit common muscles, bones and conduits of the oropharyngeal region. This anatomical intricacy is a source of potential conflicts and requires an extra layer of coordination. Feeding requires precise coordination between breathing and swallowing to prevent life-threatening tracheo-pulmonary aspiration: during the swallowing phase of feeding — where a synchronous descent of the soft palate and retraction of the tongue facilitate intra-oral transport of the food bolus — upper airway resistance is increased. During breathing on the other hand, phasic inspiratory input to the tongue maintains pharyngeal airway patency. To coordinate these motor acts, swallowing begins during the expiratory phase of the breathing cycle and breathing is briefly inhibited during a swallow, followed by post-swallow expiration (**Troche et al., 2011**). The need for such orofacial coordination mechanisms is made evident by pathological conditions in which it fails: in neurodegenerative disorders, such as Parkinson's disease, this sequence becomes abnormal: swallowing occurs more often during the inspiratory phase and inspiration can follow a swallow, resulting in increased incidences of dysphagia and aspiration pneumonia, a significant cause of mortality (**Gross et al., 2008**).

A striking feature of many orofacial motor actions is that despite the complexity of their coordination, they can be controlled in isolation from higher brain centers, by the pons and medulla, as demonstrated in decerebrate animals (**Woods, 1964**). In particular, the medulla and pons can orchestrate sophisticated orofacial feeding (ingestive) movements, even in the absence of descending control, including from the cortex, as reviewed in (**J. Travers et al., 2000; J. B. Travers & Norgren, 1983**). Possibly the earliest observation of swallowing in a decerebrate animal was in (**Miller and Sherrington, 1915**). A later notable reference is (**Grill and Norgren, 1978**) who report a complex behavioral sequence of rejection of quinine in "thalamic" rats (in which the thalamus is preserved) (**Fig. 1**).

Thus, the hindbrain contains entire neural circuits sufficient for a certain level of coordinated, adaptive oromotor activity. It obviously harbors motor nuclei for orofacial muscles and primary sensory nuclei that feedback onto them; but also interneurons that connect the two and coordinate, or "pattern" the behaviors. I will devote the next chapter to the neural circuits for ingestive behaviors (to the exclusion of swallowing), preceded by a presentation of the muscles and bones (the "motor plant") that they mobilize.

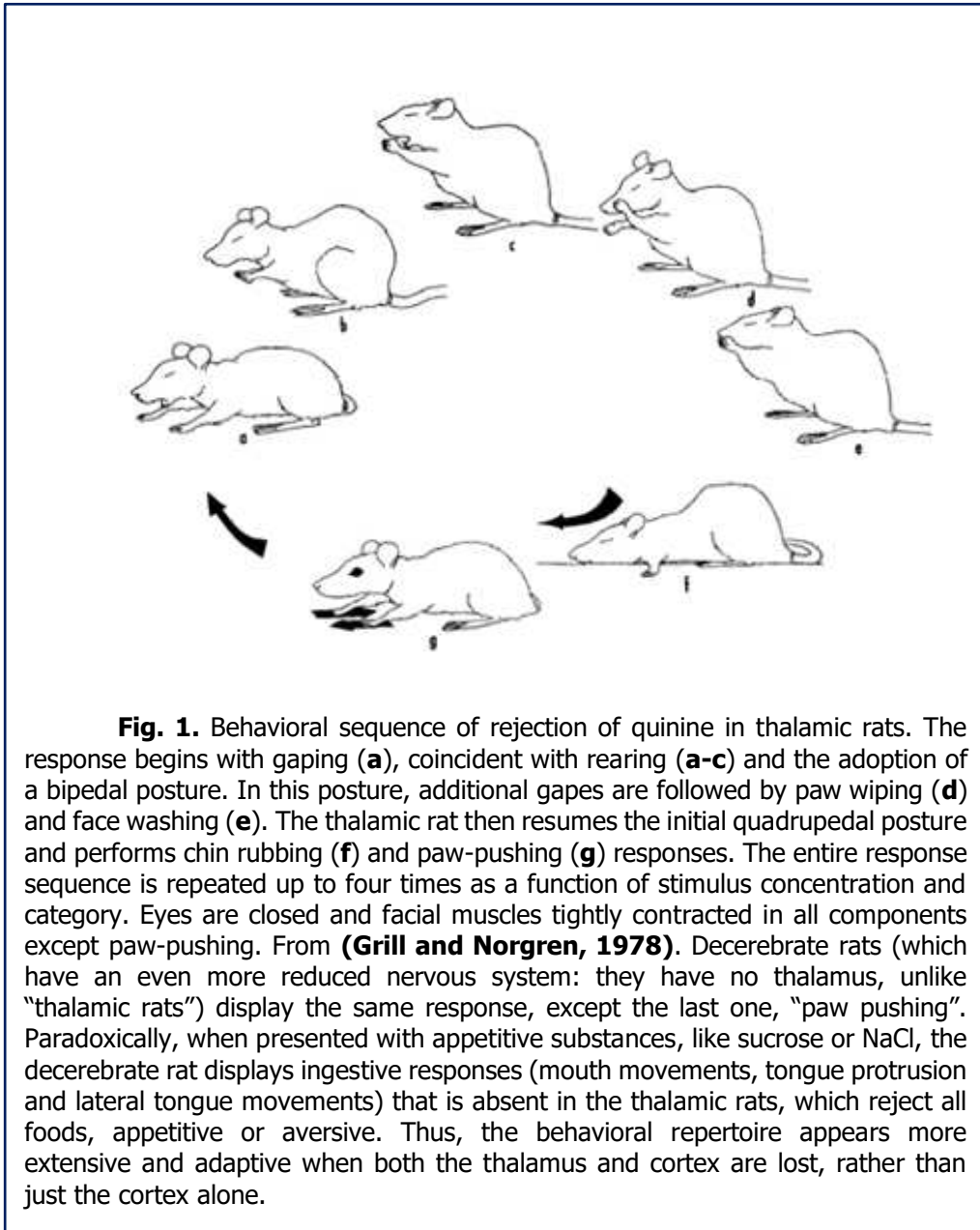


Fig. 1. Behavioral sequence of rejection of quinine in thalamic rats. The response begins with gaping (**a**), coincident with rearing (**a-c**) and the adoption of a bipedal posture. In this posture, additional gapes are followed by paw wiping (**d**) and face washing (**e**). The thalamic rat then resumes the initial quadrupedal posture and performs chin rubbing (**f**) and paw-pushing (**g**) responses. The entire response sequence is repeated up to four times as a function of stimulus concentration and category. Eyes are closed and facial muscles tightly contracted in all components except paw-pushing. From (**Grill and Norgren, 1978**). Decerebrate rats (which have an even more reduced nervous system: they have no thalamus, unlike "thalamic rats") display the same response, except the last one, "paw pushing". Paradoxically, when presented with appetitive substances, like sucrose or NaCl, the decerebrate rat displays ingestive responses (mouth movements, tongue protrusion and lateral tongue movements) that is absent in the thalamic rats, which reject all foods, appetitive or aversive. Thus, the behavioral repertoire appears more extensive and adaptive when both the thalamus and cortex are lost, rather than just the cortex alone.

1.2. THE MOTOR PLANT FOR FEEDING MOVEMENTS

The main muscles involved in solid or liquid food intake, i.e., for biting, licking (or lapping, the main method for drinking in many terrestrial vertebrates), intraoral transport, and chewing for reduction before swallowing, are briefly reviewed here. Swallowing itself falls outside the scope of my PhD work and of this review.

Food intake involves movements of the jaw and the tongue. The jaw is used to close and open the mouth by being respectively “adducted” and “abducted”. The adductor muscles, that pull the mandible towards the maxillary bone comprise the **masseter**, **medial pterygoid** and **temporalis**. The abductor muscles, that pull the mandible down towards the hyoid bone, comprise two sets of muscles: the “**suprahyoid**” muscles (**geniohyoid**¹, **mylohyoid**, **stylohyoid**, **anterior** and **posterior digastric**) and the **infrahyoid** muscles which stabilize the hyoid by pulling it down towards the shoulder girdle (the **omo-hyoid**, **sterno-hyoid**, **sterno-thyroid** and **thyro-hyoid**) (**Fig. 2b**). Finally, the **platysma** (**Fig. 2b**), a superficial muscle that inserts onto the lower lip and chin and on the shoulder-girdle is also in a position to help open the jaw and lower the lip, but there is actually very little data on the role of this muscle, which is largely dispensable in humans (and can be removed for cosmetic reasons (but see **Fig. 6**).

The movements of the tongue are extremely complex and effectuated by 16 muscles (i.e., 8 paired muscles) that move it forward (protrusion or protraction) or backward (retrusion or retraction) and, usually simultaneously change its shape: lengthen it during protraction and shorten it during retraction. Protraction is effectuated by one main muscle (**genioglossus**) and retraction by 3 muscles — **hyoglossus**, **styloglossus**, and **palatoglossus**). Changes of shape are effectuated by four orthogonally related intrinsic tongue muscles (**verticalis**, **transversus** —for elongation—, **superior** and **inferior**

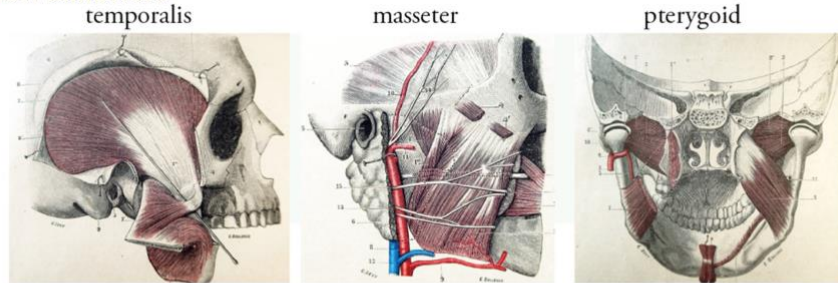
¹ The **geniohyoid** has two bony points of attachment (the genu of the mandible and the hyoid bone) that puts it in a “suprahyoid” position, i.e., able to share a role with the suprahyoids in lowering (abducting) the jaw. But it might also do the opposite, i.e., raise or pull forward the hyoid bone towards the genu of the mandible, which would facilitate tongue protrusion, and make it functionally a lingual muscle, despite its attachments to bones only, and not to the tongue. In this respect, it could be considered a detached fascicle of the genioglossus, or an accessory tongue muscle, as suggested by (Latarjet & Testut, 1948) who treat it in the chapter on “the muscles of the tongue” (not “on the neck”), “*because of its more or less intimate connections with the genioglossus*” (whose most horizontal fibers of the horizontal compartment are also attached on the hyoid bone, see **Fig. 2**).

longitudinalis for shortening)(Fregosi & Ludlow, 2014).

From a developmental and evolutionary standpoint, the muscles for feeding belong to two classes, with quite distinct ontogenies (Sambasivan et al., 2009): the **suprahyoids** are derived from the branchial (or “visceral” arches); while the **infrahyoids** and **tongue** muscles, forming together the larger group of “**hypobranchial muscles**”, are derived, like locomotory muscles, from somites, whose derivatives migrate into the head². This dichotomy was one of the major observations used by Romer (**Romer, 1972**) to theorize the bipartite vertebrate body, “somatic and visceral”, each part devoted respectively to interactions with the environment and to homeostasis. It makes sense that the somatic and visceral bodies, thus muscles, intermingle in the head, the interface of the outside and inside world, where, during feeding, the outside world actually penetrates and becomes part of the inside world. The two classes of muscles are innervated by distinct motoneuronal classes (see below).

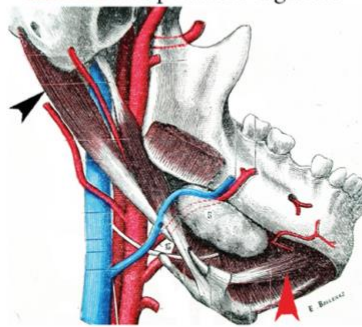
² A definitive test of the status of the **geniohyoid** (whose position and function are ambiguous between tongue muscle and suprahyoid, see note 1) would come from examining its developmental origin: does it derive, like tongue muscles, from the cervical somites? Or from branchiomeric mesoderm, like suprahyoid muscles?

A. Jaw adductors

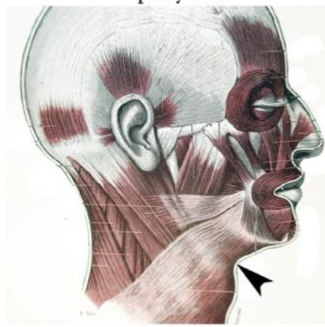


B. Jaw abductors

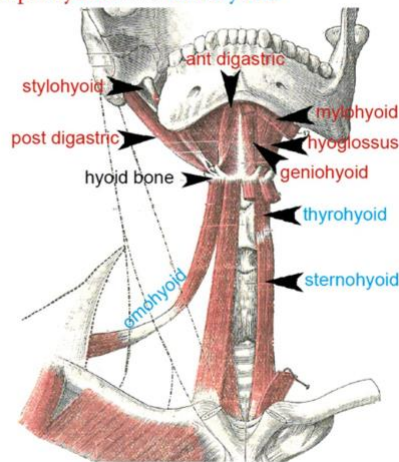
(i) anterior and posterior digastric



platysma



(ii) suprahyoids and infrahyoids



extrinsic tongue muscles

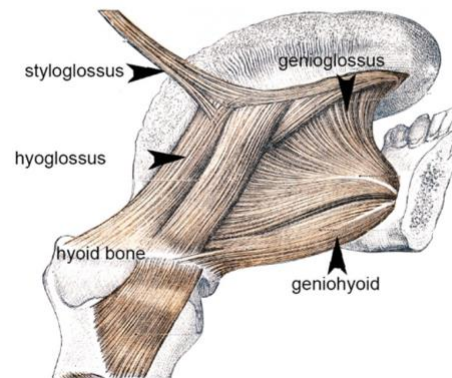


Fig. 2: Orofacial muscles involved in food ingestion in humans (adapted from Testut, 1931 and Toldt, 1912). All these muscles have equivalents in rodents. **a**) Jaw adductors: From left to right are shown the temporalis (with deflected masseter), the masseter (with vascular and nervous relationships) and pterygoid (only the deep fascicle is a jaw adductor). **b**) (i) The jaw abductors include the platysma and the suprahyoids (among which the posterior and anterior digastric), assisted by the infrahyoids(ii) which anchor and stabilize the hyoid bone. The geniohyoid, by its attachments, belongs to the suprahyoids muscle but is related in function, and possibly origin, to the genioglossus, an extrinsic lingual muscle.

1.3. BRAINSTEM MOTOR CONTROL OF FEEDING

1.3.1. Cranial motor nuclei for ingestive orofacial movements

Motor nuclei that command the orofacial muscles comprise two classes of motoneurons types that are ontogenetically, thus presumably phylogenetically, unrelated: nuclei made of branchial (or visceral) motor neurons, in the pons and medulla, that project in the trigeminal and facial nerves and innervate the branchial arch-derived suprahyoids; and a column made of somatic motor neurons, that extends from the medulla to the spinal cord and projects in the hypoglossal and cervical nerves and innervate the somite-derived hypobranchial muscles. I will review these motor nuclei, stressing features that are relevant to my experimental work.

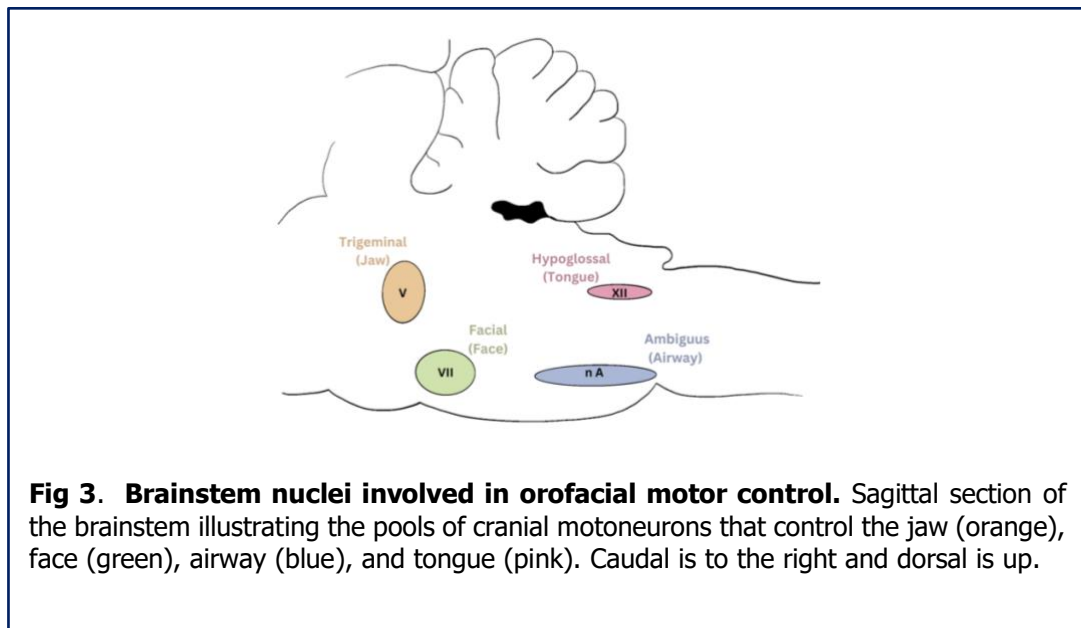


Fig 3. Brainstem nuclei involved in orofacial motor control. Sagittal section of the brainstem illustrating the pools of cranial motoneurons that control the jaw (orange), face (green), airway (blue), and tongue (pink). Caudal is to the right and dorsal is up.

1.3.2. Motor nucleus of the trigeminal nerve (Mo5)

The trigeminal motor nucleus is located in the pons (**Fig. 3**) and innervates all jaw-closing muscles (**masseter, pterygoid** and **temporalis**) and two of the jaw opening muscles (**mylohyoid** and **anterior belly of the digastric**).

It is a “branchiomotor” (or general visceral motor) nucleus. This entails that its progenitors arise in a special domain of the ventricular zone of the hindbrain (called “pMNV”), at the level of the second and third rhombomeres (r2 and r3) (which become part of the pons in the adult CNS). The neural progenitors express and depend on the pan-visceral homeodomain transcription factor *Phox2b* (see below). They give rise to a postmitotic progeny that switches on the paralogue of *Phox2b* - *Phox2a* - , migrate dorso-laterally in the mantle zone, and settle close to the forming trigeminal ganglion. Their axons form the “motor root” of the trigeminal nerve (nV).

The trigeminal motor nucleus is often presented as a single nucleus, subdivided into a dorso-lateral division that targets the jaw closing muscles and a ventro-medial division that targets the jaw opening ones (**Mizuno et al., 1975**). A more realistic description (**Paxinos & Franklin, 2004**) is to distinguish two nuclei: a “main nucleus” (that we shall call Mo5), that innervates the jaw closing muscles (**temporal, masseter** and **pterygoids**), and an “accessory nucleus” of Mo5 (Acc5) that innervates the jaw openers (**mylohyoid** and **anterior digastric**) (**Fig. 4** and see below for further comments on this partition).

1.3.3. Motor nucleus of the facial nerve (Mo7)

The facial motor nucleus, also a branchiomotor nucleus, but located in the medulla (**Fig. 3**), innervates muscles of the face and ears and three jaw opening muscles: the **posterior digastric, stylohyoid** and **platysma** (**Figs. 5,6**). Strikingly, it is also divided into a main nucleus (Mo7) and accessory nucleus (Acc7). The somatotopy of Mo7 has been studied in many species (concerning rodents, mainly in rats). (**Ashwell, 1982**) described a somatotopic representation in mouse by HRP labeling of various muscles (**Fig. 5**). However, details vary from other assessments in mouse or rat, and no photographic data is provided. It is likely that this somatotopy, especially for the intermediate part of Mo7, would benefit from being revisited with modern techniques.

1.3.4. Relationship of the accessory nuclei of the trigeminal and facial nerves (Acc5 and Acc7)

An unconventional view of these two nuclei/subnuclei will be presented here, based on a synthesis of the literature and original data from the lab. As

mentioned previously, both the trigeminal and facial nerves have a main nucleus (respectively Mo5 and Mo7) and an accessory one (respectively Acc5 and Acc7). Intriguingly, Mo5 and Acc5 have opposite actions, and in parallel, display contrasting anatomic and ontogenetic features, while Acc5 and Acc7 share a function and anatomic and ontogenetic features:

i) Anatomically, Acc5 is clearly separated from Mo5 as can be seen on the ISH of VAcHT on a coronal section at P56 from the Allen Brain Atlas (**Fig. 4**). Conversely, there is a quasi-continuity between Acc5 and Acc7, as exemplified by the position of motor neurons filled from the posterior digastric (a target of Acc7) on a parasagittal section (**Fig. 7**).

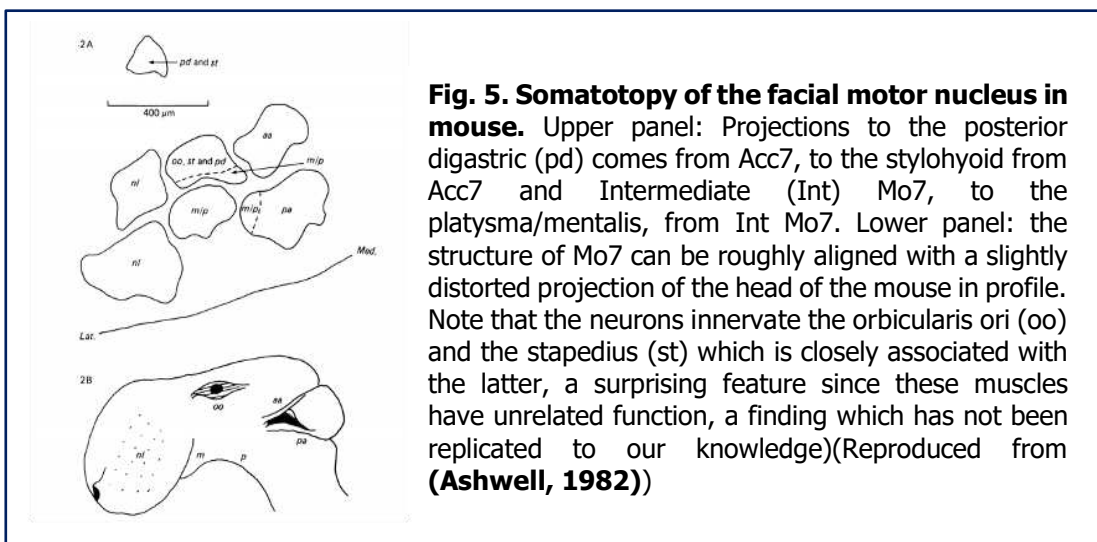
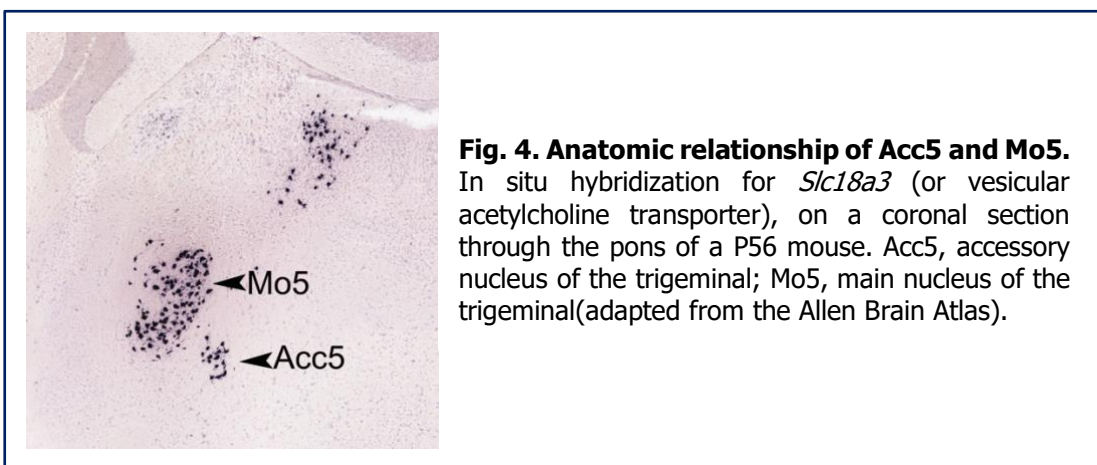
ii) Developmentally, trigeminal motor neurons have a dual rhombomeric origin in r2 and r3 (**Lumsden & Keynes, 1989**), which largely correspond, at least in mouse, to the partition into Mo5 and Acc5 (see our data in **Fig. 8**). Remarkably, this rhombomeric origin of Acc5, in r3, is close to that reported for Acc7, at the border between r3 and r4 (**Auclair et al., 1996**)(**Fig. 9**).

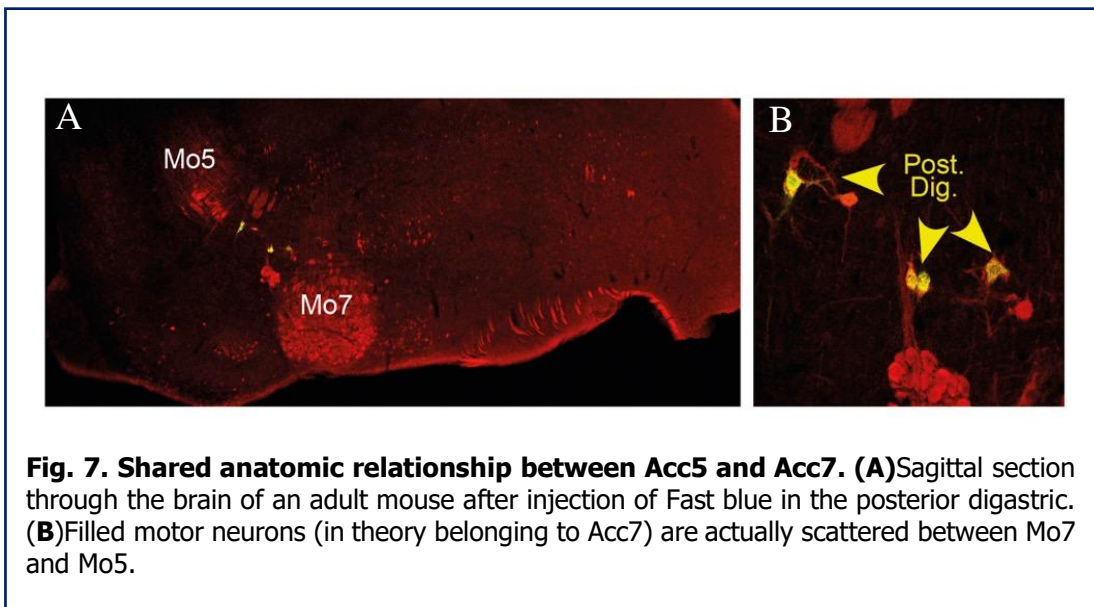
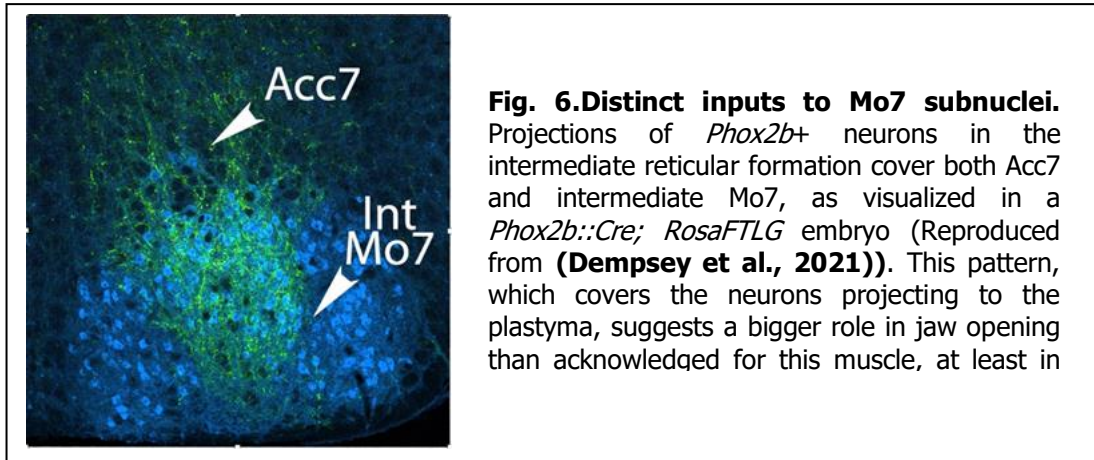
iii) Histologically, Acc5 neuronal somas are differently shaped compared to those of Mo5 (fusiform, versus polygonal) and similar to those of Acc7 (**Székely & Matesz, 1982**).

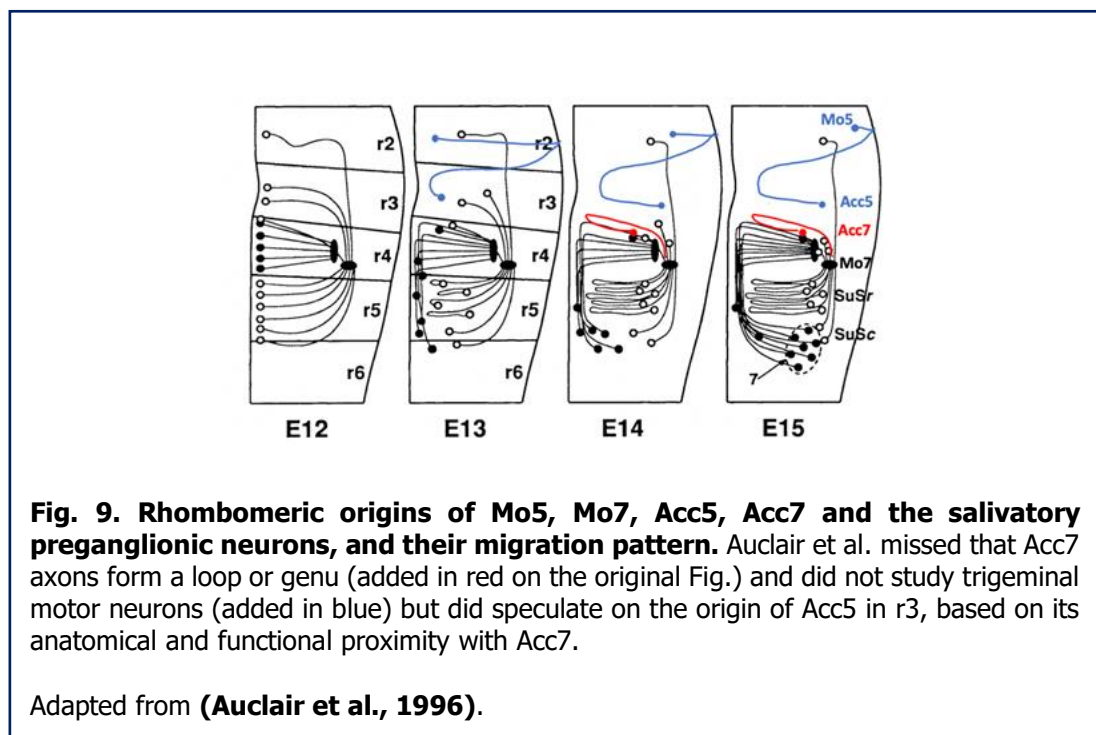
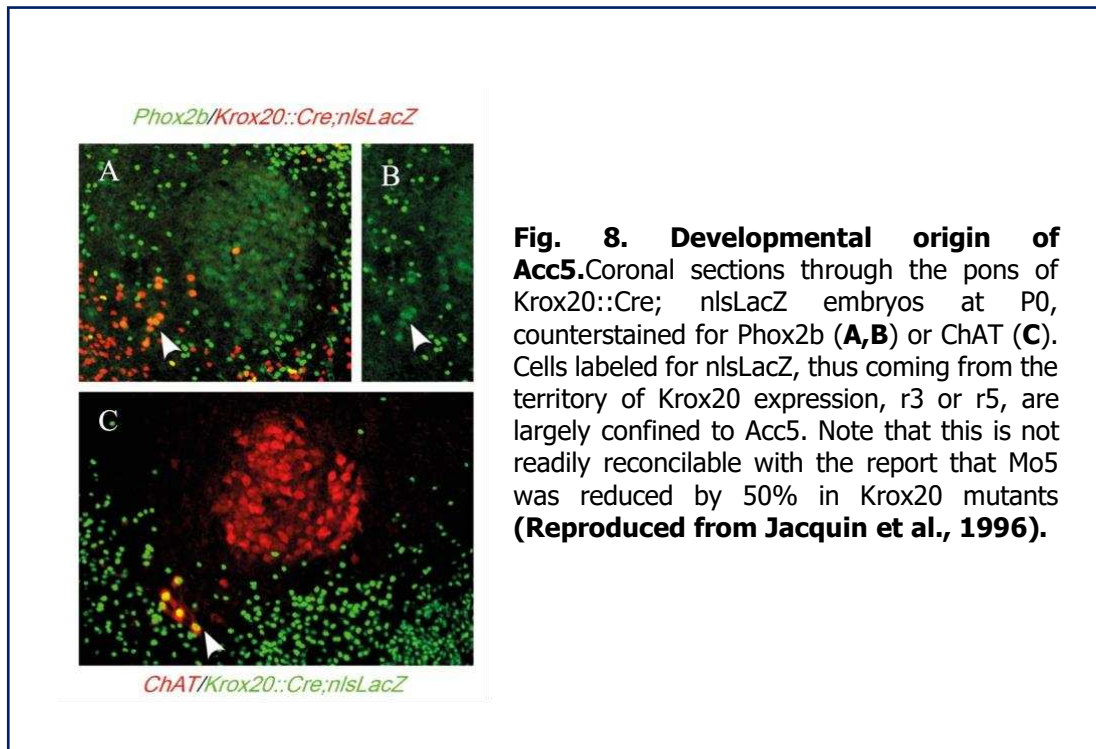
iv) Possibly the most striking contrast between Mo5 and Acc5, is that only the latter forms a "genu" in cat (**Nomura & Mizuno, 1983**) as well as in rat (**Székely & Matesz, 1982**). This *genu* manifests that, during ontogeny, the neuronal somas of Acc5 (unlike those of Mo5) migrate to their lateral location separately from their axon. Again, this is a feature shared with Acc7 (**Székely & Matesz, 1982**) — and indeed Mo7. This original mode of migration might explain that Acc5 and Acc7 (but not Mo5), are slightly disorganized in *reeler* mutants (**Terashima et al., 1993, 1994**)

For all the reasons above, Acc5 is more related to Acc7 than to Mo5, and one could almost propose that Acc5 and Acc7 are a single "accessory" nucleus (Acc), devoted to jaw abduction — albeit anatomically dichotomous, in reference to their nerves of projection, respectively trigeminal (nV) and facial (nVII). A caveat to this radical view is the ancient notion of registration of motor nuclei with branchial arches (**Gavalas et al., 1997**): Acc5 together with Mo5 innervate muscles derived from the first branchial arch, while Acc7 together with Mo7 innervate muscles derived from the second arch. A caveat to this caveat, though, is that a major argument for deriving the targets of Acc5 (mylohyoid and anterior digastric), from the first arch — despite their

dual attachment to first and second arch derivatives (jaw and hyoid bone)—seems to have been that they are innervated by the trigeminal nerve — a somewhat circular argument, see for example (**Gasser, 1967**). A final argument comes from teratology: the anterior digastric, normally innervated by Acc5 through the inferior alveolar branch of the mandibular nerve (thus nV), occasionally receives a branch of nVII in humans (**Kawai et al., 2003**). The cells of origin of this rare innervation pattern might be in Acc5 and ectopically project in nVII, or reside ectopically in Acc7, but in either case, this anomaly suggests yet another kinship of Acc5 and Acc7.







1.3.5. Motor nuclei for the hypobranchial muscles (tongue muscles and infrahyoids)

The motor neurons for the hypobranchial muscles (lingual muscles, **intrinsic** and **extrinsic, geniohyoid** (which can be considered an accessory tongue muscle, see above) and the 4 infrahyoid muscles: **omohyoid, sternohyoid, sternothyroid** and **thyrohyoid**) are located in the caudal hindbrain and rostral spinal cord: they form the hypoglossal nucleus (Mo12), its accessory nucleus (Acc12) and an unnamed motor nucleus in caudal continuity with Mo12, that projects in the first cervical nerves (and that we shall call for that reason "MoC").

All these motoneurons are of the somatic type, similar to those for the trunk and limbs: born in the pMN domain of ventricular progenitors, in rhombomere 7 and the rostral spinal cord, under the control of *Olig2*, *Neurog1* and *Neurog2* (**Novitch et al., 2001; Zhou et al., 2001**), thus genetically unrelated to branchiomotor neurons ³.

A large body of literature has been devoted to their somatotopy, especially for Mo12, to explain the sophisticated coordination of 8 pairs of tongue muscles required for eating, swallowing, vocalizing etc. I will restrict my review to the most robust findings:

One of the clearest illustrations of the somatotopy of Mo12 can be found in (**McClung & Goldberg, 2002**), who make use of the fact that the hypoglossal nerve (nXII) has two main branches, lateral and medial, whose respective deletion can reveal the origin of the other: injections in the whole tongue after cutting the **right lateral nXII** (which innervates the **retrusor** muscles) fill the left **ventral** compartment (**Fig. 10A,B**); after cutting the **left medial nXII** (which innervates the **protruder** muscles), fills the right **dorsal** compartment (**Fig. 10C**). Thus, the dorsal compartment projects to the retrusors and the ventral compartment to the protruders.

Further refinements, although less clearly documented, were proposed for the protrusor (ventral) compartment, to the effect that extrinsic muscles would have their motor neurons situated laterally (**Fig. 10E**), and intrinsic

³ An argument in favor of the tongue status of the **geniohyoid** (see above) is that it is innervated by Mo12, like tongue muscles, and unlike bona fide suprahyoid muscles, innervated by branchiomotor neurons.

ones, medially (**Fig. 10D**).

Concerning the infrahyoids, (**Kitamura et al., 1986**) show that their motoneurons form a ventral column in the cervical spinal cord in quasi-continuity with Mo12. The 'bridge' consists of a small group of neurons, the "supraspinal nucleus", which innervates the smallest and most rostral of the infrahyoid muscles: the **thyro-hyoid (Fig. 11)**.

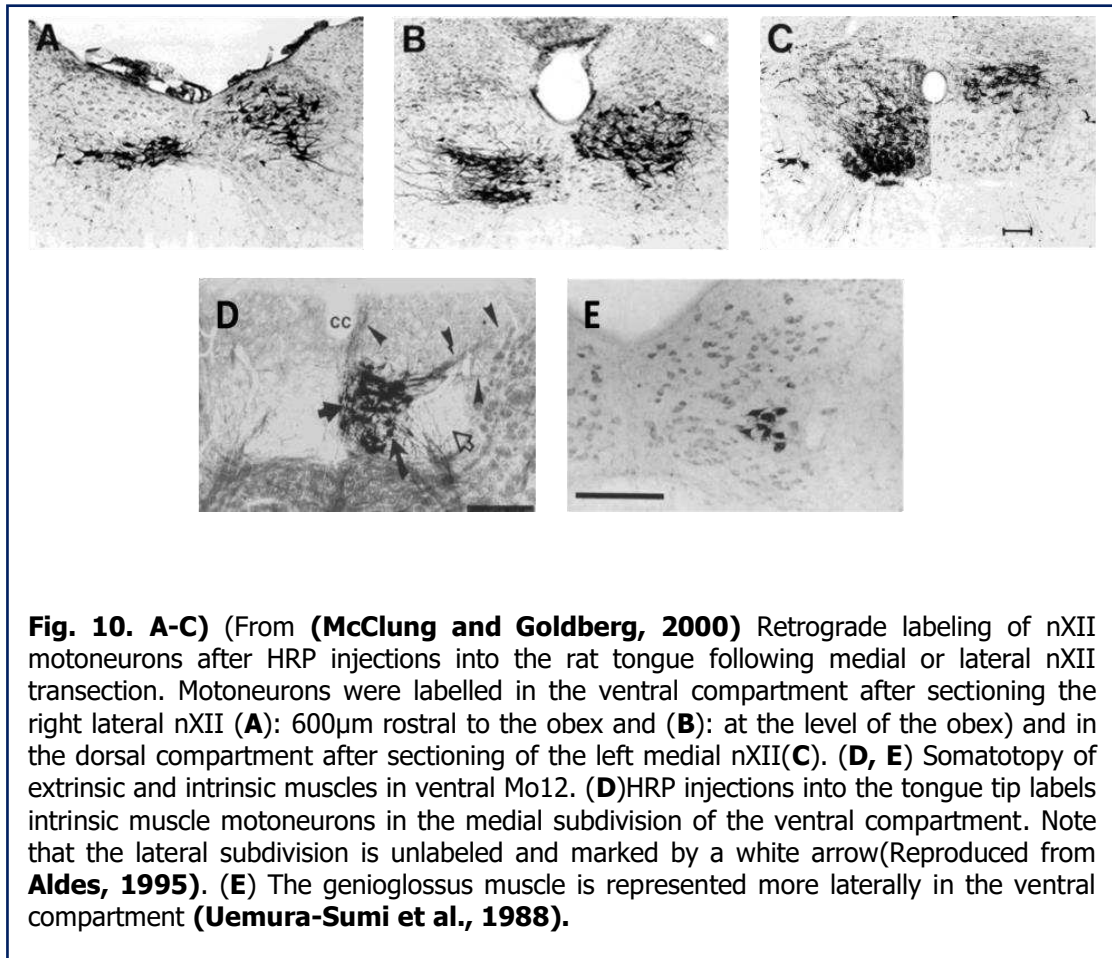


Fig. 10. A-C) (From (**McClung and Goldberg, 2000**) Retrograde labeling of nXII motoneurons after HRP injections into the rat tongue following medial or lateral nXII transection. Motoneurons were labelled in the ventral compartment after sectioning the right lateral nXII (**A**): 600μm rostral to the obex and (**B**): at the level of the obex) and in the dorsal compartment after sectioning of the left medial nXII(**C**). (**D, E**) Somatotopy of extrinsic and intrinsic muscles in ventral Mo12. (**D**)HRP injections into the tongue tip labels intrinsic muscle motoneurons in the medial subdivision of the ventral compartment. Note that the lateral subdivision is unlabeled and marked by a white arrow(Reproduced from **Aldes, 1995**). (**E**) The genioglossus muscle is represented more laterally in the ventral compartment (**Uemura-Sumi et al., 1988**).

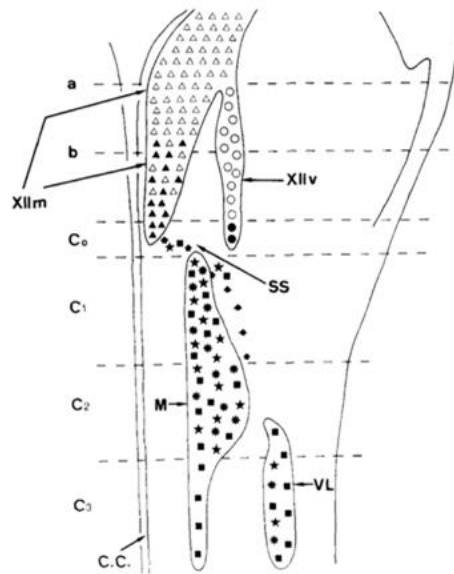


Fig. 11. Hypobranchial motoneurons. Outline drawing of the rat caudal medulla oblongata and upper cervical spinal cord, summarizing the locations of labeled hypobranchial motoneurons. The hypobranchials form a sequence of cell columns extending caudally from Mo12 (noted XIIIm and XIIv) via the supraspinal nucleus (SS) to the medial(M), then the ventrolateral nuclei(VL) of the ventral horn of C1-C3. Triangles denote lingual motoneurons, circles motoneurons for the geniohyoid, stars and squares motoneurons for hypobranchials. From **(Kitakura et al.,1986)**.

1.4. BRAINSTEM SENSORY CONTROL OF FEEDING

1.4.1. *First order sensory neurons for ingestive orofacial movements*

i. General overview

Food ingestion triggers multi-modal somatosensory inputs from various orofacial receptors, some unique to the orofacial region (**Avivi-Arber et al., 2011**). Although inessential to the general motor patterns of consummatory behaviors (as will be discussed below), they are required for their cycle-to-cycle fine tuning. Inputs from the perioral, oral and intraoral regions modulate an extensive repertoire of ingestive movements, including the grasping, positioning, manipulation, and licking movements involved in intraoral transport. The feedback modulation of orofacial movements that they provide acts both directly on brain stem-based circuits and via higher brain centers. Like the motor pathways, they fall into two large physiological categories, which are also anatomical and developmental: somatic (for mechanoreception—including touch and proprioception—, pain and heat) and visceral, more precisely “special visceral”, (for taste).

Reflecting the diversity of sensory modalities that orofacial primary sensory neurons convey, their embryonic origin is remarkably diverse, even beyond the somatic/visceral dichotomy: the neural crest for the touch and pain receptors of the proximal ganglia of nerves VII, IX and X; a combination of neural crest and a *sui generis* placode for the touch and pain receptors of the trigeminal ganglion; the epibranchial placodes for the “special visceral” taste afferents in the distal ganglia of nerves VII, IX and X ; and, more surprisingly, the central nervous system for the proprioceptors of the mesencephalic nucleus of the trigeminal nerve (Mes5).

ii. The trigeminal ganglion

Orofacial somatic inputs (touch, heat, and pain) are largely conveyed to the CNS by the trigeminal (V) nerve—whose cell bodies are located in the V ganglion. Unlike dorsal root ganglia or the proximal ganglia of nerves VII, IX and X, the trigeminal ganglion has a dual embryonic origin, in the pontine neural crest and a specific placode, the trigeminal placode. Its receptors relevant for feeding are more specifically located in the maxillary (V2) and

mandibular (V3) divisions of the ganglion, the ophthalmic division (V1) supplying the orbital and supraorbital regions of the face.

The maxillary nerve innervates the hard and soft palates, the oral mucosa of the maxillary vestibule, the maxillary dentition as well as gingiva and periodontal ligaments. The mandibular nerve innervates the oral mucosa of the cheek, anterior two-thirds of the tongue, mandibular dentition, periodontal ligaments, gingiva, and anterior mandibular vestibule. The central axons of maxillary and mandibular neurons enter the brainstem through the sensory root of nV and project to the second order sensory neurons of the trigeminal complex (VBNC) (see section below). From there, pathways for the processing of sensory-related information reach higher centers and the cortex in ways described in section 5.

In addition to periodontal pressure receptors, the trigeminal ganglion also contains proprioceptors for muscle spindles (found exclusively in jaw-closing muscles), and from periodontal ligaments, but remarkably both types of receptors are found in a completely different location in a nucleus known as the mesencephalic trigeminal nucleus (Mes5). This enigmatic nucleus is particularly relevant to my work and is treated in detail below.

iii. The mesencephalic trigeminal nucleus (Mes5)

The mesencephalic trigeminal nucleus is a collection of first-order sensory neurons that form a streak of cells from the caudal mesencephalon all the way to the pons, just rostral to Mo5 (**Fig. 12A, B**).

Mes5 neurons are the first-born neurons in the mesencephalon (the more caudal position of part of Mes5 in the adult resulting from a presumed migration) and they form the first fiber tract in the entire CNS (**Fig. 12B**). Their development is poorly understood. It was originally proposed, on the basis of extirpation experiments in chicken, to derive from neural crest cells which somehow manage to reenter the brain (**Narayanan & Narayanan, 1978**). This developmental sequence, although surprising, had the obvious appeal of providing a common ontogeny for all primary sensory neurons. However, this origin was questioned: (**Hunter et al., 2001; Louvi et al., 2007**) provide a review of previous studies and find that Mes5 is derived from midbrain progenitors expressing the signaling molecule *Wnt3a*, switched on in the mesencephalic midline *after* emigration of neural crest. Thus, Mes5 most likely has a central origin. The fact that similar neuronal types (proprioceptors) have disparate developmental origins (neural-crest for DRG or gV, CNS for

Mes5) is a rare and intriguing occurrence.

A few markers (and potential determinants) of Mes5 have been documented: the transcription factors *Brn3a* (**Fedtsova & Turner, 1995**) and *Drg11* (**Wang et al., 2007**) (in common with DRG neurons), the transcription factor *Etv1/Er81* (**Arber et al., 2000**) (**Eng et al., 2001**) (in common with DRG proprioceptors) and *Onecut/HNF6* (**Espana & Clotman, 2012**). In *Brn3a* KO, Mes5 disappears histologically by E18.5 (**Ichikawa et al., 2005**) but is reported to be present at E15.5 (data not shown by (**Espana & Clotman, 2012**)). In *Drg11*KO, no Mes5 cell is found in postnatal mice, but normal numbers of cells are found at E11.5 and at E12.5, which are dramatically reduced at E13.5. Thus, neither *Brn3a* and *Drg11* are involved in differentiation or survival, rather than generation, of Mes5 neurons, for which no determinant is known so far.

Mature neurons of Mes5 resemble dorsal root ganglion neurons in being unipolar, or rather *pseudo*-unipolar. The "united processes" (**P. F. Luo et al., 1991**) form what is sometimes called the *mesencephalic root of the trigeminal nerve* (despite the fact that a root normally resides outside the CNS) and bifurcate far from the cell body, to give off a branch that exits the CNS, and a branch that remains in it and projects caudally in the medulla, forming the "*tractus of Probst*". (**Dessem & Taylor, 1989**) provide reconstructions of individual cells of Mes5 traced from the nerve to the masseter spindles (**Fig. 12C**).

The peripheral axons, after exiting the pons via the ventral ("motor") root of the trigeminal nerve (which is thus mixed rather than purely motor), project in all three nerves emanating from the trigeminal ganglion, and from there, into the ethmoidal branch of the **ophthalmic nerve**, the palatal and superior alveolar branches of the **maxillary nerve**, and the pterygoid, temporal, masseteric and inferior alveolar branches of the **mandibular nerve** (**Corbin, 1940**). They innervate the muscle spindles of the masticatory muscles, and to a lesser extent the periodontal ligaments, gums and hard palate. Logically, Mes5 is absent from jawless vertebrates (**Hunter et al., 2001**) and is thought to have evolved with the jaw.

Mes5 neurons have a much richer connectivity than proprioceptors elsewhere in the nervous system. For one thing, due to their unique position inside the CNS, they receive numerous inputs onto their soma (listed in (**Morquette et al., 2012**)). In addition, they have numerous outputs, rather unexpectedly given the restriction of their peripheral fields and the paucity of the sensory modalities that they convey. Below are provided an exhaustive list of these sites, reported over several decades (with various degrees of

agreement — in some cases no diagnosis has yet been made of synaptic sites) and synthesized from **(Matesz, 1981)(Raappana & Arvidsson, 1993)(Rokx et al., 1986)(Zhang et al., 2001)(Zhang et al., 2005)(Shigenaga et al., 1989):**

(1) A rostral projection to the *nucleus of Darkschewitsch* at the level of the posterior commissure.

(2) Caudal projections are made through the tractus of Probst, which navigates far caudally as schematized in **Fig. 12D**, to:

- i) The *supratrigeminal nucleus* (Sup5) along the rostral border of Mo5, the most prominent area of terminal labeling from Mes5 neurons. But also, the intertrigeminal and juxtratrigeminal portions of the peritrigeminal area, as well as the principal and oralis sensory nuclei of the trigeminal (see below, interneuron chapter).
- ii) Hindbrain motor nuclei: Mo5, Acc5, Acc6, Acc7, Mo7, Mo12 and the nucleus ambiguus (MoA).
- iii) The reticular formation caudal to Sup5, described as “lateral, parvicellular reticular formation, but also in more medial parts of the reticular formation, especially in the caudal brainstem”. This might correspond in part to the IRt, not yet described in the early 90’s (see chapter on the reticular formation). Indeed, we have shown **(Dempsey et al., 2021)** that Phox2b⁺ neurons of the IRt, which are premotor to jaw opening and tongue retractors and participate in a rhythmic licking CPG (see Results section), are postsynaptic to Mes5 .
- iv) The nucleus of the solitary tract.
- v) The spinal cord, down to at least the second cervical segment.

No function can easily be deduced from this list of projection sites, some of which are functionally antagonistic (e.g., the jaw closing Mo5 versus the jaw opening Acc5 and Acc7), others too broad to make obvious sense (reticular formation), others still, unrelated to orofacial movements (spinal cord). Collectively, they suggest much broader functions in orofacial motility (and beyond) than the only two which have been discussed so far to our knowledge: jaw posture and bite strength. A possible hint of this is that the gross phenotypes of the knockout for both *Drg11* and *Brn3a* KO (see above) include

neonatal lethality evocative of dramatic feeding defects: *Drg11* KO are underweight before weaning (suggesting defect in suckling) and starve to death after weaning with overgrown incisors. Rescued by trimming the incisors and fed liquid food from an open-face shallow bowl, the pups can't lick and have to sloppily insert food in their mouth. *Brn3a* KO die before 24 hours with no visible milk in the stomach, and no rhythmic suckling response can be obtained by "stimulating the lips with a canula" unlike in wild types et heterozygotes (**Xiang et al., 1996**) [an effect later summarized by (**Ichikawa et al., 2005**) as "the knockout disrupts the rhythmic jaw and closing movements"], while (**McEvelly et al., 1996**) mentions a "swallowing deficiency". The mutants have no general insensitivity to tactile stimuli (like pinching), but no righting reflex probably due to deficits in other proprioceptors or mechanoreceptors. A caveat to the conclusion on *Mes5* that one can draw from the lethal *Drg11* and *Brn3a* KO phenotypes, is that both genes are required in the differentiation of the trigeminal ganglion and are also expressed in the principal and spinal nuclei of the trigeminal nerve. The phenotypes might therefore reflect wider roles of the genes, in the entire trigeminal sensory system. It should be noted that complete trigeminal deafferentation, implemented in adults (**Jacquin & Zeigler, 1982**) and see below), thus including *Mes5* deafferentation, has relatively minor consequences on feeding motor behaviors, which, by contrast to the neonatal lethal *Drg11* and *Brn3a* KO, could suggest that the role in ingestive behaviors of trigeminal sensory neurons, both central and peripheral, is much bigger in the neonates than in the adult.

Physiologically, the role of *Mes5* has been studied by recordings in anesthetized or alert animals, and by lesions of the nucleus itself or of branches of the trigeminal nerve (deafferentation).

The most diverse roles — and sometimes contradictory — have been put forward for *Mes5*. One central paradox that complicates the field is that periodontal receptors and spindle receptors, which collectively make up *Mes5*, could be expected to fire in opposite situations: periodontal receptors when pressure is increasing on the teeth, i.e., when the jaw is adducted (either totally, or partially on a morsel of food), while the spindle receptors should fire when the jaw openers are stretched, i.e., when the jaw is abducted. Certainly, the paradox arises only if *Mes5* is considered to behave as a homogeneous entity — which might not be the case. But few studies have explored a potential heterogeneity of *Mes5*: periodontal and spindle receptors are not well segregated (although the former might be enriched caudally (**Nomura & Mizuno, 1985**), they have the same morphology, and are all glutamatergic. The latter might synapse on masseter motoneurons more frequently than the

former (**Chul Bae et al., 1996**) but details of their respective, possibly contrasted connectivity are not available.

Two lines of speculation and research illustrate the efforts required to solve the paradoxes in the role of Mes5 during chewing:

- i) Concerning spindle receptors, one model implicates the gamma motor neurons in a constant resetting of spindle length as a function of a “temporal template”, which represents the *expected* upward jaw movement during chewing. This could explain that their discharge increases as the muscle contracts in cases where an unexpected obstacle slows the movement, and thus contribute to augment bite strength by a “servo-mechanism” (**A. Taylor & Appenteng, 1981**). In practice, it also means that their firing pattern does not reflect jaw position and is hard to predict. This line of reasoning echoes recent reappraisal of muscle spindles elsewhere in the body (**Dimitriou, 2022**).
- ii) Another intriguing line of thought involves a compartmentalization of Mes5 neurons: the central axon would be capable of conducting ectopic, antidromic action potentials and thus behaving like a bona fide interneuron, that for example, could conduct signals from the masticatory CPG to Mo5 through its collaterals, in isolation of the peripheral axon and soma (**Westberg et al., 2000**). In this audacious scenario (which has echoes in other systems; e.g., (**Connors & Ahmed, 2011**), the peripheral inputs to these neurons lose their relevance.

In summary, by highlighting one property or another, Mes5 has been implicated in the following scenarios:

- Periodontal receptors could *inhibit* jaw closing (to protect teeth against excessive pressure, e.g., when a piece of stone is encountered in the food)
- Periodontal receptors could *enhance* jaw closing (to increase bite force in response to increased toughness of the food).
- Periodontal receptors could participate in the masticatory-salivary reflex.
- Spindle receptors could counteract masseter elongation (in a postural reflex).
- Spindle receptors could increase masseter contraction (by a gamma-motoneuron dependent servo-mechanism).

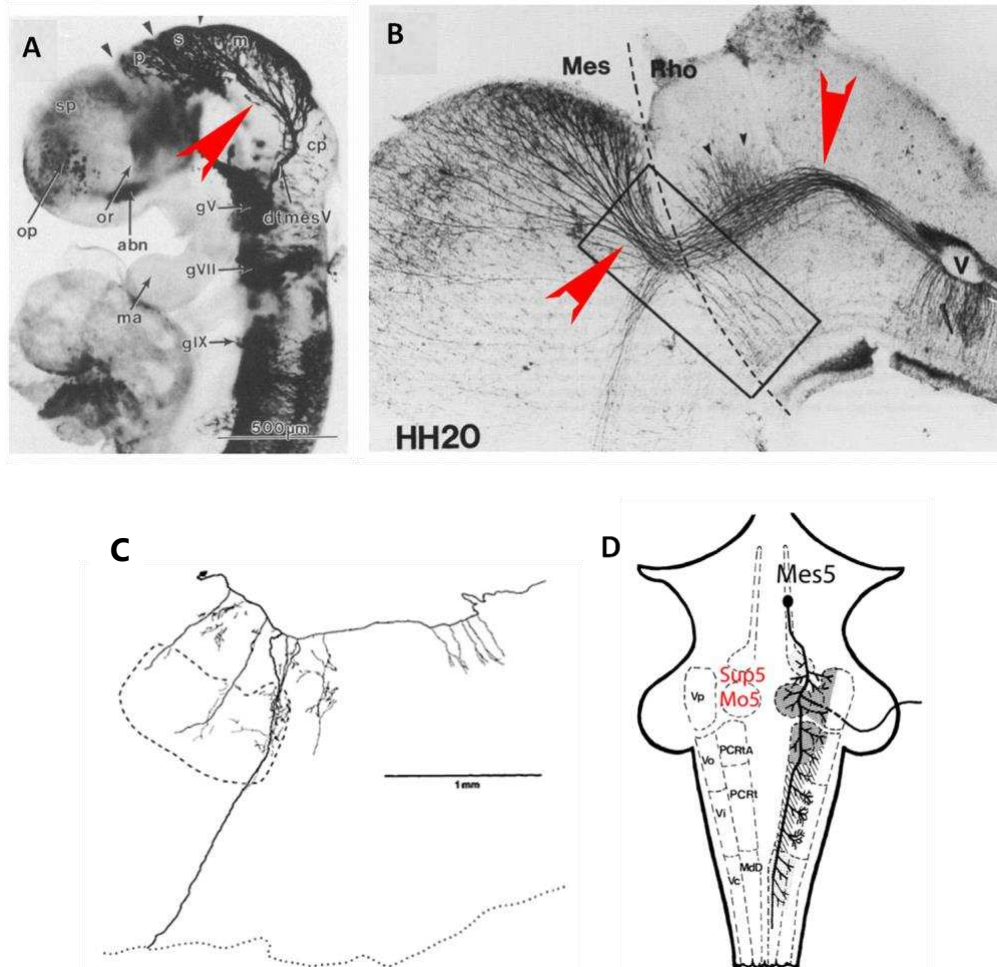


Fig. 12. Morphology and projection pattern of the mesencephalic trigeminal nucleus (Mes5). **A, B**) Lateral view of a whole mount (**A**) and flat mount (**B**) of a chick embryo at HH20 (axonal tracts are immunostained for the SC1/BEN adhesion molecule), showing origin of the Mes5 in the mesencephalon. Its axonal tracts have already crossed the midbrain-hindbrain boundary at this stage and are extending to the root of the fifth ganglion (V, the ganglion has been removed). (From **Chedotal et al., 1995**). They are the earliest-born neurons of the midbrain, and their axons pioneer major axonal tracts in the brain. **C**) Sagittal reconstruction of a masseter muscle spindle afferent axon in the rat. The dotted line indicates the ventral limits of the hindbrain and the dashed line denotes the borders of Mo5. The axon enters the brainstem through the trigeminal motor root, travels dorsomedially within the brainstem to terminate in the caudal portion of Mo5 and supplies several collaterals as it courses through it. It then bifurcates dorsomedial to Mo5 into an ascending branch in the tract of the mesencephalic nucleus and a descending branch in the tract of Probst. **D**) Horizontal view of the midbrain and hindbrain, showing the extensive course of Mes5 axons in the hindbrain. The descending branch gives off several collaterals as it courses in the tractus of Probst, supplying the reticular formation dorsal and caudal to Mo5 (From **Dessem and Taylor, 1989**).

1.4.2. Second order sensory neurons for ingestive orofacial movements

i. The principal and spinal trigeminal nuclei (Pr5 and Sp5)

The maxillary and mandibular branches of the trigeminal ganglion enter the brainstem to innervate the brainstem trigeminal complex (VBNC), which comprises a main (principal) and spinal sensory nucleus (Pr5 and Sp5, respectively). Pr5 is located within the caudal aspect of the pons lateral to the trigeminal motor nucleus. Sp5 is an elongated nucleus which spans from the pons to the substantia gelatinosa of the upper cervical cord (**Fig. 13**).

Pr5 conveys vibration and tactile sensation (2-point discrimination and fine touch), in addition to proprioceptive (Golgi tendon organ) input from the temporo-mandibular joint (**Price & Daly, 2022**).

A somatotopic representation of the face exists within Pr5 and is faithfully maintained at each projection level in the thalamus and somatosensory cortex. This representation is inverted because of the growth of the face and brain along different axes during development. Accordingly, the caudal to rostral axis of the face can be mapped along the lateral to medial axis of the mature Pr5, such that the lateral part receives inputs from the lower jaw via the mandibular branch (Fig. 14) while the medial portion receives inputs from maxillary branch afferents supplying the upper jaw (and whiskers in rodents) (**Erzurumlu et al., 2010**).

Pr5 has a dual origin in r2 and r3 during development: the dorsal division (which corresponds to the rostral division at early stages) is comprised only of r2-derived progeny, whereas the ventral (i.e., caudal at early stages) division of Pr5 is made up exclusively of r3-derived progeny (**Erzurumlu et al., 2010**). Axons of second-order neurons in the ventral division of Pr5 cross the median raphe and ascend contralaterally before projecting to the dorsolateral ventral posteromedial (VPM) thalamus. Axons originating in dorsal Pr5 project to the ventromedial VPM. Third-order VPM thalamus neurons then terminate in the face primary somatosensory cortex (S1).

The topographic peripheral afferent connections from the trigeminal ganglion to Pr5 in the brainstem and the axonal mapping of Pr5 to higher order centers depend on a set of shared anteroposterior cues that pattern both the rhombomeres and the neural crest/placode progenitors of the trigeminal

ganglion during development (**Erzurumlu et al., 2010**).

Sp5 is the termination site of primary trigeminal afferents descending through the spinal trigeminal tract, which is positioned laterally to it. Minor general somatic afferents from the ear, tongue, pharynx and larynx are supplied by the proximal ganglia of the VII, IX, and X cranial nerves (**Walker, 1990**) (**Fig. 13**), but will not be reviewed here. Sp5 segregates rostrocaudally into the pars (subnucleus) **oralis**, **interporalis**, and **caudalis** (**Olszewski, 1950**), each relaying a specific sensory modality to the CNS: e.g., the pars oralis, as well as the pars interporalis, transmit discriminative tactile sensation from the face, while the pars caudalis transmits pain and temperature sensations from the ipsilateral face. Axons of second-order sensory neurons in Sp5 cross the midline, join those of the ventrolateral Pr5 and ascend contralaterally in the ventral trigeminothalamic tract to project to the ventral posteromedial thalamus, whose projections terminate in S1 (**Price & Daly, 2022**). Subpopulations of premotor interneurons within the Sp5 also relay sensory feedback information onto motoneurons and are involved with mediating reflex jaw-opening (**Kidokoro et al., 1968**)(**Donga & Lund, 1991**)(**Takatoh et al., 2013a**)(**Stanek et al., 2014a**)

Somatotopy also exists in the spinal trigeminal nucleus and is maintained throughout its three subnuclei: sensory inputs from the lateral face project caudally to the pars caudalis, those from the middle part of the face terminate in the pars interporalis, and those from the central portion of the face project to the rostralmost division, the pars oralis.

ii. The nucleus of the solitary tract

Second-order sensory interneurons in the rostral nucleus tractus solitarius (NTS) receive gustatory inputs from taste receptors via the distal ganglia of the VII, IX and X cranial nerves (respectively geniculate, petrosal and nodose), and relay these stimuli to several oromotor nuclei (Mo5, Mo7 and Mo12), to intramedullary preganglionic parasympathetic salivatory neurons as well as to the adjacent medullary reticular formation to modulate oromotor reflexes, namely taste-elicited ingestion and rejection behaviors (i.e. gaping) (**Grill & Norgren, 1978**).

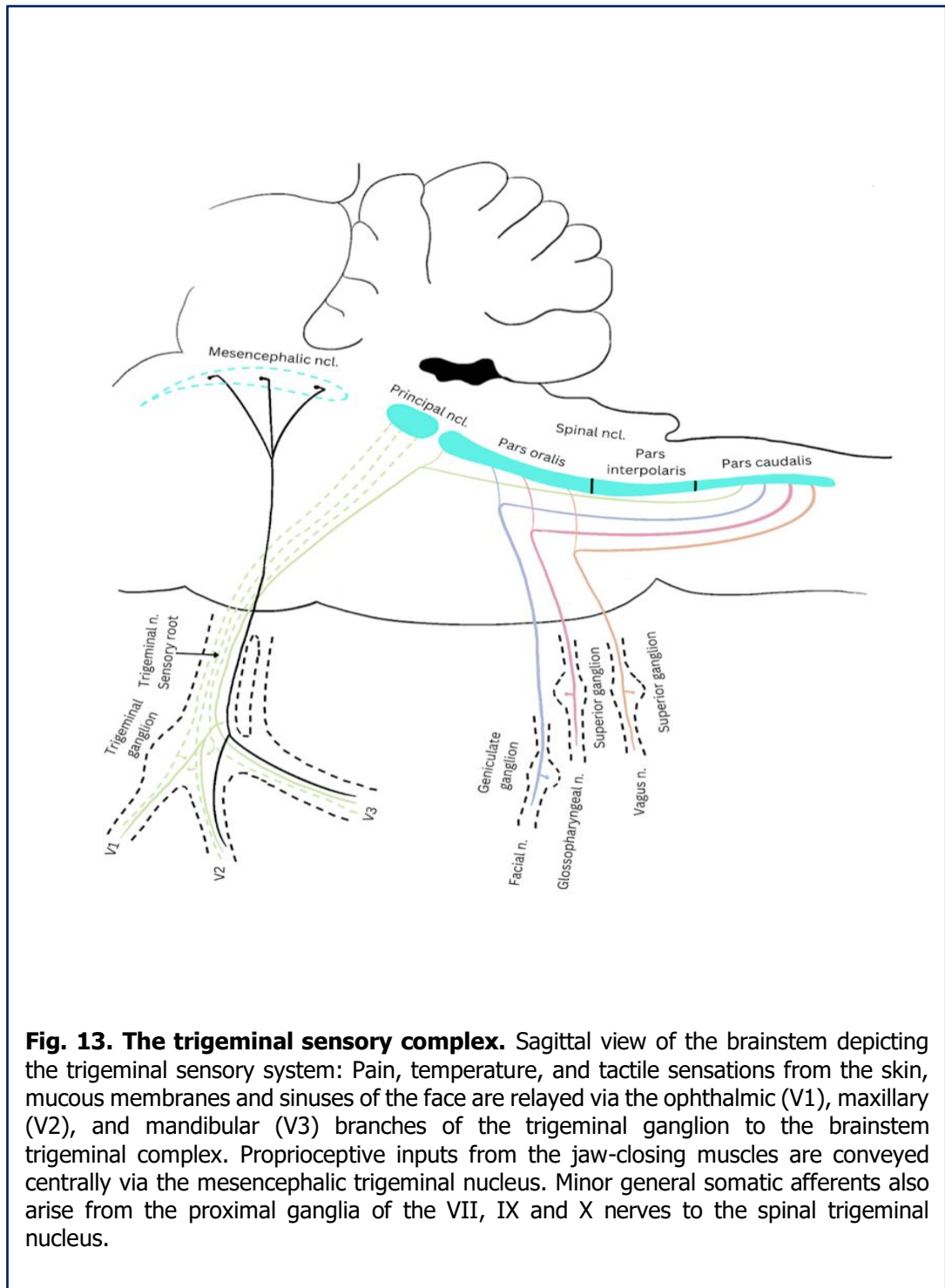


Fig. 13. The trigeminal sensory complex. Sagittal view of the brainstem depicting the trigeminal sensory system: Pain, temperature, and tactile sensations from the skin, mucous membranes and sinuses of the face are relayed via the ophthalmic (V1), maxillary (V2), and mandibular (V3) branches of the trigeminal ganglion to the brainstem trigeminal complex. Proprioceptive inputs from the jaw-closing muscles are conveyed centrally via the mesencephalic trigeminal nucleus. Minor general somatic afferents also arise from the proximal ganglia of the VII, IX and X nerves to the spinal trigeminal nucleus.

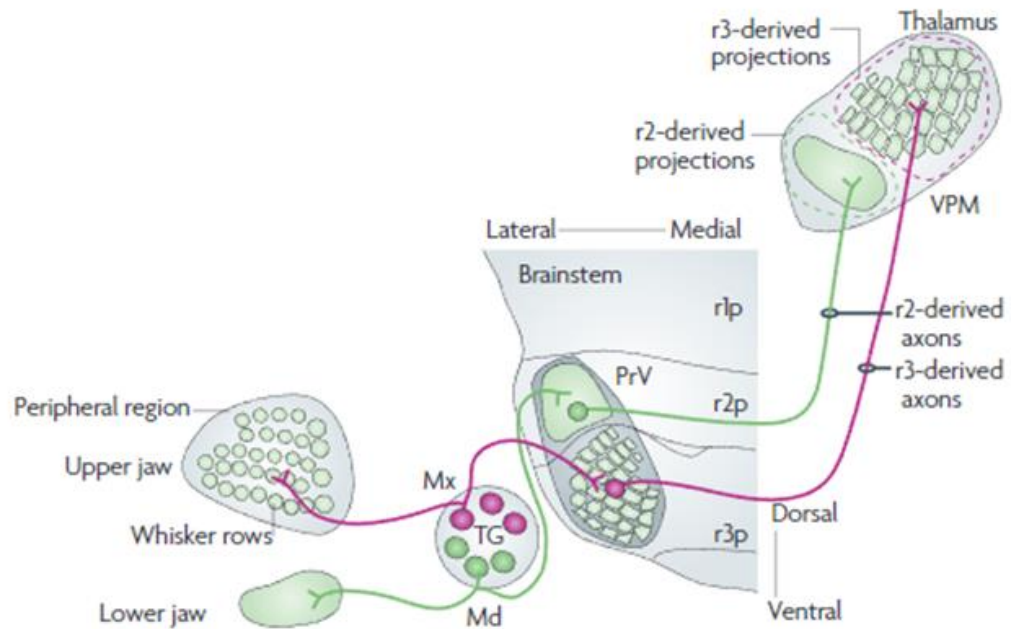


Fig. 14. Orofacial somatotopic representation in Pr5 nucleus. The caudal to rostral axis of the face can be mapped along the lateral to medial axis of the mature Pr5, such that the lateral part receives inputs from the lower jaw via the mandibular branch (green) and the medial part receives maxillary branch afferents (pink) from the upper jaw and whiskers. This topographic map of the orofacial sensory region is thought to arise as a result of shared anteroposterior positional cues that pattern both rhombomere-derived and neural crests/placode progenitors of the Pr5 and trigeminal ganglion respectively. In turn, differential patterning of Pr5 progenitors at distinct rostrocaudal levels (which remain physically segregated in the mature nucleus) underlies the somatotopic representation of mandibular and maxillary face maps (Reproduced from **Erzumulu et al., 2010**).

1.5. REGULATION OF OROFACIAL BEHAVIORS BY HIGHER-ORDER BRAIN CENTERS

The activity of brainstem orofacial CPGs is gated by descending inputs from the cortex, cerebellum, basal ganglia, and superior colliculus gate that are briefly discussed below.

1.5.1. Cortical control

Voluntary oromotor actions are initiated by the motor cortex which includes the face primary motor cortex (M1) as well as other motor centers, such as the premotor cortex and the supplementary motor area (SMA) (**Avivi-Arber et al., 2011b**). Accordingly, electrical stimulation of specific regions of the motor cortex induces various forms of oromotor activity : e.g., microstimulation of the ALM (anterolateral motor cortex) triggers bouts of directional licking (**Economo et al., 2018; N. Li et al., 2015**) while that of the cortical masticatory area (CMA) — corresponding to an anterior area (Area A) of the orofacial motor cortex — evokes rhythmic jaw movements in various species (**Goldberg & Tal, 1978; Liu et al., 1993**). Stimulation of different parts of the CMA induces diverse jaw movement kinematics in mammals (**Y. Nakamura & Katakura, 1995**). This technique was employed to establish 'motor maps' for orofacial muscles – essentially cortical motor representations of face muscles — which revealed a segregation in the cortex according to function: muscles involved in 'ingestive' movements are represented medially while those participating in 'exploratory' ones are represented laterally (**Lindsay et al., 2019**).

In rodents, the motor cortex supplies very few monosynaptic inputs to cranial motoneurons, so that its modulatory influences on oromotor behaviors are primarily indirect (**Grinevich et al., 2005; Takatoh et al., 2013**). Pyramidal tract (PT) neurons located in layer 5 of the motor cortex are the only source of cortical outputs to brainstem interneuronal areas involved in orofacial motor control (**Economo et al., 2018; Lemon, 2008**).

M1 has several roles in the control/modulation of oromotor activity:

- i) It is involved in the planning of oromotor movements (e.g., the population dynamics of ALM-PT neurons located in upper layer 5b (thalamus-projecting) is coherent with preparatory activity prior to orofacial movement (**Economo et al., 2018**).

- ii) It is involved in the execution of orofacial movements(e.g., Medulla-projecting ALM-PT neurons in lower layer 5b demonstrate population dynamics that is predictive of movement onset **(Economo et al., 2018)**).
- iii) It is involved in sensory gating. e.g., stimulation of the vibrissa motor cortex exerts a permissive role on sensory transmission to the thalamus via disinhibition of vibrissa responses in extrathalamic Gabaergic in circuits of the zona incerta that tonically inhibit this relay**(Urbain & Deschênes, 2007)**).

While the motor cortex initiates voluntary movements, both motor and primary somatosensory(S1) cortices are active during movements**(Umeda et al., 2019)**.To modulate oromotor function, the face M1 integrates somatosensory inputs from the orofacial region, which are mostly relayed to it via layer 4 of S1, which receives bilateral orofacial inputs via the thalamic somatosensory nuclei **(Fig 15)** in a somatotopic fashion. Moreover, the face S1 actively processes inputs from face M1 and has efferent projections to brainstem circuits involved in oromotor functions **(Avivi-Arber et al., 2011)**. Indeed, studies have shown that discrete as well as rhythmic jaw, tongue and facial movements can be elicited by micro-stimulation of the face S1 **(Avivi-Arber et al., 2011)**).

It should be noted that other cortical areas outside the sensorimotor cortex are involved in the control of orofacial movements (e.g., a posterior area (P-area) in the agranular insular cortex has been identified as a second CMA in rats **(Maeda et al., 2014)**).

1.5.2. Superior colliculus

The superior colliculus (SC) is a midbrain structure involved in sensorimotor integration and is organized into seven layers: three superficial (zonal, superficial gray and optic), two intermediate (intermediate gray and intermediate white) and two deep layers (deep gray and deep white). The "intermediate" and "deep" layers are collectively referred to as the "motor-related SC" **(H. W. Dong, 2008)**. Four SC zones (medial, centromedial, centrolateral, and lateral) that extend radially across the layers along the medial-lateral and rostral-caudal axes can be distinguished in rodents based on distinct cortical inputs**(Benavidez et al., 2021)**.As such, inputs from face S1 in rodents**(Benavidez et al., 2021)**and from face M1 in primates **(Tokuno et al., 1995)** are conveyed to the rostral lateral (deep) SC.

The SC regulates orofacial movements either directly via inputs to orofacial brainstem motor nuclei or indirectly via (predominantly contralateral) inputs to interneurons (**Benavidez et al., 2021**). For example, it has been shown that stimulation of the SC modulates vibrissa kinematics (e.g., amplitude and set point of whisking) via monosynaptic projections to facial motoneurons but also via the IRt (**Kaneshige et al., 2018**). Glutamatergic Pitx2+ SC neurons project to both the IRt and PCRt, and it has been suggested that the latter pathway may be involved in biting during predatory hunting (**Xie et al., 2021**).

1.5.3. Cerebellar control

Descending inputs from the cerebellum also modulates and activates several types of orofacial movements via direct projections to brainstem motor nuclei or via CPGs. The deep cerebellar nuclei (DCN) constitute the output channel of the cerebellum that conveys Purkinje cell output (the output neurons of the cerebellar cortex) to premotor areas and other brain targets and consist of four nuclei: the fastigial (medial) nucleus, two interposed (intermediate) nuclei and the dentate (lateral) nucleus, which is by far the largest DCN subnucleus.

Purkinje cell simple spike activity is locked to rhythmic licking in the rodent cerebellum (**Bryant et al., 2010; Cao et al., 2012**) and spiking activity in medial deep cerebellar nucleus (mDCN) neurons also correlates with licking (**Lu et al., 2013**). Furthermore, it has been shown that the ipsilateral mDCN is directly premotor to genioglossus motoneurons (**Lu et al., 2013; Takatoh et al., 2021a**) and decerebellate rodents have significantly slower licking frequencies (**Bryant et al., 2010**). Stimulating all deep cerebellar nuclei (DCN) in monkeys elicits tongue movements and functional specificity related to tongue movement kinematics exists within each nucleus (**Bowman & Aldes, 1980**)

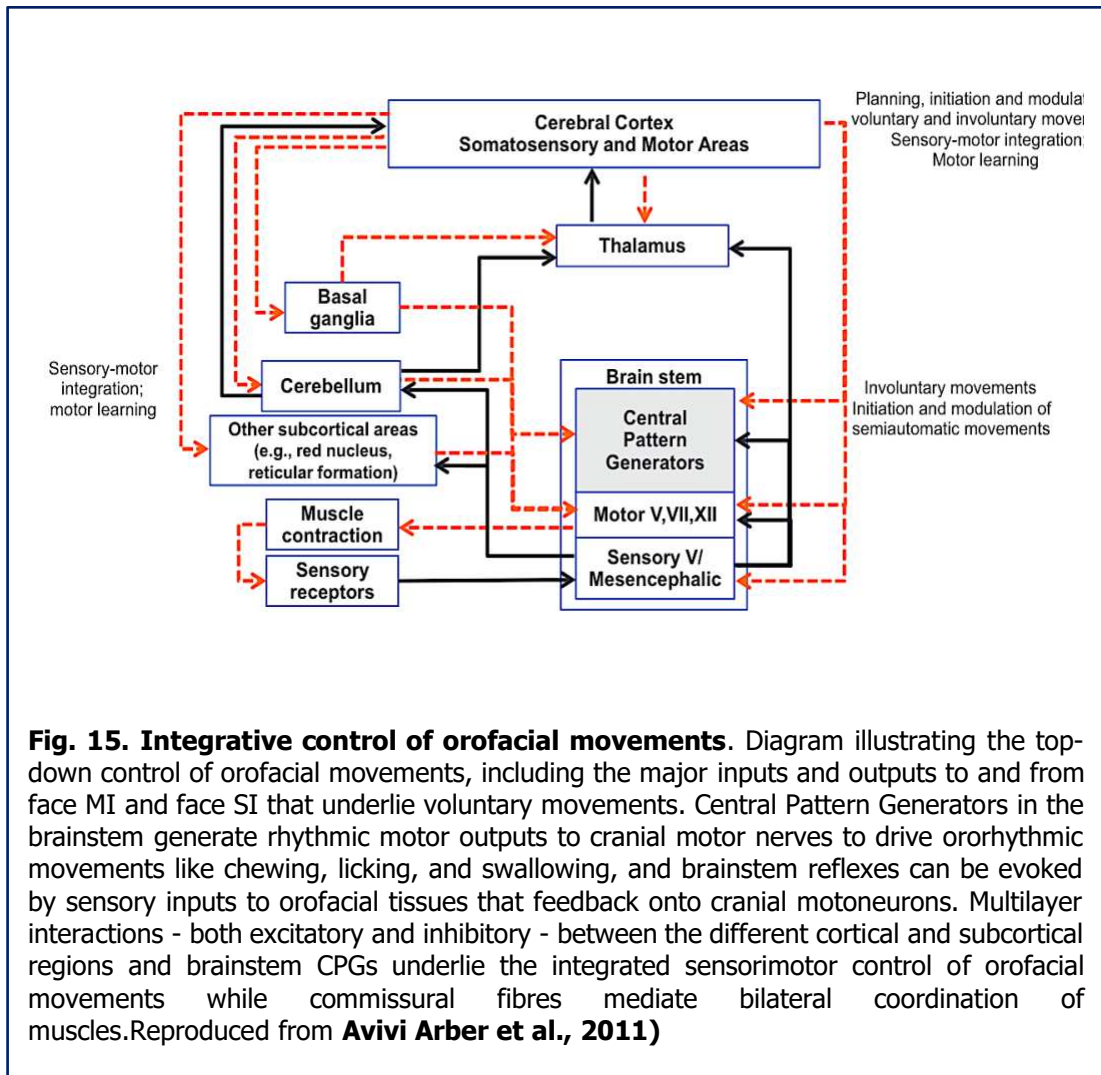
Another oromotor behavior that is subject to descending cerebellar control is whisking. It is known that Purkinje cell spiking encodes distinct aspects of vibrissa kinematics (e.g., vibrissa direction versus vibrissa set-point) and accordingly form different functional ensembles based on synchronous firing (**Bosman et al., 2010**). It has more recently been shown that the ipsilateral intermediate DCN in adult mice contains vibrissa premotor neurons (**Takatoh et al., 2021a**). Interestingly, compelling evidence also points towards a subset of bilaterally projecting mDCN neurons as substrates for cerebellar-mediated coordination of brainstem respiratory and orofacial

(whisking and licking) CP(R)Gs(Lu et al., 2013). Premotors to jaw-closing motoneurons were also recently found in the contralateral mDCN in adult mice (Takatoh et al., 2021a).

1.5.4. Basal ganglia

Descending projections stemming from the basal ganglia via the substantia nigra pars reticulata (SNR: the principal output nucleus of the basal ganglia) are thought to modulate orofacial behaviors via the medullary reticular formation — including the PCRt (Yasui et al., 1994, 1995) and supra as well as intertrigeminal areas— either directly or via the deep superior colliculus (nigrotectal pathway), or both(Yasui et al., 1992). Indeed, it has been shown that the firing rates of many lateral SNR neurons are time-locked to individual licks (Yasui et al., 1992) and optogenetic excitation of Gabaergic nigrotectal projections selectively suppresses the activity of lick-modulated SC neurons and disrupts spontaneous licking (Rossi et al., 2016). Moreover, many orofacial-related cortical output pathways project indirectly to the brain stem via the basal ganglia(Sessle, 2009). Consistent with this, pharmacological manipulations of basal-ganglia networks can elicit rhythmic jaw movements in anesthetized rodents, and orofacial motor deficits arise following the ablation of specific basal ganglia components(Sessle, 2009).

Extensive cortical and subcortical circuit interactions that integrate orofacial sensory afferent inputs to modulate brainstem CP(R)G activity underlie the integrative sensorimotor control of orofacial movements (Fig. 15).



1.6. INTERNEURONS OF THE RETICULAR FORMATION

1.6.1. *The reticular formation*

Long ago (**Herrick, 1948**), the reticular formation was conceived as a zone of integration between the ventral motor column and dorsal sensory one (on the model of the spinal cord). W.W. Blessing (**Blessing, 1997**) comments that for Herrick, in the spinal cord as well as in the hindbrain, "*there is a dorsal sensory input zone, a ventral motor output zone and an intermediate zone for coordination and integration of inputs and outputs. In the hindbrain, boundaries between the intermediate zone and the other two zones are blurred, especially in the more ventral regions*". Blessing suggests that Herrick's vision was fundamentally right, especially in that it excluded anything diffuse or non-specific in the reticular formation, which was all about precise connectivity, but that this concept was unduly abandoned in the 1950's, under the influence of Magoun, Moruzzi, the Scheibels and others, who introduced the notion of an "ascending reticular activating system" and the idea that this part of the brain was relatively unstructured. Blessing adds (**Blessing, 1997**) that the diffuse concept of the reticular formation is still very much alive, and that fighting it is "*by no means a straw-man assignment*". The situation has certainly changed in the past 20 years. Yet, this part of the brain lags behind others in terms of localization of defined cell types. The task is actually daunting if one believes the statement of Olszewski according to which "*the variety of cell types found in a cubic centimeters of volume of the rhombencephalon [...] is greater than in any other part of the central nervous system*" (cited in (**Blessing, 1997**)).

1.6.2. *Regions of the reticular formation and the slow birth of the IRt*

To this date, the reticular formation is divided into regions on the rostrocaudal and dorsoventral axis, based on a not altogether coherent set of criteria: topological, histological and hodological. Until the mid 90's, the reticular formation was divided in two regions only on the latero-medial axis (which topologically —i.e., embryologically — is dorso-ventral): two "tegmental fields", lateral and medial respectively called "parvocellular" and "gigantocellular" regions. The inadequacy, or arbitrariness, of this partition emerged progressively and a third region was distinguished, sandwiched between the two, and called for that reason "Intermediate".

An important reference in the prehistory of the “intermediate reticular formation” (IRt) is **(Holstege & Kuypers, 1977)**, who, based on the location of neurons premotor to Mo5, Mo7 and Mo12 felt compelled to subdivide the lateral tegmental field (my emphases): “*On the basis of the distribution of labeled fibers, the lateral tegmental field may, in turn, be subdivided into a **medial** and a **lateral** part. Thus, the bulbar tegmentum appears to be composed of **three longitudinal zones**, that is, the lateral part of the lateral tegmental field, the medial part of the lateral tegmental field, and the medial tegmental field.*”. This was elaborated by **(J. B. Travers & Norgren, 1983)**, also in the context of tracing premotor neurons to most hindbrain motor nuclei : “*First, although projections originated from specific regions of the reticular formation, these regions **did not always correspond to classical divisions** established by cytoarchitectural analysis. For example, the medullary reticular formation has been divided into medial gigantocellular and lateral parvocellular fields [...] A substantial proportion of the neurons projecting to mV from the rostral medullary reticular formation, however, **were sandwiched between the two**. These results correspond well with autoradiographic analysis in the cat **(Holstege et al., '77)** [...] Thus, the bilateral clusters of labeled neurons that project to oral motor nuclei could be grouped functionally with the **medial "effector" Reticular Formtion.***”

Two years later, by a completely different route, Paxinos defined the IRt and named it for the first time in his classic Atlas of the Rat Brain (1986): “*Intermediate reticular nucleus: the zone between the gigantocellular and the parvocellular reticular nuclei contains some large, as well as medium and small sized cells, and is more reactive for AChE than its neighbors. Considering its cytoarchitecture and position we have called this area the **intermediate reticular nucleus***”.

Seven years later (1992), Larry Swanson **(Swanson.,1992)** still failed to mention the Intermediate reticular nucleus — only the Parvocellular and the Gigantocellular — and refers to Olszewski **(Meessen & Olszewski, 1949)** for cytoarchitectonics.

All in all, the flurry of studies on premotor neurons in the mid-eighties, either just precedes the official birth of the IRt, or have yet to integrate it, since they describe the premotor neurons as residing in the PCRt — which greatly complicates reference to these papers.

Even the partition of the reticular formation into 3 dorsoventral regions (rather than 2) demarcated by straight lines, which is the current norm, does not readily fit with cytoarchitectonic features, or otherwise defined neuronal types. For example, many groups of neurons identified by their projections

(e.g. **(Stanek et al., 2014)**) straddle these borders, which might have little reality. Finally, on the rostro-caudal axis, the regions that surround IRT ventrally and dorsally are named “gigantocellular” and “parvicellular” from the level of the genu of the facial nerve to the rostral end of MoA, but further caudally are called “medullary reticular formation” (respectively ventral and dorsal) **(Paxinos & Franklin, 2004)**, without much anatomical or physiological justification for this change of terminology.

More recently, efforts have been devoted to defining neuron types in the reticular formation with genetic — and by implication developmental— criteria. In the hindbrain, a limited set of transcription factors can define a cartesian grid of progenitor domains for different classes of neurons: on the rostro-caudal axis, the expression borders of *Hox* genes align perfectly with the rostro-caudal boundaries of transient segments of the neural tube called rhombomeres **(Fig. 16A.) (Krumlauf et al., 1993; Lumsden & Krumlauf, 1996)**, which constrain the generation of some types or subtypes of neurons (such as motoneurons, or serotonergic neurons **(Pattyn et al., 2003)**). Similarly, on the dorso-ventral axis, 16 cardinal domains each express a discrete set of transcription factors, and give rise to specific neuronal types **(Gray, 2008a; Sieber et al., 2007; Storm et al., 2009) (Fig. 16B,C)**. Thus, combinations of transcription factors (and downstream effectors) may (to different degrees) specifically identify subpopulations of neurons within the medullary reticular formation **(Gray, 2013)**.

A number of relatively recent studies have used transgenic lines whereby a *cre* recombinase is driven by the promoter of developmental TFs to functionally interrogate cell-type specific circuits in the hindbrain reticular formation. Notable case studies include:

- i) It has long been known that the gigantocellular reticular nucleus (GRN) of the medullary reticular formation contains reticulospinal neurons involved in locomotion **(Drew et al., 1986)**, but this region contains diverse neuron types — including both inhibitory and glutamatergic interneurons that are spatially intermingled, thus hindering the selective study of neuron subtypes in this region. **(Bretzner & Brownstone, 2013)** subsequently showed that the transcription factor *Chx10* defines a subpopulation of V2aglutamatergic reticulospinal neurons (derived from the *Lhx3+* P2 domain) in the GRN — leading to a genetic entry point for refined functional manipulation of a defined circuit for locomotor control, which was found to specifically contribute to stopping,

steering and modulation of locomotion(**Bouvier et al., 2015; Cregg et al., 2020; Usseglio et al., 2020**)

- ii) PreBötC CPG neurons in the ventral medullary reticular formation have classically been defined using neuropeptide markers and their receptors – namely the neurokinin type1 receptor (NK1R)(**Gray et al., 2001**) and somatostatin (SST)(**Tan et al., 2008**), but both neuropeptides are expressed throughout the ventral medulla and SST+ neurons are not required to generate the rhythm (**Bouvier et al., 2010; Y. Cui et al., 2016; Nattie & Li, 2002; Schindler et al., 1996**) later showed that the transcription factor *Dbx1*– expressed in ventral (V0v) hindbrain progenitors— defines the rhythmogenic core of the preBötC in the medulla.
- iii) Other groups of neurons can only be defined by combined sets of transcription factors. E.g., the RTN (Retrotrapezoid nucleus) —a central chemoreceptor located immediately ventral to *Phox2b*-expressing branchiomotor neurons of the facial (VII) nucleus — is molecularly defined by the combined expression of *Vglut2*(excluded from motoneuronal cells) and *Phox2b*, or *Atoh1* and *Phox2b* transcription factors(**Guyenet et al., 2012; Ruffault et al., 2015**).

In some cases, neuropeptides and/or calcium-binding proteins can also be useful markers of neural types in the reticular formation. (**Takatoh et al., 2022**) have shown that the expression of the calcium-binding protein Parvalbumin (PV) defines a subpopulation of inhibitory neurons in the whisking oscillator in the intermediate reticular formation (vIRtPV). This molecular identification has enabled targeted ablation of these cells —providing unprecedented insight into the mechanism of rhythm generation for whisking.

Nevertheless, heterogeneity can persist within circuits defined by a single gene, such as a transcription factor. For example, in the *Chx10* population, two populations with distinct anatomical, physiological and connectivity properties (local interneurons and reticulospinal neurons) have been identified(**Chopek et al., 2021; Usseglio et al., 2020**). Similarly, *Dbx1* expression demarcates a large rostrocaudal domain of progenitors in the V0v domain of the hindbrain, and the distribution of functionally distinct *Dbx1*-derived neurons is not spatially discrete (e.g., it defines non-rhythmic local premotor neurons within the preBötC itself but also a subpopulation of glutamatergic premotor neurons to Mo12 in the intermediate reticular

formation (IRt) dorsal to the preBötC(**Revill et al., 2015**). It is likely that the combination of stereotaxic location and two genes (TFs or peptides), which can be used to drive different recombinases (Cre and Flp), would provide in many cases the optimal operational definition of a neuronal population. A logistical limitation of this approach is the difficulty in obtaining, characterizing and managing colonies of genetically modified mice, upstream of the physiological studies.

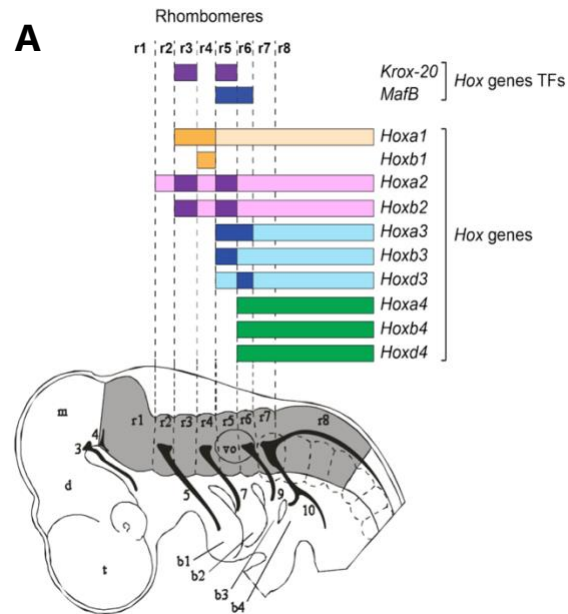
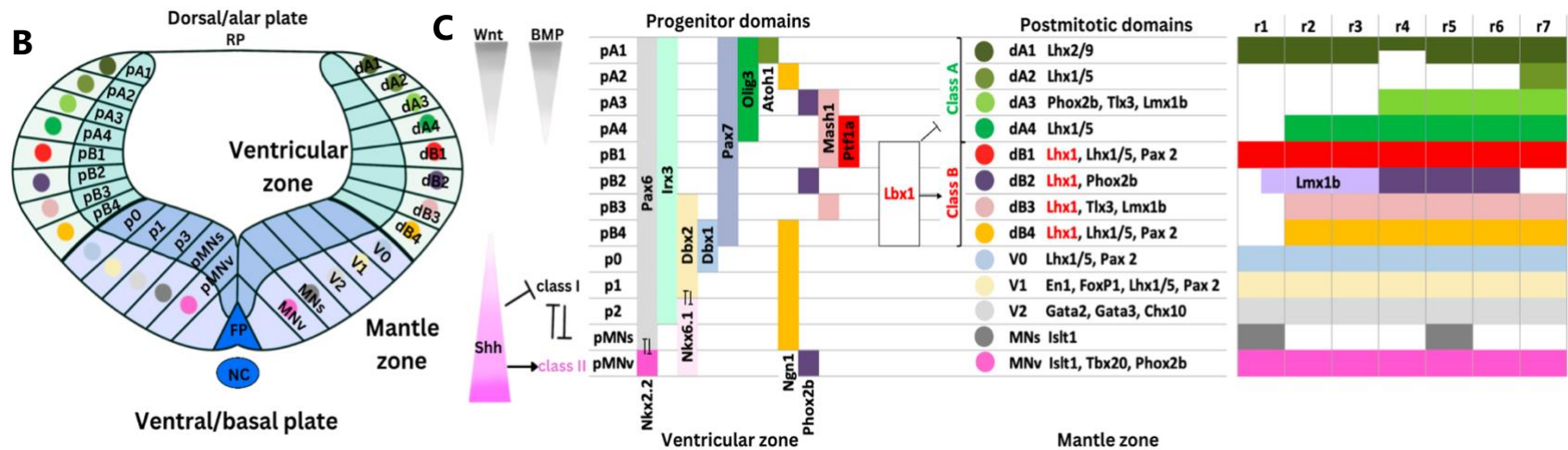


Fig. 16. Neuronal cell fate specification along the rostrocaudal and dorsoventral axes of the hindbrain. (A) Lateral view of an E9 embryo depicting the developmental segmentation of the hindbrain into 8 rhombomeres (grey shading), that align with the boundaries of expression of Hox genes. Dashed lines denote interrhomomeric boundaries. Digits refer to the cranial nerve nuclei. Note that branchiomotor nerves derived from particular rhombomeres project to specific pharyngeal arch derivatives. The bars indicate the different Hox gene expression as well as the transcription factors (TFs) that regulate Hox gene expression, with darker shades signifying higher expression levels. **(B)** Schematics depicting the dorsoventral organization of a rhombomere into 13 domains. Each domain consists of progenitors in the ventricular zone and postmitotic neurons that migrate into the mantle zone. **(C)** Dorsalizing signals from the overlying ectoderm and roof plate (Wnt and BMP) and ventralizing signals (Shh) produced by the notochord and floor plate control the nested expression of basic loop helix (bHLH) and homeodomain (HD) proteins (transcription factors) along the dorsoventral axis. Combinations of transcription factor expression constitute 'lineage-specific' genetic codes which define distinct progenitor (pA1-pMNv) and postmitotic (dA1-MNv) domains, and provide markers to identify specific subsets of neurons in neuronal circuits (**Jessell, 2000**). Note that not all the dorsoventral domains are present throughout the AP axis of the hindbrain. Orthogonal patterning along the AP and DV axes gives rise to distinct rhombomere-specific microcircuits that contribute to the complexity of hindbrain sensorimotor systems (adapted from **(Di Bonito and Studer, 2017)**).



1.7. PREMOTOR NEURONS

The exploration of the reticular formation is intimately linked to the search for premotor neurons, originally by injection of retrograde tracers in motor nuclei, more recently by retrograde monosynaptic tracings from oropharyngeal muscles.

In their seminal study, **Travers et al., (2005)** describe the distribution of bilaterally projecting premotors to the motor trigeminal (Mo5) and hypoglossal nucleus (Mo12) in the brainstem after injecting Fluorogold (FG) into Mo5 and Cholera Toxin into Mo12 in the same animal. Mo5 pre-motor neurons were found to be distributed equally across different rostrocaudal levels of the parvocellular (PCRt) and intermediate (IRt) subdivisions (**Fig.17 I-L**), while bilaterally-projecting and hypoglossal-projecting neurons were enriched in the Intermediate reticular formation (**Fig.17 J,K**).

More recently, **Stanek et al., (2014)** and **Takatoh et al., (2021)** carried out retrograde monosynaptic tracing of genioglossus, masseter and vibrissa muscles in postnatal mice and in adults respectively to survey the specific premotor circuitry for tongue protruding, jaw closing and whisker pad muscles. Consistent with the findings of **Travers et al.,(2005)** premotor neurons for tongue protruders were found enriched in the reticular formation adjacent to the Mo12 itself, particularly in the IRt (**Fig. 17C**). In the pons, labeled prehypoglossal motor neurons were located in regio h around Mo5 (**Fig.17 D**).Concerning jaw closing muscle, labeled premotors were located dorsocaudally in the contralateral IRt and PCRt (**Fig.17 E,F**) as well as in the supratrigeminal nucleus and peritrigeminal zones (**Fig.17 G**).Primary sensory afferent neurons in Mes5 are also premotor to Mo5 (**Fig.17 H**).Vibrissa premotor networks were densely labelled in the vibrissa zone of the IRt (vIRt),located medial to the nucleus ambiguus(NA) as well as in the preBötC (**Fig.17 A**). Premotor sites that also receive vibrissa primary sensory afferents were labelled in the SpVO (**Fig.17 B**).

Importantly, these studies demonstrated that functionally-identified premotors in the reticular formation are highly heterogeneous with respect to neurotransmitter phenotypes. For example, Glutamatergic, GABAergic, cholinergic, and nitrergic neurons are all found in the PCRt and IRt that project to various orofacial muscles (**Stanek et al., 2014; Takatoh et al., 2013; J. B. Travers et al., 2005**) highlighting the need to complement monosynaptic tracing schemes with a genetic strategy to manipulate functionally-identified cell-type specific circuits in these regions. Paradoxically, the former authors then proceed to functionally characterize a heterogeneous population of

premotors (Gabaergic and Glutamatergic) in the Supratrigeminal nucleus dorsal to Mo5 based on projection criteria alone (**Stanek et al., 2016**).

1.7.1. Central rhythm/pattern generators

Another major object of study in the reticular formation are central rhythm/pattern generators. Indeed, a striking property of many movements controlled by the hindbrain is their rhythmicity. This is the case for breathing, whisking, chewing, licking or lapping, swallowing (at least when ingesting liquids), and some types of vocalization (**Wei et al., 2022**).

For many years, it was thought that rhythmic movements were produced by chains of reflexes. The 'reflex chain' hypothesis stipulated that alternating movements were successively triggered by the sensory response to the previous movement (**Fig. 16A: right**). Concerning chewing, for example (i.e. a rhythmic abduction and adduction of the jaw), Sherrington proposed (**Sherrington, 1917**): "*On the mouth's seizing a morsel the mandible, when it has closed, e.g. voluntarily, upon whatever is between the jaws pressing it against the gums and teeth and hard palate, by so doing, as is clear from observation of the reflex, produces a stimulus which tends reflexly to reopen the jaws. That done, the central rebound of the previously reflexively inhibited jaw-closing muscles, or rather of their motoneurons, for the inhibition is central, sets in and tends to powerfully reclose the jaws again. There, closure brings into operation once again the jaw-opening stimulus. And so, after being started by a first bite, a rhythmic masticatory reflex tends to keep itself going so long as there is something biteable between the jaws.*"

However, as early as the 1900s, extensive deafferentation experiments were carried out in fish, amphibians and locusts, showing that rhythmic motor patterns for swimming and locomotion were preserved, strongly propounding the alternate hypothesis that rhythmically alternating movements are generated entirely by the CNS (**Brown & Sherrington, 1911; Wilson, 1961**). For orofacial ingestive movements, this view has prevailed since the pioneering studies of Lund (**Dellow & Lund, 1971**).

Thus, the sufficiency of the hindbrain to ensure rhythmic movements, in the absence of sensory feedback, or indeed of input from higher centers, implies that it harbors rhythmic centers. It remains that many rhythmic behaviors are sensitive to, i.e., *are modulated by* inputs from the periphery or higher brain centers. Moreover, most of them, to the notable exception of breathing, are triggered by, i.e., *are conditional to* such inputs from the periphery or higher centers.

1.7.2. General considerations on the architecture of rhythmic centers in vertebrates

The classical operational definition of a CPG distinguishes a central rhythm generator (CRG) — a network of bursting neurons that acts as a timekeeper — from a pattern generator (CPG proper) — a circuit of premotor interneurons that organize the motor sequences downstream of the CRG input (**Fig. 18C (left: abstract view)**). By far the best characterized mammalian brainstem CP(R)G is the pacemaker for breathing, thought to comprise a core oscillator known as the pre-Bötzinger complex (“preBötC”) and associated pattern generators in the ventral medulla (the “ventral respiratory column”), that relay the inspiratory command to respiratory pump muscles. The next best-studied mammalian CPG — the locomotor CPG — has been proposed to share this underlying organization (**McCrea & Rybak, 2008**).

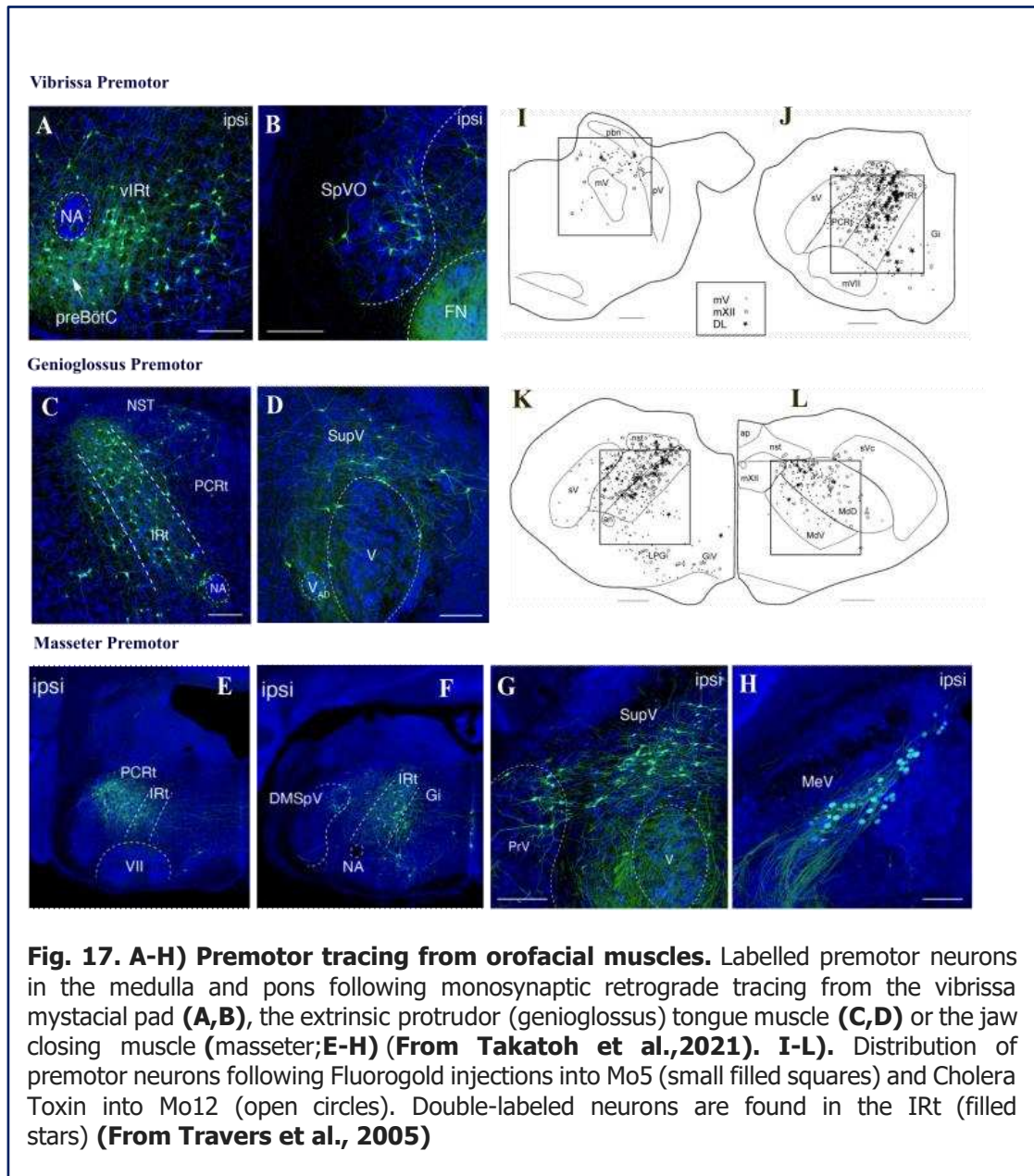
Two mechanisms may account for the production of rhythm in the CRG: it may be driven by ‘burster’ neurons that are intrinsically rhythmic, or display rhythmic behaviors as an emergent property, i.e., as a result of synaptic connections among neurons that are not intrinsically rhythmic (**Fig. 18B, (Marder & Bucher, 2001)**). This alternative is not easily sorted out in vertebrates, where the microcircuitry is often unknown. A case in point is the CRG for whisking which was declared to consist of intrinsically bursting neurons (**Deschênes et al., 2016**), but more recently found by the same lab to depend on recurrent inhibitory inputs (**Takatoh et al., 2022**).

A general assumption about CRGs is that they are located several synapses upstream of motoneurons, by contrast to the downstream CPGs which make monosynaptic contacts with motoneurons (**Grillner et al., 2000**). However, few studies directly support such an architecture and, more generally, segregation of rhythmic and patterning functions in mammalian CP(R)Gs. For example, premotor neurons may be part of the CRG itself: (**Kam et al., 2013**) showed that the preBötC contains both central rhythm and patterning elements for breathing. More recently, (**Takatoh et al., 2022**) demonstrated that the oscillator for whisking consists of a network of premotor interneurons projecting to specific pools of Mo7.

A complexity not readily accounted for by current models — which can explain such irregularities as motor burst omissions, variations in burst amplitude, and modulation by afferent inputs (**McCrea & Rybak, 2008**) — is that CPGs often express *distinct rhythms*: the preBötC can command eupnea, but also generate sighs and gasps under different neuromodulatory

states (**Lieske et al., 2000**). This may either reflect network reconfiguration to produce multiple rhythms, or the existence of several nested CPGs within the preBötC (**Toporikova et al., 2015**), or both. Similarly, it has been suggested that a multifunctional CPRG may be shared between three related orofacial movements, licking, mastication, and swallowing (**Jean, 2001; Travers et al., 1997**). The segregation between CPG and CRG may therefore represent an oversimplified, and potentially problematic, model that overlooks the dynamic reconfiguration and complex neuronal interactions occurring within a functionally versatile microcircuit for rhythm generation (**Fig. 18C(Right):Detailed view**)(**Feldman & Kam, 2015**). A more complex and potentially more realistic view of CPRGs holds that the limits of the burst generators may be constantly expanding and contracting depending on convergent excitatory inputs and sensory feedback in these circuits (**Baertsch et al., 2019; Lund, 1991**).

These conceptual difficulties highlight the dearth of current knowledge concerning the precise structural and functional architecture of mammalian CPRGs (e.g., microcircuit connectivity and cell types) for the elaboration of motor behaviors in general (**Barlow et al., 2010; Feldman & Kam, 2015**). Efforts to pursue reductionist approaches in this field — including genetic manipulation of candidate neuronal populations — are therefore warranted to help dissect and understand the network dynamics of putative CPRGs for oromotor actions.



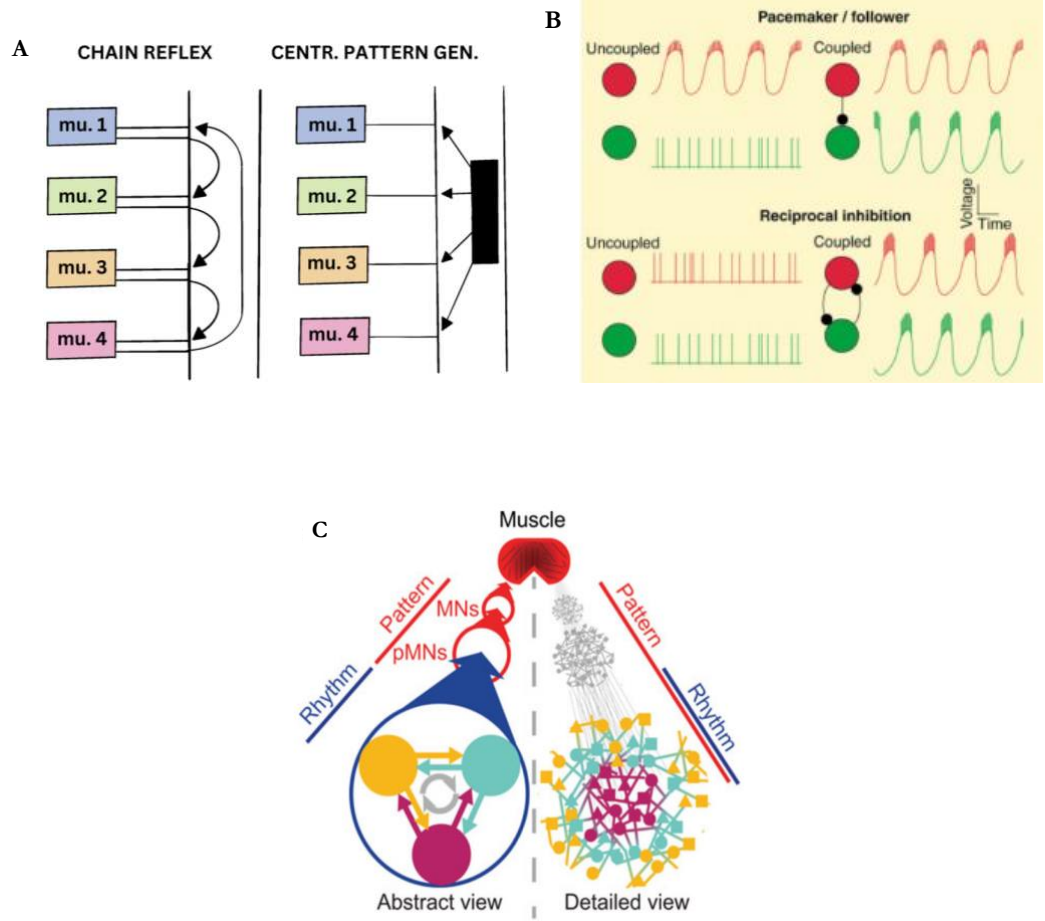


Fig. 18. Architecture of rhythmic centers in vertebrates **A)** Left: Reflex chain hypothesis. The activation of muscle 1 triggers a movement that activates receptors that in turn mobilize muscle 2, and so on and so forth to generate cyclic patterns of movements. Right: Central pattern generator hypothesis. A central pattern generator provides the phasic, patterned drive to different muscles to produce rhythmic movements. mu: muscle. Centr. pattern Gen: central pattern generator. Adapted from **(Grillner, 2011)**. **B)** In pacemaker-driven networks, a pacemaker neuron (red) can synaptically drive an antagonist (green) neuron to fire in alternation. The simplest configuration of a network oscillator comprises two neurons that are not intrinsically rhythmic, but fire in alternating bursts as a result of reciprocal inhibition. Reproduced from **(Marder and Bucher, 2001)**. **C)** Model depicting the classical view of the structure of a CPRG. Left: interactions between a core rhythm generator and independent downstream patterning elements that project to motoneuronal groups shape and relay the rhythm. Right: this model overlooks the underlying microcircuit properties, connectivity, and functional heterogeneity (illustrated by the different shapes), including the potential for the existence of multifunctional circuits (e.g., single rhythm and pattern-generating elements) within the CPRG. Reproduced from **(Feldman and Kam, 2015)**

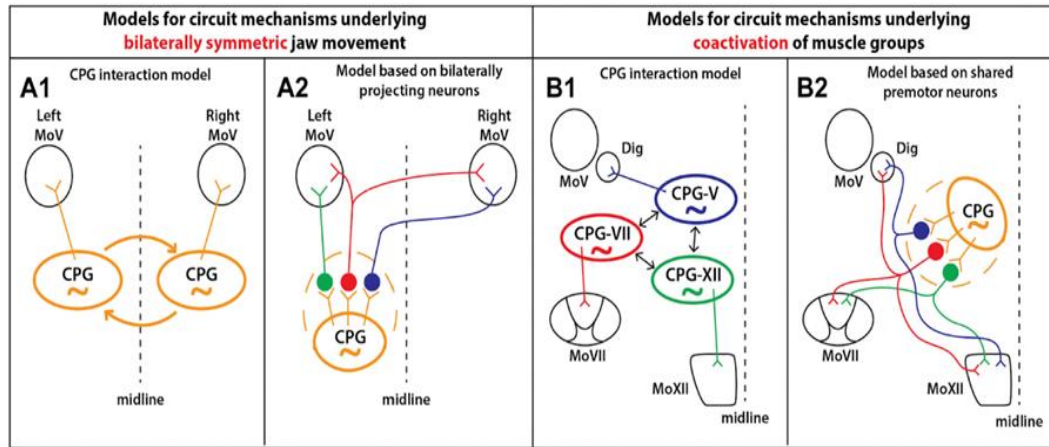


Fig. 19. Models illustrating circuit mechanisms for bilateral coordination (A1 and A2) and cross-muscle coordination (B1 and B2) during chewing. A1) Interactions between functionally equivalent independent left and right CPGs for mastication enable bilateral coordination of the jaw during chewing. **A2)** The CPG rhythm is relayed bilaterally to both trigeminal motor nuclei (MoV) via branching jaw premotoneurons. Jaw premotors can form part of the masticatory CPG (dashed outline) or represent downstream targets. **B1)** According to this model, CPGs for different muscles interact to coordinate inter-muscular activation. **B2)** Inter-muscular co-activation is mediated via shared premotor neurons that branch to supply the same input to different motor groups. Reproduced from (Stanek et al., 2014).

1.8. COORDINATION BETWEEN RHYTHMIC OROFACIAL ACTIONS

It has been proposed that premotoneurons constitute substrates for orofacial coordination between oromotor actions. Both anatomical and electrophysiological studies support this view (**Amri et al., 1990; Dong et al., 2011; Fay and Norgren, 1997; Li et al., 1993; Stanek et al., 2014; Travers et al., 2005**). Pre-ormotor neurons in the medulla have extensive intramedullary collaterals to several oromotor nuclei, effectively acting as recruitable 'modules' by CPGs and descending/sensory inputs to ensure three basic types of coordination: (i) bilateral temporal coordination between muscles on either side of the midline (**Fig.19 A1,A2**), (ii) coordination between the activity of agonist muscle groups (e.g, synchronous jaw closure/tongue retraction and jaw opening/tongue protrusion during chewing and licking) (**Fig.19 B1,B2**), and (iii) anti-phase activation of antagonist muscles (e.g., jaw closure/tongue protrusion). Notably, these branching premotoneurons are enriched in regions of the medullary reticular formation where putative CPGs for many oromotor actions have been described (**Chandler et al.,1986, Amri et al.,1990, Travers et al.,2005, Kogo et al.,2009, Nakamura et al.,2017**). This raises the question of whether premotor neurons that transmit the CPG signals are an integral part of oromotor CPGs or whether they act independently to relay the network rhythm in these systems, which would significantly extend the complexity of functions that can be ascribed to premotor interneurons.

1.9. *Phox2b*, A MASTER REGULATOR OF AUTONOMIC REFLEX CIRCUITS

Phox2b is a paired-like homeodomain protein whose expression is strictly limited to the nervous system — and, within the nervous system, to a handful of classes of neurons. This was verified in all vertebrates where it was examined: most extensively in mice, but also xenopus (**Kaneshige et al., 2018**), human (**Amiel et al., 2003**), zebrafish (**Coppola et al., 2012**) and chicken (JFB, unpublished data). This rule holds true as well in protostome and deuterostome invertebrates (**Dufour et al., 2006b**)(**Nomaksteinsky et al., 2013a**)(**Pujol et al., 2000**).

A striking feature— to this date, rather enigmatic — of *Phox2b* expression is that the vast majority of *Phox2b+* neuron types identified so far match the anatomical and physiological concept proposed by Blessing (**Blessing, 1997a**) of “visceral neurons, afferent and efferent” (to replace the old notion of “autonomic nervous system” that excluded sensory neurons and interneurons), i.e. those neurons that maintain bodily homeostasis through the reflex control of the digestive, cardiovascular and respiratory functions (**Fig. 20**).

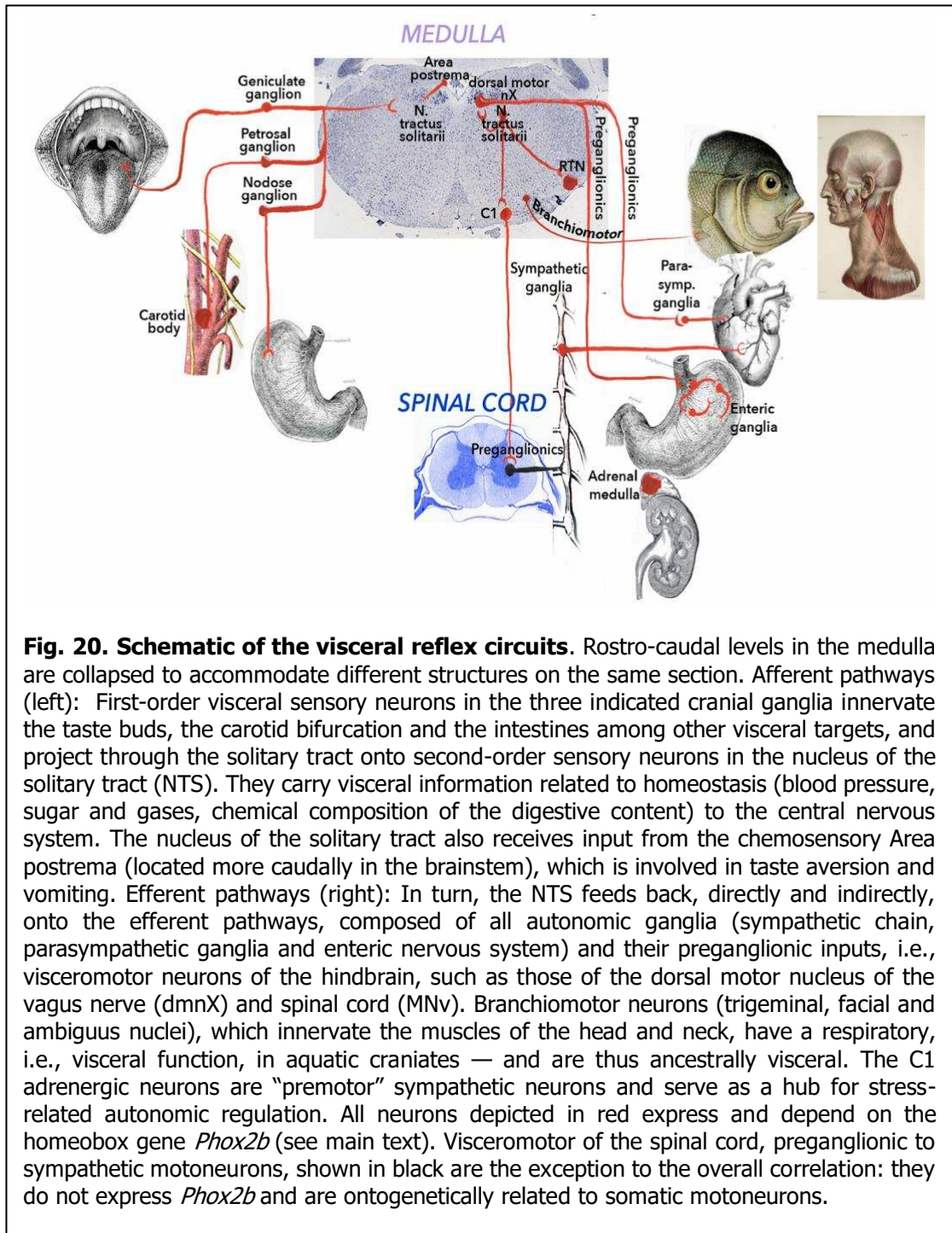
On the afferent path of these visceral reflexes, *Phox2b* is expressed in primary visceral sensory neurons, that form the three distal ganglia of cranial nerves VII, IX and X: the geniculate, petrosal and nodose ganglia, as well as in the carotid body, a chemosensory organ presynaptic to the petrosal ganglion (that senses, for example, blood oxygen). It is also expressed in central targets of these primary sensory neurons, the second-order visceral sensory neurons of the hindbrain (that form the nucleus of the solitary tract (NTS)) and the nearby chemosensory center, the area postrema (AP), responsible for chemically-induced vomiting and conditioned taste aversion. On the efferent path, *Phox2b* is expressed in all autonomic ganglia (sympathetic, parasympathetic and enteric) as well as their presynaptic neurons, the “general visceral motor” (VM) neurons of the hindbrain — to the notable exclusion of preganglionic sympathetic neurons, located in the spinal cord. Sympathetic premotor neurons, or at least the majority of them (the C1 adrenergic center) express *Phox2b* (**Fig. 20**). In all the neural types listed above, *Phox2b* is not only a marker but a determinant. All *Phox2b*-positive neurons that switch it on, either at the dividing progenitor or early post-mitotic precursor stage, depend on it for their differentiation: in *Phox2b* KO embryos, they are either not born, die, or switch fate. Details of these dependencies fall beyond the scope of this introduction.

In addition, *Phox2b* is expressed in the branchiomotor (BM) neurons

that form Mo5, Mo7, MoA (pars compacta) and Mo11 (spinal accessory nucleus) cranial motor nuclei, which innervate the branchial arch-derived muscles that motorize the face and neck. Those motor neurons are neither included in the classical concept of “autonomic nervous system”, nor in the set of visceral motor neurons recognized by Blessing (who incorrectly classifies BM neurons as “somatic”). However, this exclusion is unwarranted from a larger zoological, developmental, and evolutionary perspective, as will be discussed later.





Finally — and central to my PhD work — *Phox2b* is expressed in large populations of pontine and medullary interneurons, whose function was mostly unknown until recently. One exception is the retrotrapezoid nucleus (**Ruffault et al., 2015b**)(**Stornetta et al., 2006**), a locus for CO₂ sensing (**Guyenet & Bayliss, 2015**) in the brainstem, which is yet another node of homeostatic circuits .

My work characterizes three additional populations of *Phox2b*⁺ interneurons in the pons and medulla. They turn out to be presynaptic to orofacial motor neurons (many of which are *Phox2b*⁺, see above) and are likely involved in solid and liquid food intake. These data expand the landscape of *Phox2b*⁺ circuits and provide some of the first links in the reticular formation between neuronal function and genetic identity (beyond neurotransmitter phenotype).



RESULTS 1: A MEDULLARY CENTER FOR LAPPING IN MICE

A medullary centre for lapping in mice

Bowen Dempsey¹, Selvee Sungeelee¹, Phillip Bokinić ², Zoubida Chettouh¹, Séverine Diem ³, Sandra Autran³, Evan R. Harrell⁴, James F. A. Poulet ², Carmen Birchmeier⁵, Harry Carey⁶, Auguste Genovesio¹, Simon McMullan⁶, Christo Goriđis¹, Gilles Fortin^{1,7} & Jean-François Brunet ^{1,7}✉

It has long been known that orofacial movements for feeding can be triggered, coordinated, and often rhythmically organized at the level of the brainstem, without input from higher centers. We uncover two nuclei that can organize the movements for ingesting fluids in mice. These neuronal groups, IRT^{Phox2b} and Peri5^{Atoh1}, are marked by expression of the pan-autonomic homeobox gene *Phox2b* and are located, respectively, in the intermediate reticular formation of the medulla and around the motor nucleus of the trigeminal nerve. They are premotor to all jaw-opening and tongue muscles. Stimulation of either, in awake animals, opens the jaw, while IRT^{Phox2b} alone also protracts the tongue. Moreover, stationary stimulation of IRT^{Phox2b} entrains a rhythmic alternation of tongue protraction and retraction, synchronized with jaw opening and closing, that mimics lapping. Finally, fiber photometric recordings show that IRT^{Phox2b} is active during volitional lapping. Our study identifies one of the subcortical nuclei underpinning a stereotyped feeding behavior.

¹Institut de Biologie de l'ENS (IBENS), Inserm, CNRS, École normale supérieure, PSL Research University, Paris, France. ²Max Delbrück Center for Molecular Medicine in the Helmholtz Association (MDC), and Neuroscience Research Center, Charité-Universitätsmedizin, Berlin, Germany. ³Université Paris-Saclay, CNRS, Institut des Neurosciences NeuroPSI, Gif-sur-Yvette, France. ⁴Institut Pasteur, INSERM, Institut de l'Audition, Paris, France. ⁵Developmental Biology/Signal Transduction, Max Delbrueck Center for Molecular Medicine, and Cluster of Excellence NeuroCure, Neuroscience Research Center, Charité-Universitätsmedizin, Berlin, Germany. ⁶Faculty of Medicine, Health & Human Sciences, Macquarie University, Macquarie Park, NSW, Australia. ⁷These authors contributed equally: Gilles Fortin and Jean-François Brunet. ✉email: jfbrunet@biologie.ens.fr

The hindbrain (medulla and pons) is a sensory and motor center for the head and the autonomic (or visceral) nervous system. Large areas therein defy conventional cytoarchitectonic description and are subsumed under the label “reticular formation”¹. Over decades, the reticular formation has slowly emerged from “localizatory nihilism”², and regions defined by stereotaxy [e.g., ref. 3], or cell groups defined by their projections [e.g., ref. 4] have been implicated in a variety of roles: premotor neurons to orofacial or respiratory muscles^{5, 6}, and—underpinning the sophisticated residual behaviors observed in decerebrate animals⁷—rhythm and pattern generators for chewing, whisking, breathing, and sighing^{3, 5, 8–11}. Licking is another rhythmic behavior for which a hindbrain rhythm generator is predicted¹² although the evidence is mostly extrapolated from chewing, the two behaviors possibly sharing some neuronal substrate⁹.

However, the parsing of the reticular formation into genetically defined neuronal groups, endowed with specific connectivity and roles, has only begun^{13–17} and lags behind other parts of the brain, such as the cortex or the spinal cord. Among the most specific genetic markers of neuronal classes are transcription factors, in particular, homeodomain proteins [e.g., refs. 18, 19]. *Phox2b* is one such gene, which marks (and specifies) a limited set of neurons in the peripheral nervous system and the hindbrain, including the reticular formation. The expression landscape of *Phox2b* is strikingly unified by physiology: most *Phox2b* neurons studied to date, partake in the sensorimotor reflexes of the autonomic nervous system, that control bodily homeostasis²⁰. An apparent exception is branchial motor neurons, that motorize the face and neck^{1, 21} but their kinship to visceral circuits, aptly highlighted by their alternative name of “special visceral”, is revealed by their exclusive ancestral functions in aquatic vertebrates, in feeding and breathing—thus visceral indeed. To this broadened picture of the visceral nervous system, in charge of vital functions and maintenance of the interior milieu, we now add two groups of *Phox2b* interneurons, located in the reticular formation of the hindbrain, that are premotor to orofacial muscles and can command licking or lapping, a rhythmic feeding behavior essential for the intake of liquids in many terrestrial vertebrates.

Results

The reticular formation harbors *Phox2b*⁺ orofacial premotor neurons. We visualized the total projections of *Phox2b* interneurons that are located in the reticular formation. The vast majority of these neurons are glutamatergic, thus express the glutamate vesicular transporter *Vglut2*, as shown by expression of the *Cre* and *Flpo*-dependent reporter *RC::Fela* in a *Phox2b::Flpo;Vglut2::Cre* background (Supplementary Fig. 1a). We used this neurotransmitter phenotype to implement an intersectional strategy that excludes the potentially confounding widespread projections of other *Phox2b*⁺ neurons, in the locus coeruleus²², which are noradrenergic. We designed an intersectional allele (*Rosa^{FRTtomato-loxSypGFP}* or *Rosa^{FTLG}*) (Fig. 1a) which expresses one of two fluorophores, exclusively: the action of flippase (*Flpo*) will trigger cytoplasmic expression of *tdTomato* (*tdT*), while additional action of *Cre* recombinase, will extinguish *tdT* in the cell soma and switch on instead a fusion of synaptophysin with GFP (*Syp-GFP*) transported to presynaptic sites²³. When *Flpo* was driven by the *Phox2b* promoter, and *Cre* by the *Vglut2* promoter, i.e., in *Phox2b::Flpo;vGlut2::Cre;Rosa^{FTLG}* pups, at P4 *tdT* was expressed, as expected, in the soma of the singly recombined motoneurons (which are *Phox2b*⁺, but not glutamatergic), but lost from the doubly recombined interneurons (which are *Phox2b*⁺ and glutamatergic) (Supplementary Fig. 1b). The latter, in turn,

had switched on *Syp-GFP* in their synaptic boutons, which covered remarkably discrete structures of the hindbrain (Supplementary Fig. 1b and Fig. 1b), among which motor nuclei (whose function will be discussed later) featured prominently: (i) most branchiomotor (*Phox2b*⁺) nuclei—the trigeminal motor nucleus (Mo5) and its accessory nucleus (Acc5), the facial nucleus (Mo7) (albeit only its intermediate lobe) and its accessory nucleus (Acc7), the nucleus ambiguus (MoA); (ii) two somatic (*Phox2b*[−]) motor nuclei: the hypoglossal nucleus (Mo12), and a nucleus in the medial ventral horn, at the spinal-medullary junction, which innervates the infrahyoid muscles²⁴ (and Supplementary Fig. 1c), and that we call MoC (to denote its projection through the upper Cervical nerves)²⁴. Other cranial motor nuclei were free of input from *Phox2b*⁺/*vGlut2*⁺ interneurons: those for extrinsic muscles of the eye (oculomotor (Mo3) and trochlear (Mo4)), and for the spinal accessory nucleus (Mo11), which innervates the sternocleidomastoid and trapezius muscles (Supplementary Fig. 1d). The abducens nucleus (Mo6) however, did receive boutons (Supplementary Fig. 1d). Thus, somewhere in the reticular formation, are *Phox2b*⁺ orofacial premotor neurons, which we then sought to locate.

To locate *Phox2b*⁺ orofacial premotor neurons, we used retrograde transsynaptic viral tracing from oromotor muscles. We injected a G-defective rabies virus variant encoding the fluorophore *m-Cherry*²⁵ together with a helper virus encoding G and the fluorophore YFP (*HSV-YFP-G*) in the posterior belly of the digastric muscle (Fig. 1c) (a jaw-abductor), known to be innervated by Acc7^{26, 27}. Predictably, the only seed neurons (i.e., that co-express the rabies virus-encoded mCherry and the helper virus-encoded YFP) were found in Acc7 (right panel in Fig. 1c). Premotor neurons, presynaptic to the seed motoneurons (i.e., that express only the rabies virus-encoded mCherry) and which, in addition, were *Phox2b*⁺, were found at two sites only: (i) the intermediate reticular formation (IRt) (Fig. 1d) and (ii) “regio h”, arranged in “shell form” around Mo5²⁸, more commonly called the peritrigeminal region (Peri5)²⁹ (Fig. 1e). We found the same pattern of *Phox2b*⁺ premotor neurons for the geniohyoid muscle (a hyoid protractor and jaw-abductor) (Supplementary Fig. 2a), innervated by the accessory compartment of Mo12 (Acc12)²⁴; and we found a subset of this pattern for the genioglossus (a tongue protractor and/or jaw-abductor) (Supplementary Fig. 2b) and for the intrinsic muscles of the tongue (Supplementary Fig. 2c) (both innervated by Mo12), whereby *Phox2b*⁺ premotor neurons were restricted to the IRt. On the other hand, the masseter (the main jaw-closing muscle) and the thyroarytenoid (that motorizes the vocal cords) had totally distinct premotor landscapes (Supplementary Fig. 2d, e)^{30, 31}.

We next sought to characterize genetically and developmentally the *Phox2b*⁺ orofacial premotor neurons located in Peri5 and IRt.

Transcriptional signature and developmental origin of Peri5^{Atoh1} and IRt^{Phox2b}. The *Phox2b*⁺ premotor nucleus that occupies Peri5, we shall call Peri5^{Phox2b} (Fig. 2a, b). Because it surrounds, shell-like, a nucleus with a history of *Phox2b* expression (Mo5 + Acc5) it cannot be selectively accessed with *Phox2b*-based tools, even refined by stereotaxy. We thus restricted our study to a distinct subnucleus of Peri5^{Phox2b}, which unlike the rest of the nucleus co-expresses *Phox2b* with another transcription factor, *Atoh1*³² and that we shall call Peri5^{Atoh1} (Fig. 2b–d). Peri5^{Atoh1} is made of 2052 ± 184 cells (*n* = 4) at late gestation (E18.5), is premotor to the posterior digastric (Supplementary Fig. 2f), and can be selectively targeted in an intersectional *Phox2b::Flpo;Atoh1::Cre* background^{16, 33} (Fig. 2e). Peri5^{Atoh1} cells express *Lbx1* (Fig. 2f), thus originate from the dB progenitor domain³⁴. More precisely

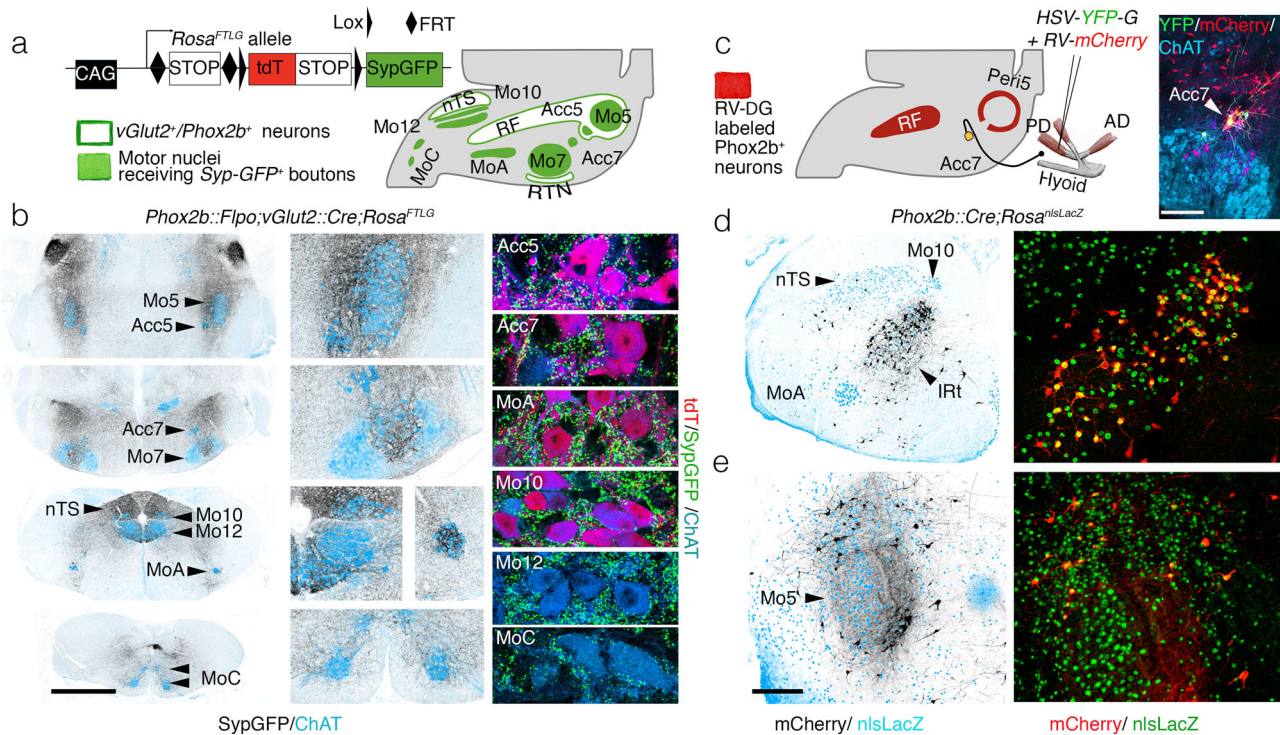


Fig. 1 Premotor status of reticular formation *Phox2b*⁺ interneurons. **a** *Rosa*^{FLG} allele used for intersectoral transgenic labeling of boutons from *vGlut2*⁺/*Phox2b* interneurons (left) and schematic of the results (right). **b** Coronal sections through the hindbrain of a *Phox2b::Flpo; vGlut2::Cre; Rosa*^{FLG} mouse at P4, showing synaptic boutons (black) from *vGlut2*⁺/*Phox2b* interneurons in relation to motor nuclei (ChAT⁺, blue) at low (left), and higher (middle) magnifications, and close-ups of boutons (green) on motoneurons (right), which are either *Phox2b*⁺ (purple) or *Phox2b*⁻ (blue). **c** (left) Strategy for monosynaptically restricted transsynaptic labeling of premotor neurons from the posterior digastric muscle (PD) in a *Phox2b::Cre; Rosa*^{nlslacZ} mouse, with G-deleted rabies virus (RV) encoding mCherry and complemented by a G-encoding helper HSV virus (*HSV-YFP-G*), and summary of the results. (right panel) The only seed neurons are Acc7 motoneurons, double-labeled by the *HSV-G* and *RV-mCherry* viruses. **d, e** Coronal sections through the hindbrain at P8 showing labeled premotor neurons (black on the left panels) in the IRT (**d**) and Peri5 (**e**), which for the most part (72.7% ± 3.5 SEM, *n* = 4 animals) express *Phox2b* (right panels). AD anterior digastric, IRT intermediate reticular formation, nTS nucleus of the solitary tract, PD posterior digastric, Peri5 peritrigeminal area, RF reticular formation, RTN retrotrapezoid nucleus. Scale bars, **b** 1 mm for the left column, **c** 250 μm, **d, e** 500 μm.

they belong to its dB2 derivatives, at the leading edge of whose migration stream they become detectable at E11.5, near the incipient Mo5 (Fig. 2g).

The *Phox2b*⁺ premotor nucleus that occupies IRT, we shall call IRT^{*Phox2b*} (Fig. 2a). It shares with the nearby nTS the *Phox2b*⁺/*Tlx3*⁺/*Lmx1b*⁺ signature and an origin in *Olig3*⁺ progenitors (i.e., the pA3 progenitor domain³⁵) (Fig. 2a, h). It is distinguished, however, by the expression of the transcriptional cofactor *Cited1* (Fig. 2i). IRT^{*Phox2b*} segregates topographically from nTS at E13.5 (Fig. 2i) from which it can thus be told apart by stereotaxy. The border between the two nuclei is marked by the intramedullary root of Mo10 (Fig. 2j). Unlike nTS, IRT^{*Phox2b*} does not receive any input from the tractus solitarius (Fig. 2k). Also unlike the nTS, IRT^{*Phox2b*} neurons are intermingled with glutamatergic neurons of other types (*Phox2b*-negative) (Supplementary Fig. 3). Thus, IRT^{*Phox2b*} and nTS are two structures related by lineage, which acquire distinct molecular, topological, and hodological identities.

Peri5^{*Atoh1*} and IRT^{*Phox2b*} target jaw opening and tongue muscles.

We confirmed the premotor status of Peri5^{*Atoh1*} and IRT^{*Phox2b*} in adult animals by anterograde tracing with viral and transgenic tools (Fig. 3). For Peri5^{*Atoh1*}, we used the *Rosa*^{FLG} allele recombined by *Phox2b::Flpo*³³ and *Atoh1::Cre*¹⁶ (Fig. 3a). The GFP⁺ boutons covered Acc5, intermediate Mo7, Acc7, Mo10, Mo12, and MoC (Fig. 3a–f). In Mo12, the rostro-ventral compartment was excluded (Fig. 3d, e). Because the retrotrapezoid nucleus (RTN) is also *Atoh1*⁺/*Phox2b*⁺¹⁶, thus could

confound this pattern, we confirmed the projections of Peri5^{*Atoh1*} by anterograde tracing with a *Cre*-dependent adeno-associated virus (AAV) expressing *mGFP* and *Syp-mRuby*³⁶ injected in Mo5 of a mouse harboring both, *Phox2b-Flpo* and an *Atoh1-Cre* that is dependent on *Flpo* (*Atoh1::FRTCre*)¹⁶ (Supplementary Fig. 4a, b). Using the same vector, this time stereotactically injected in IRT^{*Phox2b*} of a *Phox2b::Cre* mouse, we found the projections from IRT^{*Phox2b*} in the same motor nuclei as those from Peri5^{*Atoh1*} (Fig. 3g–l)— with the sole difference that in Mo12, the ventral compartment was targeted, rather than the dorsal one (compare Fig. 3j, k with Fig. 3d, e).

To map putative collaterals of *Phox2b*⁺ premotor neurons, we performed a retrograde transsynaptic tracing experiment from the posterior digastric in a genetic background that, in addition, labels the boutons of all *Phox2b*⁺ neurons with GFP (*Phox2b::Cre; Rosa::Syp-GFP*) (Fig. 3m). Double-labeled terminals (*m-Cherry*⁺; *Syp-GFP*⁺)—thus, sent by neurons that are both, *Phox2b*⁺ and premotor to the posterior digastric—were found, in addition to Acc7 (the motor nucleus of the injected muscle), in Acc5, intermediate Mo7, Mo12, and MoC (Fig. 3n–q). Thus, *Phox2b*⁺ orofacial premotor neurons to Acc7 are collateralized in a way that hardwires Acc5, intermediate Mo7, Acc7, Mo12, and MoC to activate their target muscles together.

The combined action of head motor nuclei innervated by Peri5^{*Atoh1*} and IRT^{*Phox2b*} should mobilize the jaw, lower lip and tongue: Acc5 and Acc7 innervate the four suprahyoid muscles^{37–39}, which depress the jaw via the hyoid apparatus. Intermediate Mo7 innervates the *platysma*³⁹, probably a jaw

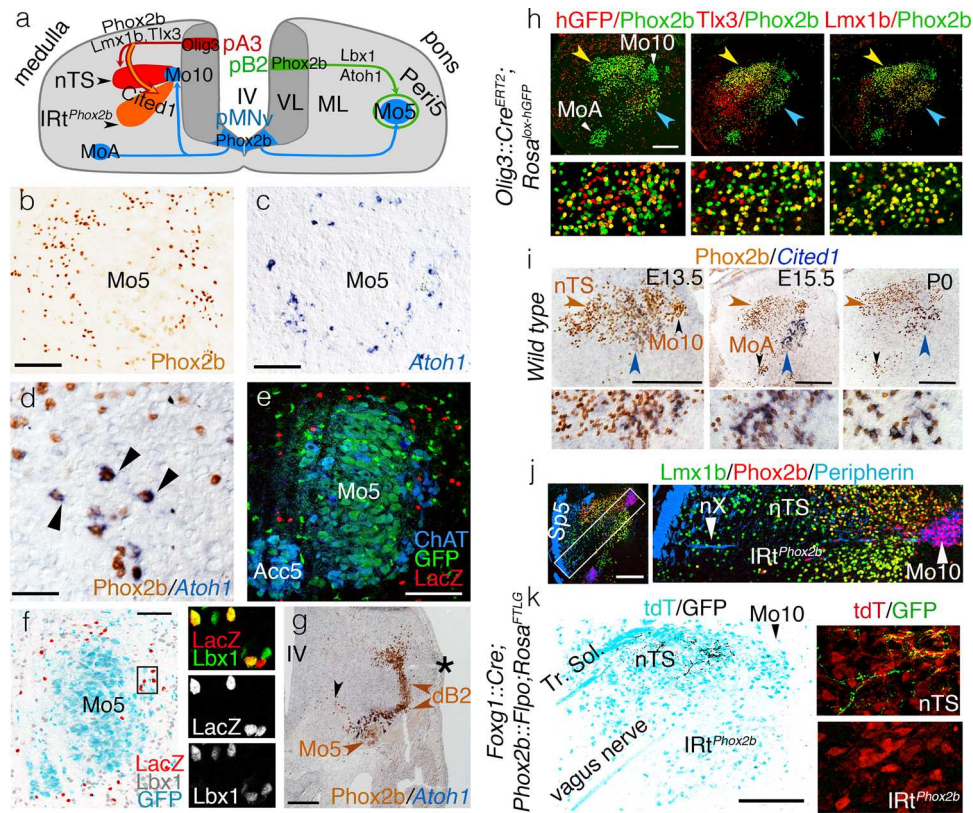


Fig. 2 Ontogenetic definition of IRt^{Phox2b} and $Peri5^{Atoh1}$. **a** Two schematic hemisections of the embryonic medulla (left) or pons (right), showing the origin of branchiomotor nuclei (Mo5, MoA, and Mo10), $Peri5^{Phox2b}$ and IRt^{Phox2b} in progenitor (p) domains of the ventricular layer (VL), their settling sites in the mantle layer (ML), and their transcriptional codes. **b–d** Coronal sections through the pons at E18.5, showing $Peri5^{Phox2b}$ (**b**) or $Peri5^{Atoh1}$ (**c, d**) labeled with the indicated antibody or probe. $Peri5^{Atoh1}$ cells co-express *Phox2b* and *Atoh1* (arrowheads in **d**). **e** Coronal sections through Mo5 in a *Phox2b::Flpo;Atoh1::Cre;Fela* mouse at P0, showing the doubly recombined (nlsLacZ⁺) cells of $Peri5^{Atoh1}$ (red). **f** Coronal section through Mo5 in a *Phox2b::Flpo;Atoh1::Cre;Fela* mouse, where *Phox2b*⁺ motoneurons are GFP⁺ (cyan) and *Phox2b*⁺/*Atoh1*⁺ neurons are nlsLacZ⁺ (red), counterstained for *Lbx1* (gray at low magnification, green in the close-ups). **g** Coronal section through the pons at E11.5 showing the migrating *Phox2b*⁺ Mo5 and dB2 precursors (black and brown arrowheads, respectively) and, at their meeting point, $Peri5^{Atoh1}$ cells that have switched on *Atoh1*. Asterisk: lateral recess of the IVth ventricle (IV). **h** Coronal sections through nTS (yellow arrowhead) and IRt^{Phox2b} (blue arrowhead) at E18.5, at low magnification (upper) or at high magnification for the IRt (lower), stained with the indicated antibodies. A history of *Olig3* expression is revealed by recombination of the histone-GFP (*hGFP*) reporter in the *Olig3::Cre^{ERT2}* background (left). Mosaicism is likely due to incomplete induction of Cre. Virtually all cells of IRt^{Phox2b} (98% ± 0.2 SEM, *n* = 3 animals) co-expressed *Lmx1b* with *Phox2b*. **i** Coronal sections through nTS (brown arrowhead) and IRt^{Phox2b} (blue arrowhead) at indicated stages at low magnification (upper) and high magnification for the IRt (lower), immunostained for *Phox2b* and in situ hybridized for *Cited1*. **j** Coronal section at E15.5 showing that nTS and IRt^{Phox2b} are separated by the medullary root of the vagus nerve (nX). Sp5 spinal trigeminal tract. **k** Coronal section through the nTS and IRt^{Phox2b} of an adult, showing the central boutons of epibranchial ganglia (that express *Foxg1*^{T2} and are labeled by *SypGFP* in a *Foxg1^{ires}Cre;Phox2b::Flpo;Rosa^{FTLG}* background) in the nTS, but not IRt^{Phox2b} (left). Magnified details (right). Scale bars, **b, c** 125 μm, **d, e** 50 μm, **f** 100 μm, **g, h, j, k** 200 μm, and **i**, 250 μm.

depressor⁴⁰, and a *mentalis*³⁹, which, together with the *platysma*, pulls down the lower lip. Ventral Mo12, targeted by IRt^{Phox2b} , innervates tongue protractors⁴¹, while dorsal Mo12, targeted by $Peri5^{Atoh1}$, innervates tongue retractors⁴². Finally, MoC innervates the infrahyoid muscles, classically viewed as stabilizers of the hyoid during jaw lowering, but which probably collaborate with the suprahyoids in a more complex fashion⁴³. Thus, $Peri5^{Atoh1}$ and IRt^{Phox2b} appear connected so as to, collectively, lower the jaw, while retracting or protracting the tongue, respectively.

In addition, anterograde tracing from IRt^{Phox2b} in a *Phox2b::Cre* background and from $Peri5^{Atoh1}$ in a *Phox2b::Flpo;Atoh1::Cre* background revealed, respectively, massive projections of IRt^{Phox2b} to the peri5 region (Fig. 3h) and of $Peri5^{Atoh1}$ to the IRt region. (Supplementary Fig. 4c). We could not assess the precise cellular targets of IRt^{Phox2b} , but those of $Peri5^{Atoh1}$ included IRt^{Phox2b} (Supplementary Fig. 4d, inset), suggesting reciprocal connections of the two nuclei.

$Peri5^{Atoh1}$ and IRt^{Phox2b} can trigger tongue and jaw movements. We optogenetically stimulated IRt^{Phox2b} or $Peri5^{Atoh1}$ in head-fixed awake animals. To do so, we injected a Cre-dependent AAV that directs expression of the soma-targeted excitatory opsin stCoChR, either in IRt^{Phox2b} of *Phox2b::Cre* mice (Fig. 4a) or in $Peri5^{Atoh1}$ of *Phox2b::Flpo;Atoh1^{FTRCre}* mice (Fig. 4b). Single light pulses (100 ms) on IRt^{Phox2b} evoked a wide opening of the mouth accompanied by tongue protraction, which terminated upon cessation of the pulse (Fig. 4a), while the same stimulus applied to $Peri5^{Atoh1}$ triggered only mouth opening, of smaller amplitude (Fig. 4b). Thus, both nuclei can open the mouth, in agreement with their projections on the motoneurons for the suprahyoid and infrahyoid muscles (Fig. 1b and Supplementary Figs. 2a, 3), while IRt^{Phox2b} but not $Peri5^{Atoh1}$ can protract the tongue, in line with the targeting of hypoglossal motoneurons for tongue protractors by the former and tongue retractors by the latter (Fig. 3d, e, j, k). Delivering the stimulus at 4, 5, or 7 Hz led to a faithful repetition of the movement (Supplementary Fig. 5a)

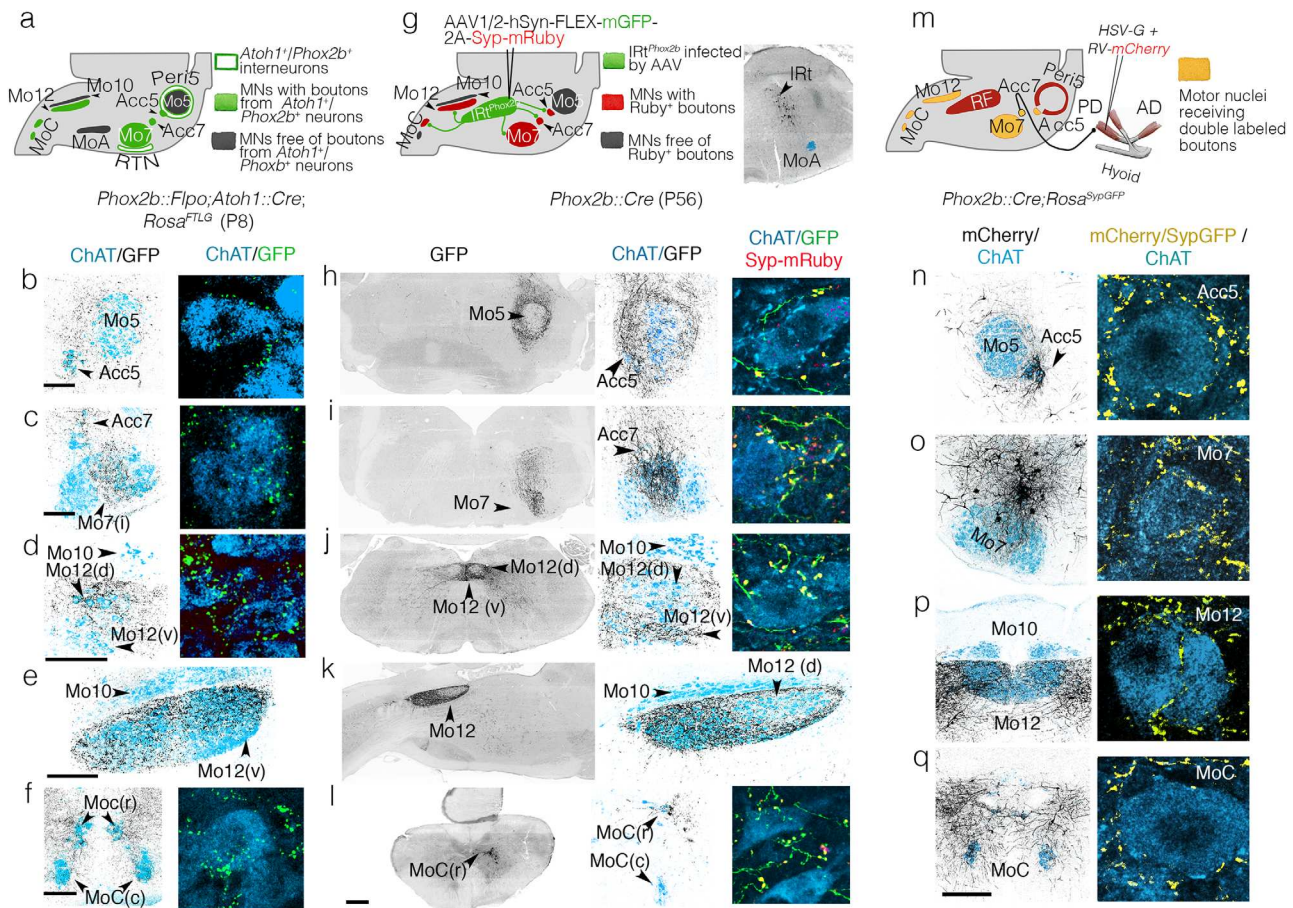


Fig. 3 Projections of IRT^{Phox2b} and $Peri5^{Atoh1}$ on hindbrain motoneurons. **a** Strategy for the transgenic labeling of projections from $Peri5^{Atoh1}$ (and RTN) and summary of the results; **b-f** Coronal (**b-d, f**) or parasagittal (**e**) sections through a P8 hindbrain showing GFP -labeled boutons (black) on motoneurons (blue) at medium (left) and high (right) magnification. **g** Strategy for the viral tracing of projections from IRT^{Phox2b} and summary of the results (left), and $mGFP$ -labeled infected cells of IRT^{Phox2b} (right); **h-l** Coronal (**h-j, l**) or parasagittal (**k**) sections through a P56 hindbrain showing the GFP -labeled fibers (black) of IRT^{Phox2b} neurons at low (left) and medium (middle) magnifications, and in extreme close-ups (right), together with Syp - $mRuby$ labeled boutons (yellow) on motoneurons (blue). **m** schematic for retrograde tracing of premotor neurons for the right posterior digastric muscle, in a $Phox2b::Cre;Rosa^{SypGFP}$, and summary of the results. **n-q** (left) Coronal sections through the hindbrain at P8 showing the $mCherry^+$ projections (black) of premotor neurons on the motor nuclei ($ChAT^+$, blue); (right) close-ups on motoneurons receiving double-labeled Syp - $GFP/mCherry$ boutons (yellow). Scale bars, **b-f** 200 μm for the left column, **h-l** 500 μm for the left column, **n-q** 200 μm for the left column.

showing that IRT^{Phox2b} can operate in this frequency range. As expected from the premotor status of IRT^{Phox2b} , lengthening the light pulse on IRT^{Phox2b} to 200 ms analogically prolonged the mouth opening and tongue protraction (Fig. 4c). Unexpectedly, however, further lengthening led to the termination of the initial movement and its rhythmic repetition at around 7 Hz (Fig. 4c, Supplementary Fig. 5b, and Supplementary Movie 1), a frequency similar to that of naturally occurring licking (Supplementary Fig. 5c)⁴⁴. Conversely, prolonged illumination of $Peri5^{Atoh1}$ only prolonged the initial mouth opening (Fig. 4d, Supplementary Fig. 5d, and Supplementary Movie 2). Thus, a contrast between the actions of photo-stimulated $Peri5^{Atoh1}$ and IRT^{Phox2b} lies in the ability of the latter to translate stationary excitation into a rhythmic series of oromotor movements, akin to naturally occurring licking⁴⁴.

IRT^{Phox2b} is active during volitional licking. We then tested whether IRT^{Phox2b} is active during spontaneous fluid ingestion. We recorded the bulk fluorescence⁴⁵ of IRT^{Phox2b} in head-fixed $Phox2b::Cre$ mice, injected in IRT^{Phox2b} with a Cre -dependent AAV encoding the calcium indicator $jGCaMP7s$ ⁴⁶ and implanted

with an optical cannula (Fig. 4e). During freely initiated bouts of licking from a water-spout, we observed a systematic increase in fluorescence of IRT^{Phox2b} immediately upon deflection of the jaw that preceded individual licks or bouts of lapping (Fig. 4f, g, Supplementary Fig. 5e, and Supplementary Movie 3). Thus, IRT^{Phox2b} neurons, capable of triggering a licking behavior with physiological frequency, are active during such spontaneous behavior. Importantly, IRT^{Phox2b} encompasses the location of many neurons previously identified as rhythmically active during licking⁹. Stationary optogenetic stimulation of this nucleus might emulate the effect of sustained drive from the licking area of the oromotor cortex⁴⁷⁻⁵⁰.

Inputs to IRT^{Phox2b} . Although decerebrated mammals can display reflexive licking^{7, 51}, volitional or self-initiated licking requires higher brain centers. To explore the substratum for this requirement, we traced the inputs to IRT^{Phox2b} by co-injecting it with a pseudotyped G-defective rabies virus variant encoding $mCherry$ and a helper virus that depends on Cre , in a $Phox2b::Cre$ background (Fig. 5a). The vast majority of inputs (about 90%) were in the brainstem (Fig. 5b), which could explain

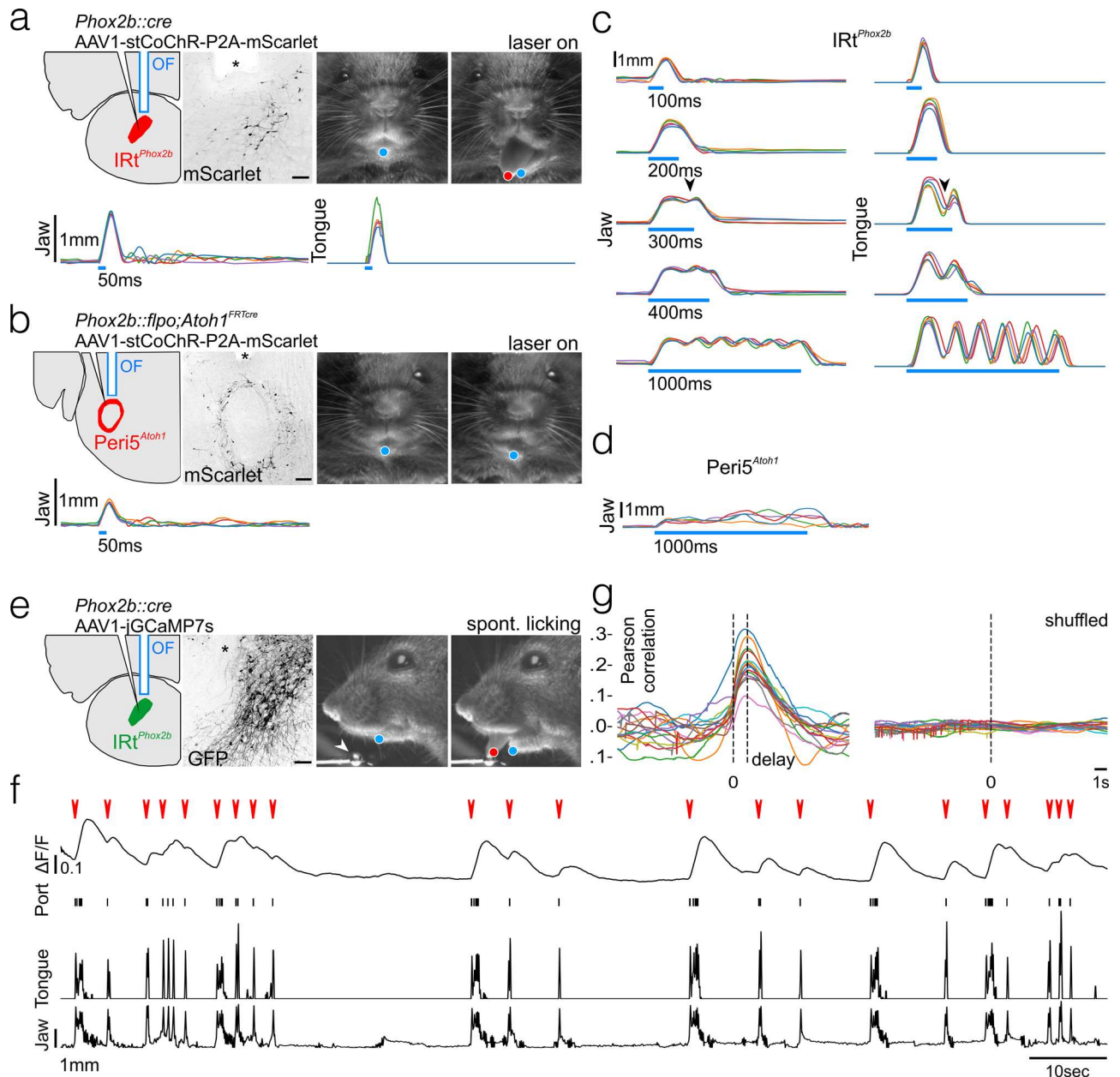


Fig. 4 Orofacial movements triggered by IRT^{Phox2b} and Peri5^{Atoh1} and activity of IRT^{Phox2b} during voluntary licking. **a** (Upper left) Schematic of the viral injection and fiber-optic implantation for stimulation of IRT^{Phox2b}, and transverse section through the hindbrain showing transduced IRT^{Phox2b} neurons and position of optical fiber (OF, asterisk); scale bar 100 μm. (Upper right) Example frames of the mouse face before and during stimulation including DeepLabCut tracked position of the jaw (blue) and tongue (red). (Lower) Individual traces of tracked jaw and tongue position on the Y-axis upon 50 ms stimulation (five trials). **b** (Upper left) Schematic of the viral injection and fiber-optic implantation for stimulation of Peri5^{Atoh1} and transverse section through the hindbrain showing transduced Peri5^{Atoh1} neurons and position of optical fiber (asterisk); scale bar 200 μm. (Upper right) Example frames of the mouse face before and during stimulation including DeepLabCut tracked position of jaw (blue). (Lower) Individual traces (five trials) of tracked jaw position on the Y-axis upon 50 ms stimulation. **c** Individual traces (five trials) of the tracked jaw (left) and tongue (right) position on the Y-axis upon stimulation of IRT^{Phox2b} of increasing length. A repetitive movement is triggered by stimulation beyond 300 ms (arrowhead). **d** Individual traces (five trials) of tracked jaw position on the Y-axis upon a 1000 ms stimulation of Peri5^{Atoh1}. The jaw remains open and quivers non-rhythmically during the stimulus. **e** (Left) Schematic of viral injection and optical fiber implantation for observation of IRT^{Phox2b} activity, and transverse section through the hindbrain showing transduced IRT^{Phox2b} neurons and position of optical fiber (asterisk); scale bar 100 μm. (Right) Example frames of the mouse face before and during a bout of licking from a lick port (arrowhead), during a photometry recording, including DeepLabCut tracked position of the jaw (blue) and tongue (red). **f** Example trace of change in bulk fluorescence of IRT^{Phox2b} during a recording session (~2 min) of unitary licking events and licking bouts (red arrowheads), contact events with the lick port, and movements of the tongue and the jaw on the Y-axis. **g** (left) Superimposed correlation curves between licking activity and calcium activity (each curve corresponding to one of 15 recording sessions, each 1–5 min, in one mouse) which peaked at 1.2 s after lick port contact; (right) no peak was observed after shuffling the data.

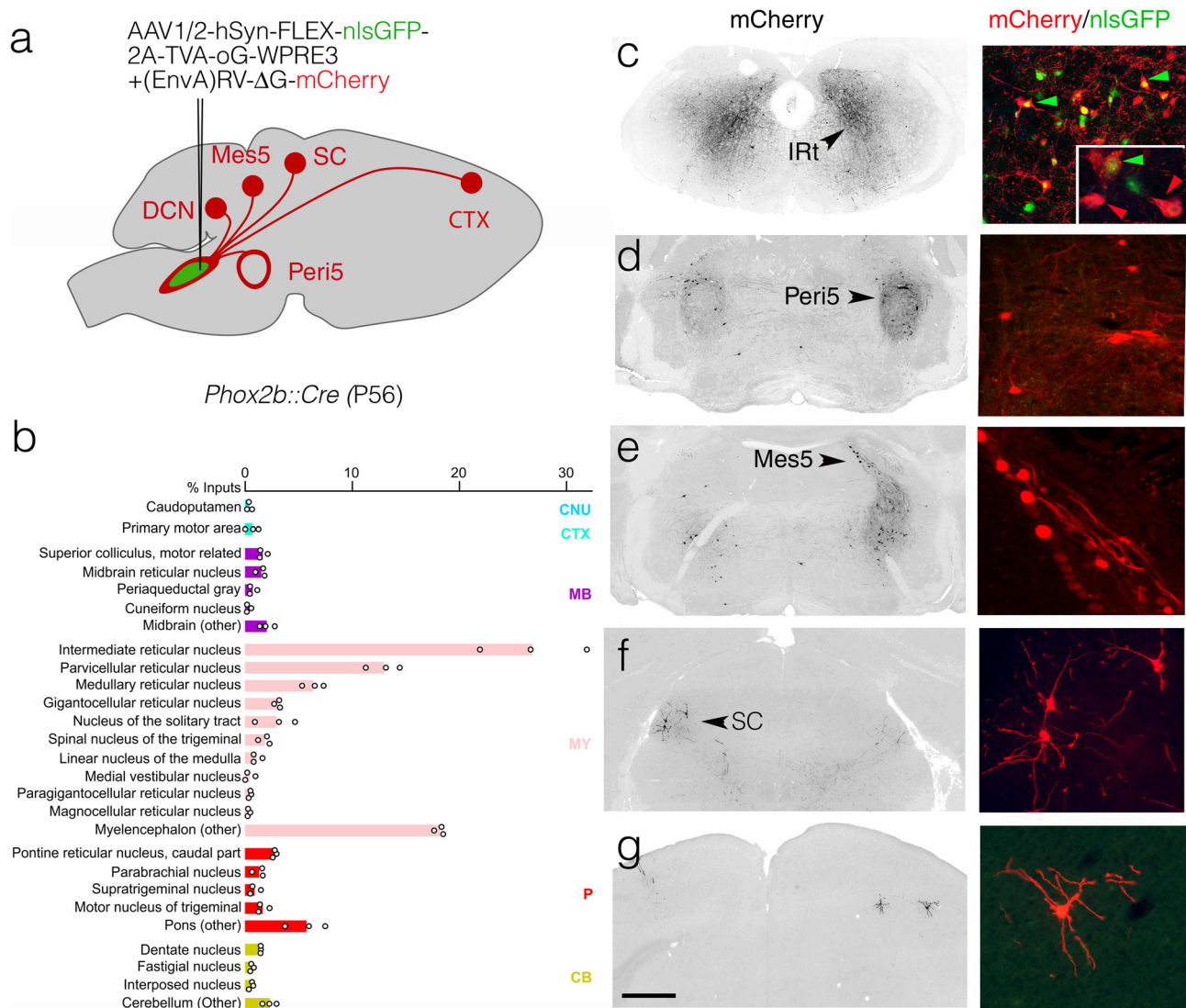


Fig. 5 Inputs to IRT^{Phox2b}. **a** Strategy for the retrograde transsynaptic labeling of input neurons to IRT^{Phox2b} with exemplar sites of input. **b** Bar graph of the relative percentage of monosynaptic input neurons labeled from IRT^{Phox2b} starter neurons, displayed per brain region as defined in the Allen Brain Atlas ($n = 4063$ input cells and $n = 598$ starter cells, from $n = 3$ animals; individual values as circles; seeding efficiency = 7.4 inputs/starters ± 1.8 SEM). Rabies labeled input neurons were largely ($74.5 \pm 1.1\%$ SEM) restricted to the medulla (pink, MY) and exhibited a slight but consistent ipsilateral bias ($55.6 \pm 3.0\%$ SEM). Major sources of these medullary inputs were the intermediate, gigantocellular, and parvocellular reticular nuclei. Inputs from the cortex, midbrain, and pons represented a minority of rabies-labeled neurons ($1.6 \pm 0.3\%$ SEM, $6.4 \pm 0.5\%$ SEM, and $12.3 \pm 1.1\%$ SEM respectively). **c-g** Images at low magnification (left) and high magnification (right) of monosynaptic input neurons in the IRT, Peri5, mesencephalic nucleus of the trigeminal nerve, contralateral superior colliculus, and motor cortex. Green arrowheads: seed neurons; red arrowheads: ($n-1$) IRT neurons. CB cerebellum, CNU caudoputamen, CTX cortex, DCN deep cerebellar nucleus, MB midbrain, Mes5 mesencephalic nucleus of the trigeminal nerve, MY myelencephalon, P pons, SC superior colliculus. Scale bar **c-g** 1 mm.

the largely intact reflexive behavior of decerebrated animals. Among these regional inputs, many were found in IRT itself, including contralaterally (Fig. 5c)—suggesting local interconnectivity of IRT neurons, possibly related to rhythmogenesis, through recurrent synaptic connections, as hypothesized for other rhythm generating structures⁵². Other regional inputs came from the peri5 region (Fig. 5d)—likely including Peri5^{Atoh1} that we had traced anterogradely to IRT^{Phox2b} (Supplementary Fig. 4d)—the mesencephalic nucleus of the trigeminal nerve (Mes5) (Fig. 5e)—which harbors proprioceptors for the teeth and masseter, potentially allowing for a cross talk between jaw position and tongue movement⁵³, and the superior colliculi (Fig. 5f)—whose inhibition disrupts self-initiated licking⁵⁴. Finally, we found input from the cortex (Fig. 5g), where a subclass of pyramidal tract

neurons are known to directly target orofacial promotor neurons⁴⁹.

Discussion

Our study uncovers two genetically coded neuronal groups in the reticular formation, involved in orofacial movements. They are premotor to orofacial muscles and collateralized, thus in a position to coordinate the contraction of a precise set of muscles to the exclusion of others, a property previously highlighted in studies of orofacial premotor neurons (refs. 5, 6 and references therein). As such, they represent an essential hierarchical level in the orchestration of complex oropharyngeal behaviors. In addition, one of them, IRT^{Phox2b}, translates a tonic stimulation into a

rhythmic behavior. The most parsimonious interpretation of IRT^{Phox2b} is that its neurons are bifunctional: premotor through their collateralized inputs on motor nuclei, and rhythm generators, corresponding to the hypothetical licking CPG¹² or at least an element thereof, in the precise region where many lick-rhythmic neurons were previously recorded (refs. 8, 9 for reviews). It is of note that another nearby *Phox2b*⁺ nucleus, the RTN, has intrinsic rhythmic properties, in that case related to breathing, in the neonate^{15, 55}. At this stage, though, we cannot exclude that IRT^{Phox2b} contains two subtypes of neurons, one premotor and the other pre-premotor, and that it is the latter which, upon photo-stimulation, triggers rhythmic repetition; in other words, that IRT^{Phox2b} encompasses a two (or more)-level architecture, akin to models proposed for other motor behaviors^{56–59}. This possibility is made less likely by the apparent genetic homogeneity of IRT^{Phox2b}, whose neurons all co-express the transcriptional signature *Phox2b/Cited1*. Finally, the possibility that the rhythm would be generated by neurons elsewhere in the brainstem (recruited by IRT^{Phox2b} and feeding back on it) is constrained by the limited output of IRT^{Phox2b}: to motor nuclei and the *peri5* region.

In addition to rhythmic tongue protrusion and jaw opening, the entrainment of a full licking cycle requires the delayed activation of antagonistic muscles (as in several “burst generator” models of the locomotor CPG, e.g. ref. 58). One substrate for such rhythmic alternation might comprise the reciprocal projections of IRT^{Phox2b} and Peri5^{Atoh1} (Fig. 3h and Fig. S3C, D), the former targeting tongue protractors and the latter tongue retractors.

From a developmental and evolutionary perspective, it is striking that IRT^{Phox2b} and Peri5^{Atoh1} express the pan-autonomic transcriptional determinant *Phox2b*, as do several of their motoneuronal targets. Thus, the evolutionarily conserved⁶⁰ selectivity of *Phox2b* for neurons involved in homeostasis, extends beyond the reflex control of the viscera, including all sensory-motor loops involved in digestion^{20, 61}, to the executive control of ingestion, through the *Phox2b*⁺ premotor/motor arm that mobilizes visceral-arch derived muscles (Fig. 1 and Supplementary Fig. 1). The remarkable genetic monotony of these circuits breaks down at the level of the somatic (*Phox2b*[−]) lingual and hypobranchials motoneurons. Such exceptions are to be expected in the head where the visceral and somatic bodies of the vertebrate animal, *sensu* Romer⁶², must meet and cooperate, at the border of the external world and interior milieu. Indeed, feeding can be construed as a sequence of somatic (i.e., external or relational) and visceral (i.e., internal or homeostatic) actions: to take in a substrate from the environment by biting or licking/lapping up, then to incorporate it in the interior milieu by chewing and swallowing. In these actions, the hyoid bone act as a weld between visceral and somatic muscles of the head: respectively the suprahyoids, derived from visceral arch mesoderm and innervated by branchiomotor (*Phox2b*⁺) motoneurons; and the hypobranchials (infrahyoid and lingual) derived from somites and innervated by somatic (*Phox2b*[−]) motoneurons. The hyoid bone, branchiomeric muscles, branchiomotor neurons, and premotor centers Peri5^{Atoh1} and IRT^{Phox2b}, all affiliated to the visceral body—muscles and bones through their origin in branchial arch mesoderm or neural crest, neurons through their expression of *Phox2b*—are likely the ancestral agents of feeding behaviors in vertebrates. At the advent of predatory and terrestrial lifestyles, the *Phox2b*⁺ premotor centers must have recruited elements of the somatic body: the infrahyoid and lingual motoneurons, and their muscle targets, migrated into the head⁶³.

Methods

Mouse lines. The following transgenic mouse lines were used: *Phox2b::Flpo*³³, *Phox2b::Cre*⁶⁴, *vGlut2::Cre*⁶⁵, *Atoh1::Cre*¹⁶, *Atoh1::FRTCre*¹⁶, *Olig3::Cre*^{ERT2}³⁵, *Foxg1^{ires}Cre*⁶⁶, *RC::FELA*⁶⁷, *Tau::Syp-GFP*⁶⁸, *Rosa::nlsLacZ* (also known as

Tau^{mGFP})⁶⁹, and *Ai9*⁷⁰. For behavioral experiments, all mice were produced in a B6D2 background.

The *Rosa^{FTLG}* mutant mouse line was established at the Institut Clinique de la Souris (Phenomin-ICS), Illkirch, France). The targeting vector was constructed as follows. A PCR fragment containing the rat synaptophysin cDNA fused to *GFP* was cloned by SLIC cloning with a 346 bp double-stranded synthetic HSV TK pA followed by a 29 bp homology for the 5′ extremity of the 3′ *Rosa* homology arm plus a *NsiI* site, in an ICS proprietary vector containing a floxed NeoR-STOP cassette. In the second cloning step, the NeoR cassette was removed by BamHI and SpeI restriction digests and replaced by SLIC cloning with the cDNA of tdTomato. The third cloning step introduced 5′ of the floxed tdTomato-STOP cassette, a DNA fragment containing a *NsiI* site followed by a 29 bp homology for the 3′ of the pCAG, followed by an MCS. The fourth step was the cloning of an FRT-surrounded NeoR-STOP cassette previously excised from an ICS proprietary vector in the *SmaI* site of the restriction site introduced in the MCS cassette. Finally, a fifth cloning step comprised the excision of a 7.8 kb fragment containing the whole FRT-NeoR-STOP-FRT LoxP-TdTomato-STOP-LoxP Syn-YFP cassette by a *NsiI* digest and its subcloning via SLIC cloning in an ICS proprietary vector containing a pCAG (Chicken b-actin promoter preceded by a CMV enhancer) and both 5′ and 3′ *Rosa* homology arms. The linearized construct was electroporated in C57BL/6 N mouse embryonic stem (ES) cells (ICS proprietary line). After G418 selection, targeted clones were identified by long-range PCR and further confirmed by Southern blot with an internal (Neo) probe and a 5′ external probe. One positive ES cell clone was validated by karyotype spreading and microinjected into BALB/c blastocysts. The resulting male chimeras were bred with wild-type C57BL/6 N females. Germline transmission was achieved in the first litter.

The sequence of all primers for genotyping are in Supplementary Table 1.

Housing. Animals were group-housed with free access to food and water in controlled temperature conditions (room temperature controlled at 21–22 °C, humidity between 40 and 50%), and exposed to a conventional 12-h light/dark cycle. Experiments were performed on embryos at embryonic (E) days E11.5–17.5, neonate pups at postnatal day 2–8 (P2–8), and adult (P30–56) animals of either sex. All procedures were approved by the Ethical Committee CEEA-005 Charles Darwin (authorization 26763-2020022718161012) and conducted in accordance with EU Directive 2010/63/EU. All efforts were made to reduce animal suffering and minimize the number of animals, in compliance with all relevant ethical regulations for animal testing and research.

Viral vectors for tracing, optogenetic, and photometry experiments. For anterograde tracing from Peri5^{Atoh1} and IRT^{Phox2b}, we injected unilaterally 250 nl of a Cre-dependent AAV2/8-*hSyn-FLEX-mGFP-2A-Synaptophysin-mRuby* (Titer: 1.3 × 10¹² viral genomes (vg)/ml, Viral Core Facility Charité).

For retrograde transsynaptic tracing from muscles, we injected unilaterally 50 to 100 nl of a 1:1 viral cocktail comprised of *RV-B19-ΔG-mCherry* or *RV-B19-ΔG-GFP* (titer: 1.3 × 10⁹ and 5.8 × 10⁸ TU/ml respectively, Viral Vector Core—Salk Institute for Biological Studies) and an *HSV-hCMV-YFP-TVA-B19G* (titer: 3 × 10⁸ TU/ml, Viral Core MIT McGovern Institute).

For retrograde tracing from IRT^{Phox2b} we injected unilaterally 250 nl of a Cre-dependent *AAV1/2-Syn-flex-nGToG-WPRE3* (titer: 8.1 × 10¹¹ vg/ml, Viral Core Facility Charité). Two weeks later we injected *EnvA-RV-B19-ΔG-mCherry* (titer: 3.1 × 10⁸ vg/ml, Viral Vector Core, Salk Institute for Biological Studies).

For optogenetic and photometry experiments we respectively injected 250 nl of *AAV1/2-Efla-DIO-stCoChR-P2A-mScarlet* (titer: 3 × 10¹³ vg/ml, kind gift from O. Yzhar) or 250 nl of *AAV1-syn-FLEX-jGCaMP7s-WPRE* (titer: 1 × 10¹² vg/ml Addgene #104487-AAV1).

Surgical procedures

Stereotaxic injections and implants. All surgeries were conducted under aseptic conditions using a small animal digital stereotaxic instrument (David Kopf Instruments). Mice were anesthetized with isoflurane (3.5% at 1 l/min for induction and 2–3% at 0.3 l/min for maintenance). Buprenorphine (0.025 mg/kg) was administered subcutaneously for analgesia before surgery. A feed-back-controlled heating pad was used to maintain the animal temperature at 36 °C. Anesthetized animals were placed in a stereotaxic frame (Kopf), a 100 μl injection of lidocaine (2%) was made under the skin covering the skull, after which a small incision was made in the scalp and burr-free holes were drilled in the skull to expose the brain surface at the appropriate stereotaxic coordinates [anterior-posterior (AP) and med

ial-lateral (ML) relative to bregma; dorsal-ventral (DV) relative to brain surface at coordinate (in mm)]: −4.9 AP, 1.2 ML, 4.0 DV to target the Peri5^{Atoh1} neurons; −6.7 AP, 0.5 ML, 4.2 DV to target the IRT^{Phox2b} neurons. A 0.5 ML coordinate was selected for virus deliveries to the IRT^{Phox2b} to circumvent the potential infection of nTS neurons along the injecting pipette track, a 4.0 DV coordinate was selected for virus deliveries to the Peri5^{Atoh1} to target the center of Mo5. Viral vectors were delivered using glass micropipettes (tip diameter ca. 100 μm) backfilled with mineral oil connected to a pump (Legato 130, KD Scientific, Phymep, France) via a custom-made plunger (Phymep, France). The injector tip was lowered an additional 0.1 mm below the target site and then raised back to the target coordinate before infusion started (flow of 25 nl/min) to restrict virus diffusion to the site of

injection and prevent leakages along the needle track. After infusion, the injection pipette was maintained in position for 10 min, then raised by 100 μm increments to retract the pipet from the brain. For optogenetic and photometry experiments, 200 μm core optic fibers (0.39 NA and 0.57 NA, respectively) (Smart Laser Co., Ltd) were implanted following vector injections, $\sim 500 \mu\text{m}$ above the sites of interest (-4.9 AP , 1.2 ML , 3.0 DV for $\text{Peri5}^{\text{Atoh1}}$; -6.7 AP , 0.9 ML , 3.6 DV for $\text{IRT}^{\text{Phox2b}}$). The optic fibers were secured via a ceramic ferrule to the skull by light-cured dental adhesive cement (Tetric Evoflow, Ivoclar Vivadent). Mice recovered from anesthesia on a heating pad before being placed, and monitored daily, in individual cages.

Intramuscular injections. All surgeries were conducted under aseptic conditions on P2 neonates anesthetized by deep hypothermia. For induction, pups were placed in latex sleeves gently buried in crushed ice for 3–5 min and maintenance (up to 15 min) was achieved by placing anesthetized pups on a cold pack (3–4 °C). Following small incisions of the skin to expose the targeted muscles, the viral cocktail (or 0.5% Cholera toxin subunit B (CTB) (List Labs) for labeling of the infrahypoids) was injected via a pneumatic dispense system (Picospritzer) connected to a glass pipette (tip diameter ca. 0.1 mm) mounted on a 3D micromanipulator to guide insertion in the desired muscle. Typically, 5–10 pressure pulses (100 ms, 3–5 bars) were delivered while the muscular filling was checked visually by the spreading of Fast-Green (0.025%) added to the viral solution. The pipette was withdrawn and the incision irrigated with physiological saline and closed using a 10-0 gage suture (Ethilon). The mouse was placed on a heating pad for recovery and returned to the mother. Six days postinjection (4 days for CTB), pups were deeply anesthetized, transcardially perfused with 4% paraformaldehyde (PFA) in phosphate-buffered saline (PBS), and the brains were dissected out and postfixed overnight in 4% PFA, cryoprotected in 15% sucrose in PBS and stored at $-80 \text{ }^\circ\text{C}$.

Histology

Immunofluorescence. Depending on the stage, the brain was analyzed in whole embryos dissected out of the uterine horns up to E16.5, dissected out from decapitated embryos from E17.5 to P0, or after P0, dissected in cold PBS from euthanized animals perfused with cold PBS followed by 4% paraformaldehyde. Brains or embryos were postfixed in 4% paraformaldehyde overnight at 4 °C, rinsed in PBS, and cryoprotected in 15% sucrose overnight at 4 °C. Tissues were then frozen in the Tissue-Tek[®] OCT compound for cryo-sectioning (14–30 μm) on a CM3050s cryostat (Leica). Sections were washed for 1 h in PBS and incubated in blocking solution (5% calf serum in 0.5% Triton-X100 PBS) containing the primary antibody, applied to the surface of each slide (300 μl per slide) placed in a humidified chamber on a rotating platform. Incubation was for 4–8 h at room temperature followed by 4 °C overnight. Sections were washed in PBS (3 \times 10 min), then incubated with the secondary antibody in blocking solution for 2 h at room temperature, then washed in PBS (3 \times 10 min), air-dried, and mounted under a coverslip with fluorescence-mounting medium (Dako). Primary antibodies used were: goat anti-*Phox2b* (RD system AF4940, diluted 1:100), rabbit anti-peripherin (Abcam ab4666, 1:1000), guinea pig anti-Lmx1b (Müller et al., 2002, 1:1000), goat anti-ChAT (Millipore AB144p), 1:100, chicken anti- βGal (Abcam, ab9361, 1:1000), chicken anti-*GFP* (Aves Labs, GFP-1020, 1:1000), goat anti-ChAT (Millipore, AB144p, 1:100), rabbit anti-*GFP* (Invitrogen, A11122, 1:1000), rabbit anti-*Phox2b* (Pattyn et al., 1997, 1:500), rat anti-RFP (Chromotek, 5F8, 1:1000), and goat anti-CTB (List Labs, #703, 1:500). All secondary antibodies were used at 1:500 dilution: donkey anti-chicken 488 (Jackson laboratories, 703-545-155), donkey anti-chicken Cy5 (Jackson laboratories, 703-176-155), donkey anti-goat Cy5 (Jackson laboratories, 705-606-147), donkey anti-rabbit 488 (Jackson laboratories, 711-545-152) donkey anti-rabbit Cy5 (Jackson laboratories, 712-165-153), donkey anti-rat Cy3 (Jackson laboratories, 711-495-152), and donkey anti-Guinea pig Cy3 (Jackson laboratories, 706-165-148). Epifluorescence images were acquired with a NanoZoomer S210 digital slide scanner (Hamamatsu Photonics) with NDPview2+; and confocal images with a Leica SP5 confocal microscope (Leica) with Leica Application suite X. Pseudocoloring, image brightness, and contrast were adjusted using Adobe Photoshop and FIJI.

In situ hybridization and immunohistochemistry. For the *Atoh1* probe, primers containing SP6 and T7 overhangs were used to amplify a 607 bp region from a plasmid containing the full-length *Atoh1* CDS. The purified amplicon was then used as the template for antisense probe synthesis with T7 RNA polymerase using the following primers: Forward Primer: 5'-CGATTTTAGGTGACTATAGAAA TCAA-CGCTCTGTCGGAGTT-3'; Reverse Primer: 5'-CTAATACGACTCACTA TAGGACACAGGAAGGGGAT-TGGAAGAG-3'. To generate the *Cited1* probe, a 687 bp fragment of the murine *Cited1* gene was amplified from E13.5 mouse brain cDNA (superscript III kit, Invitrogen) and cloned into pGEM-T vector (Promega), using the following primers: Forward Primer: 5'-TGGGGGGCTTAAG AGCCCGG-3'; Reverse Primer: 5'-AGGTGAGGGGTAGGATGCAG-3'. pGEM clones were linearized with NotI and transcribed with SP6 or T7 RNA polymerase using the DIG RNA labeling Kit (Roche 1277073) to generate antisense or sense probes. In situ hybridization was performed on 14 μm thick cryo-sections. Sections were washed for 10 min in PBS prepared in DEPC-treated water, then washed in RIPA buffer (150 mM NaCl, 1% NP-40, 0.5% Na-deoxycholate, 0.1% SDS, 1 mM EDTA, 50 mM Tris, pH 8.0) for 20 min, postfixed in 4% paraformaldehyde for

15 min followed by rinses in PBS (3 \times 10 min). Whenever ISH was to be followed by an immunohistochemical reaction, slides were incubated for 30 min in a mixture of 100% ethanol and 0.5% H_2O_2 , washed in PBS (3 \times 10 min), then incubated in Triethanolamine containing 0.25% acetic acid for 15 min and washed again in PBS (3 \times 10 min). Antisense RNA probes were diluted in 200 μl hybridization buffer (5 \times SSC, 10% dextran sulfate, 500 $\mu\text{g}/\text{mL}$ Herring sperm DNA, 250 $\mu\text{g}/\text{mL}$ Yeast-RNA, 50% formamide) and denatured at 95 °C for 5 min, cooled briefly on ice, then diluted at 100–200 ng/ml in 17 ml hybridization buffer for incubation in slide mailers, at 70 °C overnight. The next day, slides were washed for 1 h at 70 °C in 2 \times SSC, 50% formamide, and 0.1% Tween 20 and for 1 h in 0.2 \times SSC at 70 °C. Slides were washed in B1 buffer (0.1 M Maleic acid; pH 7.5, 0.15 M NaCl, 0.1% Tween 20), 3 \times 10 min. The sections were then blocked for 1 h at room temperature by incubation in blocking buffer (B1 buffer supplemented with 10% heat-inactivated fetal calf serum). The blocking solution was replaced by an alkaline phosphatase-conjugated anti-DIG antibody (Roche diagnostics, 11093274910) diluted 1:200 in the blocking buffer, and sections were incubated overnight at 4 °C under a coverslip. The following day the slides were rinsed in B1 buffer (3 \times 10 min), equilibrated with B3 buffer (0.1 M Tris pH 9.5, 0.1 M NaCl, 50 mM MgCl_2 , 0.1% Tween 20) for 30 min and colorimetric detection of the digoxigenin-labeled probe was performed with NBT-BCIP substrate for alkaline phosphatase (Thermo Scientific). The reaction was stopped by washing the slides in PBS-0.1% Tween 20 (2 \times 5 min) and fixing in 4% paraformaldehyde for 15 min. Sections were then washed in PBS-0.1% Tween 20 for 5 min each. Sections were incubated in blocking buffer (10% fetal calf serum diluted in 0.1% Tween 20 in PBS) for 1 h at room temperature, then in blocking buffer containing the primary antibody at 4 °C overnight. The next day, slides were washed for 10 min and biotinylated secondary antibody (diluted at 1:200 in blocking buffer) was applied for 2 h at room temperature and peroxidase enzyme detection of biotinylated antibody was carried out as per manufacturer's guidelines with the Vectastain Elite ABC kits (PK-6101 and PK-4005; Vector Laboratories), followed by color development using 3, 3'-Diaminobenzidine (SIGMA FAST D4293-50SET). The reaction was stopped by washing the slides for 2 \times 5 min in Milli-Q water, then sections were allowed to air-dry completely before mounting with Aquatex (Sigma Aldrich) for microscopy. Hybridized sections were imaged with a Leica DFC420C camera mounted on a Leica DM5500B microscope.

Data analysis of histology

Counts of premotor neurons and Lmx1b neurons. Cells expressing *mCherry* and/or *nlsLacZ* were counted in a spheroid of fixed dimension and position delimitating the ipsilateral dorsal IRT, drawn on the approximately seven alternate sections that were in register with the compact formation of MoA; $n = 4$ animals, 87 ± 20 SEM premotor neurons per animal.

Cells expressing *Phox2b* and/or *Lmx1b* were counted as above from one side; $n = 3$ animals, 1321 ± 46 SEM neurons per animal.

Inputs to $\text{IRT}^{\text{Phox2b}}$. Labeled neurons were manually annotated as IRT seed neurons (*GFP* + *mCherry*+) or monosynaptic input neurons (*mCherry*+) in ImageJ. The annotated sections were aligned to the Allen Brain Atlas using QuickNII (<https://www.nitrc.org/projects/quicknii>) transforming the annotations into Allen Brain Atlas coordinates and corresponding Allen Brain Atlas brain structures were identified using CellfHelp <https://doi.org/10.5281/zenodo.5508650>. Data from individual replicates were tabulated, normalized, and pooled to generate a list of brain regions that provide monosynaptic input to $\text{IRT}^{\text{Phox2b}}$. The bar graph excludes any input below 0.3%.

Behavioral experiments

Timing and training. All behavioral experiments started 4 weeks after the viral injection. Two weeks after surgery animals were habituated to head-fixation through sessions of increasing duration (2 min) every other day, starting at 2 min on day 0 and a final duration of 10 min on day 4 which corresponded to the duration of recording sessions. Animals were given condensed milk as a reward after each session. Animals used for photometry experiments were introduced to a lick port during habituation. During acquisition or manipulation animals were head-fixed within a 5 cm tube, illuminated from below and above by an LED light. Animals were water-deprived for 12 h prior to photometry experiments.

Optogenetics. For optogenetic photostimulation of *stCoChR* expressing neurons, fiber-optic cannulae were connected to a 473-nm DPSS laser (CNI, Changchun, China) through a patch cable (200 μm , 0.37 NA) and a zirconia mating sleeve (Thorlabs). Laser output was controlled using a pulse generator (accupulser, WPI), which delivered single continuous light pulses of 50–1000 ms or trains of 100 ms pulses at 4 Hz (33% duty cycle), 6 Hz (50% duty cycle), and 7 Hz (67% duty cycle). Light output through the optical fibers was adjusted to $\sim 5 \text{ mW}$ at the fiber tip using a digital power meter (PM100USB, Thorlabs). All light stimuli were separated by minimal periods of 10 s. Laser output was digitized at 1 kHz by a NI USB-6008 card (National Instruments) and acquired using a custom-written software package (Elphy by G Saddoc, <https://www.unic.cnrs.fr/software.html>).

Photometry. For photometry experiments, a single site fiber photometry system (Doric Lenses Inc, Canada) was used to measure the excited isosbestic (405 nm) and calcium-dependent fluorescence of jGCaMP7s (465 nm). Doric neuroscience studio software system (Doric Lenses Inc, Canada) was used to operate the photometry hardware and acquire the photometry signal. Briefly, using the “lock in mode” function, 465 and 405 nm LEDs were sinusoidally modulated at 208.616 and 572.205 Hz, respectively (to avoid any electrical system harmonics at 50/60, 100/120, and 200/240 Hz) at an intensity of 30 μ W and coupled to a patch cable (diam. 200 μ m, 0.57 nA) after passing through an optical assembly (iLFMC4, Doric Lenses Inc, Canada). The modulated excitation signal was then directed through an implanted fiber-optic cannula (diam. 200 μ m, 0.57 NA) onto the IRT via the mated patch cable and the emitted signal was then returned via the same patch cable to a fluorescence detector head, mounted on the optical assembly and amplified. The raw detected signal was acquired at 12 kHz and then demodulated in real time to reconstitute the excited isosbestic (405 nm) and calcium-dependent GCaMP (465 nm) signals. Contact between the tongue and the lick port during spontaneous licking bouts were registered via an SEN-1204 capacitance sensor (Sparkfun) connected to the Arduino Uno R3 microcontroller board (Arduino) and acquired at 12 kHz via the Doric fiber photometry console.

Automated markless pose estimation. Spontaneous and light-evoked licking sequences were filmed at portrait (Fig. 4a) and profile angles (Fig. 4d) with a CMOS camera (Jai GO-2400-C-USB) synchronized by a 5 V TTL pulse. The acquired frames (800 \times 800 pixels, 120 fps.) were streamed to a hard disk using 2ndlook software (IO Industries) and compressed using a MPEG-4 codec. Portrait views were used for video tracking of optogenetically-evoked oromotor movements, while profile views were preferably used for photometry experiments, to optimize detection of the tongue, which was partially obscured by the nearby lick port when filmed from the portrait angle.

Using DeepLabCut (version 2.0.77¹), we trained 2 ResNet-50 based neural networks to identify the tip of the tongue and lower jaw from portrait and landscape views (Fig. 4a, b, d). The “portrait” network was trained on a set of 264 frames (800 \times 800 pixels) derived from 11 videos of six different mice for >400,000 iterations, reporting a train error of 1.85 pixels and test error of 6.79 pixels upon evaluation. The “profile” network was trained on a set of 90 frames (800 \times 800 pixels) from four videos of four different mice for >800,000 iterations reporting a train error of 1.66 pixels and a test error of 4.57 pixels upon evaluation. These networks were then used to generate Cartesian estimates for the Y-axis position of the jaw and tongue for experimental videos.

Data analysis

Fiber photometry. We analyzed behavioral and fiber photometry data using custom-written Python scripts (Python version 3.7, Python Software Foundation). Fiber photometry and photostimulation data were resampled to 120 Hz to match the acquisition rate of video recordings. Fiber photometry and photostimulation data were resampled to 120 Hz to match the acquisition rate of video recordings. Photometry data were first processed by applying a low-pass filter (Butterworth) to the calcium-dependent 465 nm and isosbestic 405 nm signals with a 20 Hz cut-off. The 465 nm signal was then normalized using the function $\Delta F/F = (F - F_0)/F_0$, in which F is the 465 nm signal, and F₀ is the least-squared mean fit of the 405 nm signal. For each recording session in one animal, correlations between lick port contact and calcium signals were computed for all possible shifts at 120 Hz spanning from -10 to +10 s, producing one curve per session (Fig. 3g). A null correlation curve per recording session was constructed by performing the same computation after shuffling the lick port contact (Fig. 3g). All recording sessions and all null correlation curves were averaged for each animal, to produce a single mean shifted correlation curve and a null mean correlation curve per animal (Fig. S4). The maxima values of both shifted and null mean curves were retrieved for each animal ($n = 4$). A paired *t*-test between these values indicated a shifted correlation between both signals.

Normalization of jaw and tongue pose estimation. Cartesian pixel estimates of the jaw and tongue were corrected to a 5 mm scale bar within the video frame and smoothed using the Savitzky-Golay filter. For optogenetic experiments, the jaw position was normalized to its averaged location 50–100 ms prior to stimulation. For fiber photometry experiments, the jaw position was normalized to its average location during quiescent periods between 1–3 s long. As the tongue was only present during stimulation of IRT^{Phox2b} or spontaneous lapping, we normalized the tongue distance empirically by observing the first detected instance of tongue protrusion that succeeded jaw-opening events. All positional estimates of the tongue that had a probability <5%⁷¹ were then set to the empirically determined baseline to filter out aberrant estimates of the tongue position during periods of the recording where it was not visible.

Licking frequency. For data collected during optogenetic experiments, we first obtained the onsets of each lick during the 1000 ms stimulation window. These onsets were identified as the peaks of the first derivative of each lick within a lick bout. Lick frequency was then calculated as the number of lick events divided by length of time from the last lick to the first lick within a lick bout. For data collected during fiber photometry, lick frequency was determined by the number of contact

events of the capacitance sensor divided by the length of time from the last to the first lick within a lick bout.

Statistical analysis. All data are reported as mean \pm s.e.m (shaded area). *P* values for independent samples comparison were performed using a two-tailed Student’s *t*-test.

Statistics and reproducibility. For physiological experiments, the number of experiments is indicated in the legends of the relevant figure. Tracing experiments and histological analyses were reproduced a minimum of three times.

Reporting Summary. Further information on research design is available in the Nature Research Reporting Summary linked to this article.

Data availability

The data that support the findings of this study can be found in the Source Data provided with the paper. Microscopy data are available from the corresponding author upon reasonable request. Data from the Allen Brain Atlas was used in this study. Source data are provided with this paper.

Code availability

All code for this paper can be found at the following address: <https://doi.org/10.5281/zenodo.5508650>

Received: 4 June 2021; Accepted: 27 September 2021;

Published online: 02 November 2021

References

- Herrick, C. J. *An Introduction to Neurology* (W.B. Saunders Company, 1918).
- Torvik, A. Afferent connections to the sensory trigeminal nuclei, the nucleus of the solitary tract and adjacent structures; an experimental study in the rat. *J. Comp. Neurol.* **106**, 51–141 (1956).
- Moore, J. D. et al. Hierarchy of orofacial rhythms revealed through whisking and breathing. *Nature* **497**, 205–210 (2013).
- Ruder, L. et al. A functional map for diverse forelimb actions within brainstem circuitry. *Nature* **590**, 445–450 (2021).
- Stanek, E., Cheng, S., Takatoh, J., Han, B.-X. & Wang, F. Monosynaptic premotor circuit tracing reveals neural substrates for oro-motor coordination. *eLife* **3**, e02511 (2014).
- Takatoh, J. et al. Constructing an adult orofacial premotor atlas in Allen mouse CCF. *eLife* **10**, e67291 (2021).
- Woods, J. W. Behavior of chronic decerebrate rats. *J. Neurophysiol.* **27**, 635–644 (1964).
- Moore, J. D., Kleinfeld, D. & Wang, F. How the brainstem controls orofacial behaviors comprised of rhythmic actions. *Trends Neurosci.* **37**, 370–380 (2014).
- Travers, J. B., Dinardo, L. A. & Karimnamazi, H. Motor and premotor mechanisms of licking. *Neurosci. Biobehav. Rev.* **21**, 631–647 (1997).
- Anderson, T. M. et al. A novel excitatory network for the control of breathing. *Nature* **536**, 76–80 (2016).
- Nakamura, Y., Yanagawa, Y., Morrison, S. F. & Nakamura, K. Medullary reticular neurons mediate neuropeptide Y-induced metabolic Inhibition and Mastication. *Cell Metab.* **25**, 322–334 (2017).
- Wiesenfeld, Z., Halpern, B. & Tapper, D. Licking behavior: evidence of hypoglossal oscillator. *Science* **196**, 1122–1124 (1977).
- Bouvier, J. et al. Descending command neurons in the brainstem that halt locomotion. *Cell* **163**, 1191–1203 (2015).
- Cregg, J. M. et al. Brainstem neurons that command mammalian locomotor asymmetries. *Nat. Neurosci.* **23**, 730–740 (2020).
- Thoby-Brisson, M. et al. Genetic identification of an embryonic parafacial oscillator coupling to the preBötzinger complex. *Nat. Neurosci.* **12**, 1028–1035 (2009).
- Ruffault, P.-L. et al. The retrotrapezoid nucleus neurons expressing Atoh1 and Phox2b are essential for the respiratory response to CO₂. *eLife* **4**, e07051 (2015).
- Li, P. et al. The peptidergic control circuit for sighing. *Nature* **530**, 293–297 (2016).
- Reilly, M. B., Cros, C., Varol, E., Yemini, E. & Hobert, O. Unique homeobox codes delineate all the neuron classes of *C. elegans*. *Nature* **584**, 595–601 (2020).
- Yuste, R. et al. A community-based transcriptomics classification and nomenclature of neocortical cell types. *Nat. Neurosci.* **23**, 1456–1468 (2020).

20. Brunet, J.-F. & Pattyn, A. Phox2 genes - from patterning to connectivity. *Curr. Opin. Genet. Dev.* **12**, 435–440 (2002).
21. Pattyn, A., Hirsch, M., Goridis, C. & Brunet, J. F. Control of hindbrain motor neuron differentiation by the homeobox gene Phox2b. *Development* **127**, 1349–1358 (2000).
22. Pattyn, A., Goridis, C. & Brunet, J. F. Specification of the central noradrenergic phenotype by the homeobox gene Phox2b. *Mol. Cell Neurosci.* **15**, 235–243 (2000).
23. Li, L. et al. Visualizing the distribution of synapses from individual neurons in the mouse brain. *PLoS ONE* **5**, e11503 (2010).
24. Kitamura, S., Nishiguchi, T., Okubo, J., Chen, K. L. & Sakai, A. An HRP study of the motoneurons supplying the rat hypobranchial muscles: central localization, peripheral axon course and soma size. *Anat. Rec.* **216**, 73–81 (1986).
25. Wickersham, I. R. et al. Monosynaptic restriction of transsynaptic tracing from single, genetically targeted neurons. *Neuron* **53**, 639–647 (2007).
26. Ashwell, K. W. The adult mouse facial nerve nucleus: morphology and musculotopic organization. *J. Anat.* **135**, 531–538 (1982).
27. Hinrichsen, C. F. & Watson, C. D. The facial nucleus of the rat: representation of facial muscles revealed by retrograde transport of horseradish peroxidase. *Anat. Rec.* **209**, 407–415 (1984).
28. Meessen, H. & Olszewski, J. *Cytoarchitectonic Atlas of the Rhombencephalon of the Rabbit* (Karger, 1949).
29. Morquette, P. et al. Generation of the masticatory central pattern and its modulation by sensory feedback. *Prog. Neurobiol.* **96**, 340–355 (2012).
30. Hernandez-Miranda, L. R. et al. Genetic identification of a hindbrain nucleus essential for innate vocalization. *Proc. Natl Acad. Sci. USA* **114**, 8095–8100 (2017).
31. Van Daele, D. J. & Cassell, M. D. Multiple forebrain systems converge on motor neurons innervating the thyroarytenoid muscle. *Neuroscience* **162**, 501–524 (2009).
32. van der Heijden, M. E. & Zoghbi, H. Y. Loss of Atoh1 from neurons regulating hypoxic and hypercapnic chemoresponses causes neonatal respiratory failure in mice. *eLife* **7**, 937 (2018).
33. Hirsch, M.-R., d'Autréaux, F., Dymecki, S. M., Brunet, J.-F. & Goridis, C. A Phox2b:FLPo transgenic mouse line suitable for intersectional genetics. *Genes* **51**, 506–514 (2013).
34. Sieber, M. A. et al. Lbx1 acts as a selector gene in the fate determination of somatosensory and viscerosensory relay neurons in the hindbrain. *J. Neurosci.* **27**, 4902–4909 (2007).
35. Storm, R. et al. The bHLH transcription factor Olig3 marks the dorsal neuroepithelium of the hindbrain and is essential for the development of brainstem nuclei. *Development* **136**, 295–305 (2009).
36. Beier, K. T. et al. Circuit architecture of VTA dopamine neurons revealed by systematic input-output mapping. *Cell* **162**, 622–634 (2015).
37. Terashima, T., Kishimoto, Y. & Ochiishi, T. Musculotopic organization in the motor trigeminal nucleus of the reeler mutant mouse. *Brain Res.* **666**, 31–42 (1994).
38. Shohara, E. & Sakai, A. Localization of motoneurons innervating deep and superficial facial muscles in the rat: a horseradish peroxidase and electrophysiologic study. *Exp. Neurol.* **81**, 14–33 (1983).
39. Terashima, T., Kishimoto, Y. & Ochiishi, T. Musculotopic organization of the facial nucleus of the reeler mutant mouse. *Brain Res.* **617**, 1–9 (1993).
40. Widmalm, S. E., Nemeth, P. A., Ash, M. M. & Lillie, J. H. The anatomy and electrical activity of the platysma muscle. *J. Oral Rehabil.* **12**, 17–22 (1985).
41. Aldes, L. D. Subcompartmental organization of the ventral (protrusor) compartment in the hypoglossal nucleus of the rat. *J. Comp. Neurol.* **353**, 89–108 (1995).
42. McClung, J. R. & Goldberg, S. J. Organization of motoneurons in the dorsal hypoglossal nucleus that innervate the retrusor muscles of the tongue in the rat. *Anat. Rec.* **254**, 222–230 (1999).
43. Crompton, A. W., Cook, P., Hiiemae, K. & Thexton, A. J. Movement of the hyoid apparatus during chewing. *Nature* **258**, 69–70 (1975).
44. Murakami, H. Rhythmometry on licking rate of the mouse. *Physiol. Behav.* **19**, 735–738 (1977).
45. Lerner, T. N. et al. Intact-brain analyses reveal distinct information carried by SNc dopamine subcircuits. *Cell* **162**, 635–647 (2015).
46. Dana, H. et al. High-performance calcium sensors for imaging activity in neuronal populations and microcompartments. *Nat. Methods* **16**, 649–657 (2019).
47. Komiyama, T. et al. Learning-related fine-scale specificity imaged in motor cortex circuits of behaving mice. *Nature* **464**, 1182–1186 (2010).
48. Mercer Lindsay, N. et al. Orofacial movements involve parallel corticobulbar projections from motor cortex to trigeminal premotor nuclei. *Neuron* **104**, 765–780.e3 (2019).
49. Economo, M. N. et al. Distinct descending motor cortex pathways and their roles in movement. *Nature* **563**, 79–84 (2018).
50. Li, N., Chen, T.-W., Guo, Z. V., Gerfen, C. R. & Svoboda, K. A motor cortex circuit for motor planning and movement. *Nature* **519**, 51–56 (2015).
51. Grill, H. J. & Norgren, R. The taste reactivity test. II. Mimetic responses to gustatory stimuli in chronic thalamic and chronic decerebrate rats. *Brain Res.* **143**, 281–297 (1978).
52. Feldman, J. L. & Del Negro, C. A. Looking for inspiration: new perspectives on respiratory rhythm. *Nat. Rev. Neurosci.* **7**, 232–242 (2006).
53. Luo, P., Zhang, J., Yang, R. & Pendlebury, W. Neuronal circuitry and synaptic organization of trigeminal proprioceptive afferents mediating tongue movement and jaw-tongue coordination via hypoglossal premotor neurons. *Eur. J. Neurosci.* **23**, 3269–3283 (2006).
54. Rossi, M. A. et al. A GABAergic nigrotectal pathway for coordination of drinking behavior. *Nat. Neurosci.* **19**, 742–748 (2016).
55. Onimaru, H. & Homma, I. A novel functional neuron group for respiratory rhythm generation in the ventral medulla. *J. Neurosci.* **23**, 1478–1486 (2003).
56. Cui, Y. et al. Defining preBötzing complex rhythm- and pattern-generating neural microcircuits in vivo. *Neuron* **91**, 602–614 (2016).
57. McCrea, D. A. & Rybak, I. A. Organization of mammalian locomotor rhythm and pattern generation. *Brain Res. Rev.* **57**, 134–146 (2008).
58. Dougherty, K. J. & Ha, N. T. The rhythm section: an update on spinal interneurons setting the beat for mammalian locomotion. *Curr. Opin. Physiol.* **8**, 84–93 (2019).
59. Zhong, G., Shevtsova, N. A., Rybak, I. A. & Harris-Warrick, R. M. Neuronal activity in the isolated mouse spinal cord during spontaneous deletions in fictive locomotion: insights into locomotor central pattern generator organization. *J. Physiol.* **590**, 4735–4759 (2012).
60. Nomaksteinsky, M. et al. Ancient origin of somatic and visceral neurons. *BMC Biol.* **11**, 53 (2013).
61. Pattyn, A., Morin, X., Cremer, H., Goridis, C. & Brunet, J. F. The homeobox gene Phox2b is essential for the development of autonomic neural crest derivatives. *Nature* **399**, 366–370 (1999).
62. Romer, A. S. The vertebrate as a dual animal—Somatic and visceral. *Evol. Biol.* **5**, 121–156 (1972).
63. Sambasivan, R., Kuratani, S. & Tajbakhsh, S. An eye on the head: the development and evolution of craniofacial muscles. *Development* **138**, 2401–2415 (2011).
64. d'Autréaux, F., Coppola, E., Hirsch, M.-R., Birchmeier, C. & Brunet, J.-F. Homeoprotein Phox2b commands a somatic-to-visceral switch in cranial sensory pathways. *Proc. Natl Acad. Sci. USA* **108**, 20018–20023 (2011).
65. Vong, L. et al. Leptin action on GABAergic neurons prevents obesity and reduces inhibitory tone to POMC neurons. *Neuron* **71**, 142–154 (2011).
66. Kawaguchi D, Sahara S, Zembrzycki A, O'Leary DD. Generation and analysis of an improved Foxg1-IRES-Cre driver mouse line. *Dev Biol* **412**, 139–174 (2016).
67. Jensen, P. et al. Redefining the serotonergic system by genetic lineage. *Nat. Neurosci.* **11**, 417–419 (2008).
68. Pecho-Vrieseling, E., Sigrist, M., Yoshida, Y., Jessell, T. M. & Arber, S. Specificity of sensory–motor connections encoded by Sema3e–Plexnd1 recognition. *Nature* **459**, 842–846 (2009).
69. Hippenmeyer, S. et al. A developmental switch in the response of DRG neurons to ETS transcription factor signaling. *PLoS Biol.* **3**, e159 (2005).
70. Madisen, L. et al. A robust and high-throughput Cre reporting and characterization system for the whole mouse brain. *Nat. Neurosci.* **13**, 133–140 (2010).
71. Mathis, A. et al. DeepLabCut: markerless pose estimation of user-defined body parts with deep learning. *Nat. Neurosci.* **21**, 1281–1289 (2018).
72. Hatini, V., Ye, X., Balas, G. & Lai, E. Dynamics of placodal lineage development revealed by targeted transgene expression. *Dev. Dyn.* **215**, 332–343 (1999).

Acknowledgements

We thank the animal facility of IBENS, the imaging facility of IBENS (supported by grants from Fédération pour la Recherche sur le Cerveau, Région Ile-de-France DIM NeRF (2009 and 2011), and France-BioImaging), Ofer Yitzar for the *AAV1-EF1a-DIO-stCoChR-P2A-mScarlet* vector. The mouse *Rosa^{FLTG}* mutant line was established at the Institut Clinique de la Souris (Phenomin-ICS) in the Genetic Engineering and Model Validation Department. Funding is from CNRS, École Normale Supérieure, INSERM, Association Nationale pour la Recherche ANR -15-CE16-0013 (to J.-F.B.), Association Nationale pour la Recherche ANR-17-CE16-0006 (to J.-F.B.), and ANR-19-CE16-0029 (to G.F.), Fondation pour la Recherche Médicale DEQ2000326472 (to J.-F.B.), “Investissements d’Avenir” program ANR-10-LABX-54 MEMO LIFE and ANR-11-IDEX-0001-02 PSL Research University), and Région Ile-de-France (to S.S.).

Author contributions

Conceptualization: B.D., C.G., G.F. and J.-F.B. Investigation: B.D., S.S., P.B., E.R.H., Z.C., S.D. and S.A. Formal Analysis: S.M., H.C., P.B., B.D. and A.G. Supervision: C.G., G.F., J.-F.B. and J.F.A.P. Resources: C.B. Writing: B.D., G.F. and J.-F.B.

Competing interests

The authors declare no competing interests.

Additional information

Supplementary information The online version contains supplementary material available at <https://doi.org/10.1038/s41467-021-26275-y>.

Correspondence and requests for materials should be addressed to Jean-François Brunet.

Peer review information *Nature Communications* thanks the anonymous reviewer(s) for their contribution to the peer review of this work. Peer reviewer reports are available.

Reprints and permission information is available at <http://www.nature.com/reprints>

Publisher's note Springer Nature remains neutral with regard to jurisdictional claims in published maps and institutional affiliations.



Open Access This article is licensed under a Creative Commons Attribution 4.0 International License, which permits use, sharing, adaptation, distribution and reproduction in any medium or format, as long as you give appropriate credit to the original author(s) and the source, provide a link to the Creative Commons license, and indicate if changes were made. The images or other third party material in this article are included in the article's Creative Commons license, unless indicated otherwise in a credit line to the material. If material is not included in the article's Creative Commons license and your intended use is not permitted by statutory regulation or exceeds the permitted use, you will need to obtain permission directly from the copyright holder. To view a copy of this license, visit <http://creativecommons.org/licenses/by/4.0/>.

© The Author(s) 2021

RESULTS 2: A PONTINE CENTER FOR CHEWING

A PREMOTOR CENTER FOR CHEWING

Authors

Sungeelee. S et al.

ABSTRACT

The reticular formation of the pons and medulla is known to contain neurons that participate in vital homeostatic functions such as feeding, thermoregulatory as well as cardiovascular and respiratory control. Despite these broad functional attributes, it remains poorly characterized in terms of genetically defined neuron types. The transcription factor Phox2b specifies most autonomic neurons, as well as orofacial motor nuclei. Previous work from the lab identified jaw-opener Phox2b+ premotor neurons in the intermediate reticular formation (**Dempsey et al., 2021**). Moreover, genetic anterograde tracing of all hindbrain glutamatergic Phox2b+ interneurons revealed terminals in jaw closing motor nuclei, pointing to orofacial Phox2b+ premotor populations (**Dempsey et al., 2021**). Here we explore the development, anatomy and function of another Phox2b+ interneuronal population (Sup5^{Phox2b}) located in the supratrigeminal nucleus, a region known to project to the trigeminal (jaw-closing) motor nucleus. We find that the expression of the transcription factor Phox2b in the supratrigeminal nucleus identifies a likely jaw-closing premotor center and provides access to its further functional characterization.

INTRODUCTION

Orofacial movements for ingesting food (biting, chewing, lapping, swallowing) are executed by jaw, tongue and pharyngeal muscles controlled by cranial motor nuclei of the pons and medulla: trigeminal (Mo5), facial (Mo7), ambiguous (MoA), hypoglossal (Mo12) nuclei and an unnamed nucleus for the infrahyoid muscles (hereafter MoC). The activity of the motor neurons themselves can be triggered, modulated and coordinated — in other terms patterned — by premotor centers, also situated in the pons and medulla, as evidenced by the preservation of complex feeding movements in decerebrated animals (**Miller and Sherrington, 1915; Woods, 1964**). Premotor neurons to cranial motor nuclei were mapped in many regions of the bulbar and pontine

reticular formation, most recently by monosynaptic retrograde tracing (**Stanek et al., 2014a, 2016a; Takatoh et al., 2021b, 2022**). However, to date, few hindbrain premotor neurons have been attributed genetic signatures, beyond those underlying their neurotransmitter phenotype (mostly glutamatergic, (**Ruder et al., 2021; Wei et al., 2022a**) and Gabaergic (**Han et al., 2017b; Y. Nakamura et al., 2017; Takatoh et al., 2022**) which limits our understanding and manipulation of the circuits in which they partake. We previously reported two classes of premotor neurons to jaw and tongue muscles that express the pan-autonomic and branchiomotor neuron transcriptional determinant *Phox2b* (**Dempsey et al., 2021**). They reside respectively in the medial intermediate reticular formation and peri-trigeminal area and were named IRT^{*Phox2b*} and Peri5^{*Atoh1*}. Both nuclei can trigger jaw abduction and IRT^{*Phox2b*} can also trigger tongue protrusion. Moreover, tonic activation of IRT^{*Phox2b*} in alert animals triggers a rhythmic jaw and tongue movement akin to lapping, placing IRT^{*Phox2b*} upstream of, or within the putative licking/lapping oscillator.

Here we identify a third cluster of orofacial premotor interneurons that express the homeobox gene *Phox2b*. In the adult, they reside in the pons, at the location previously described as the Supra-trigeminal nucleus (Sup5), proposed to contain premotor neurons to Mo5 a century ago by means of Golgi stains (**Lorente De No, 1922**) and recently by monosynaptic retrograde tracing (**Stanek et al., 2014a; Takatoh et al., 2021b**). Sup5^{*Phox2b*} targets Mo5, Mo12 and Mo7. Photo-stimulation of Sup5^{*Phox2b*} in alert animals robustly adducts the jaw, interrupting bouts of licking or chewing, and Sup5^{*Phox2b*} activity, monitored by fibrometry tracks licking, biting and chewing movements.

RESULTS

Ontogeny and topology of Sup5^{Phox2b}

We previously identified Peri5^{*Atoh1*}, a pontine group of *Phox2b* interneurons that co-express the *Atoh1* transcription factor and are organized as a shell around Mo5 (**Dempsey et al., 2021**). Peri5^{*Atoh1*} is included in a much larger population of *Phox2b*⁺ interneurons that occupy the regions called peritrigeminal (Peri5) (first described as *regio h* by (**Meessen & Olszewski, 1949**)) and supratrigeminal (Sup5) (first identified and named by (**Lorente De No, 1922**) and described in rat as rich in *Phox2b*⁺ cells by (**Nagoya et**

al., 2017). Both regions contain neurons that can be traced to or from Mo5 (Kolta et al., 2000; Mizuno et al., 1983), are monosynaptically labeled from the masseter (Stanek et al., 2014a; Takatoh et al., 2021b), evoke EPSPs in Mo5 motoneurons, and EMG signals in the masseter (Stanek et al., 2016b). For ease of stereotaxic access, we elected the supratrigeminal *Phox2b*⁺ population (hereafter Sup5^{Phox2b}) for further study.

The Sup5 region of mice contains many *Phox2b*⁺ neurons that cap Mo5 and lie medial to the dorsomedial principal trigeminal nucleus (Dempsey et al., 2021) (and Fig. 1a,b). Together with *Phox2b*, these cells all co-express, the vesicular glutamate transporter *Vglut2* (Fig. 1a) and the homeobox transcription *Lmx1b* (Fig. 1b).

Despite the usual description of Sup5 as “dorsal” to Mo5 (as it appears on standard coronal sections through the pontine curvature) Sup5 *Phox2b*⁺ neurons are actually rostral to it, in topological and genoarchitectonic (Puelles & Ferran, 2012) terms: in a genetic background where expression of a fluorophore is driven specifically in the second segment of the hindbrain — rhombomere 2 (r2) — (i.e. in *Hoxa2Cre::Rosa^{tdT}*) (Ren et al., 2002), Mo5 was *tdT* positive (consistent with its origin in r2) while the supratrigeminal *Phox2b*⁺ neurons resided in the *tdT*⁻territory immediately rostral to it, thus in r1 (Fig. 1c,d). This topology was already evident at E12.5, where the incipient Sup5^{Phox2b} was seen forming rostral to the *Lbx1*⁺ domain (Sieber et al., 2007), whose rostral limit coincides with the r1/r2 boundary (Schubert et al., 2001) (Fig. 1e). On the second cartesian axis of the developing hindbrain, i.e. dorsoventral, Sup5 *Phox2b*⁺ neurons appeared to arise from a stream of cells whose progenitors expressed *Phox2b*, thus from the dB2 progenitor domain (Sieber et al., 2007), and switch on *Lmx1b* post-mitotically, from r1 to r3 (arrowheads in Fig. 1f). The *Phox2b*⁺/*Lmx1b*⁺ postmitotic progeny had an unusual appearance in that it was seamlessly continuous with a wider population of *Lmx1b*⁺ cells residing in r1, in the confines of which they were entirely contained. This pattern looked ambiguously like it could result from the onset of *Lmx1b* in the *Phox2b*⁺ progeny of dB2 (yellow arrowhead in Fig 1f), and/or a localized onset of *Phox2b* in the *Lmx1b*⁺ population of r1 (for which we have no direct evidence). In *Phox2b* KO embryos, where dB2 progenitors failed to produce post-mitotic cells (red arrowhead in Fig. 2a) and remained in the state of radial glia (red asterisk in Fig. 2a), a population of *Phox2b*⁺/*Lmx1b*⁺ cells was still present in r1, albeit in reduced numbers (Fig. 2a). We surmise that their origin is from the nearby dB3 domain, whose postmitotic progeny is known to switch on *Lmx1b* (Di Bonito & Studer, 2017) and might also express *Phox2b*. All in all, despite its unifying *Phox2b*/*Lmx1b* signature, Sup5^{Phox2b} might have a dual

dB2/dB3 origin (thus possibly a cryptic heterogeneity).

Another notable topological feature of *Lmx1b*⁺/*Phox2b*⁺ cells is their close association with the axon tract of the mesencephalic nucleus of the trigeminal nerve (Mes5). Mes5^{tract} borders medially the elongated *Lmx1b*⁺/*Phox2b*⁺ locus coeruleus (**Fig. 2b**) as early as E11.5 (**Fig. 2c**) and **E10.5 (Fig. 2c)**, spreads laterally within the *Lmx1b*⁺/*Phox2b*⁺ Sup5^{Phox2b} (**Fig. 2a**) and its caudal continuation, called Probst's tract (**Corbin, 1940**), remains in close apposition to the *Lmx1b*⁺/*Phox2b*⁺ progeny of dB2 all the way to r4 (blue arrowheads in **Fig. 2b**). This spatial contiguity suggests that Mes5^{tract} and *Lmx1b*⁺/*Phox2b*⁺ cells could have a developmental relationship with each other. Since Mes5^{tract} is the earliest fiber tract of the entire brain (**Chédotal et al., 1995**) and forms before any dB2 neuron is born, we deleted Mes5 in a *Onecut1/2* null background (**Espana & Clotman, 2012**) and examined the formation of Sup5^{Phox2b}. At E13.5, in the absence of Mes5^{tract} the distribution of *Lmx1b*⁺ and *Phox2b*⁺ cells had changed in a complex manner (**Fig. 2e,f**), and the total number of *Lmx1b*⁺/*Phox2b*⁺ decreased. We are in the process of examining the mutants and earlier and later stages. More caudally, in r2 and r3 of *Onecut1/2* nulls, dB2 cells failed to switch on *Lmx1b* (Sup Fig.). Thus, the axons of Mes5 have an organizing role in the reticular formation, at least its dB2 derived cells, including Sup5^{Phox2b}, which is one of its main targets (see below).

Connectivity of Sup5^{Phox2b}

The original description of Sup5 (**Lorente De No, 1922**) was largely based on connectivity: a major site of projections from Mes5 and of inputs to Mo5. We asked whether these hodological features held true for Sup5^{Phox2b}.

We first assessed whether Sup5^{Phox2b} is premotor to Mo5 by monosynaptic retrograde tracing from the masseter in P3 pups. A modified G-deficient rabies virus expressing mCherry was co-injected into the masseter with a G-complementing helper virus expressing a YTB reporter, and brains were analyzed at P8. Seed cells co-expressing mCherry and YTB were observed ipsilaterally in the dorsolateral Mo5, consistent with the known somatotopic representation of jaw closers in this nucleus (**Sasamoto, 1979**). Monosynaptically projecting cells were observed very laterally in the Sup5 - both ipsi and contralaterally - and more importantly, all of them were found to express Phox2b. mCherry-expressing axon collaterals of monosynaptically-traced Sup5^{Phox2b} neurons can be seen crossing the midline to contralateral Mo5. Therefore, at least a subset of cells in Sup5^{Phox2b} is specifically premotor

to jaw-closing muscles in Mo5.

To visualize the brain-wide projection targets of Sup5^{Phox2b}, we next injected it with a Cre-dependent AAV construct that expresses a membrane-tethered GFP, and a red fluorophore fused to synaptophysin (Syp-Ruby) that labels synaptic boutons (**Beier et al., 2015**). Syp-Ruby boutons covered the whole surface of Mo5 and the accessory 5th nucleus (Acc5) bilaterally with ipsilateral predominance, as well as the contralateral Sup5 (**Fig 3f, g**). Other bilateral projections (with ipsilateral predominance) targeted Mo12 (more specifically its dorsal retrusor compartment) (**Fig3i**), intermediate Mo7 (**Fig3h**) and the accessory 7th (Acc7) (Sup.Fig.) nucleus as well as the pontine reticular nucleus (Sup.Fig.), ventral periaqueductal grey and deep mesencephalic nucleus (**Fig3j**) as well as broad regions of the caudal medullary reticular formation (Sup.Fig.). The ventral posteromedial thalamic nucleus received predominantly contralateral projections (Sup.Fig.).

To identify the source of descending inputs to Sup5^{Phox2b}, we first injected a cre-dependent AAV fusion construct expressing the optimized rabies glycoprotein oG and the TVA receptor in the Sup5 of *Phox2b::cre* mice. Following two weeks of expression of oG (**Kim et al., 2016**) and TVA, a second injection of an EnvA-pseudotyped G-deficient rabies virus encoding the fluorophore mRuby was made into Sup5, such that its expression was restricted to TVA-expressing neurons (seed cells). The retrograde projectome of Sup5^{Phox2b} was very discrete compared to its output targets and included, from rostral to caudal: the contralateral primary motor cortex (M1), the ipsilateral central amygdala (CeA), the contralateral deep (lateral) superior colliculus, the ipsilateral trigeminal mesencephalic nucleus, the ipsilateral lateral and medial parabrachial nuclei, the deep cerebellar nuclei (more specifically the ipsilateral dorsolateral interposed (IntPDL) subnucleus and contralateral medial dorsolateral (mDL)), the contralateral IRt and a broad region of the medullary reticular formation encompassing IRt and PCRt ipsilaterally. A large population of mRuby+/GFP- neurons occupied Sup5 itself ipsilaterally (although we could not ascertain the genetic signature of these cells).

The tracing experiments show that Sup5^{Phox2b} has both descending and ascending efferent connections with several brain regions but receives only modest afferent inputs from suprabulbar regions. These regions are largely involved in the emotional and motor regulation of the face region, suggesting Sup5^{Phox2b} might regulate jaw-related orofacial movements by acting as a major hub that sends divergent efferent inputs to orofacial motor and premotor centers for the jaw.

Sup5^{Phox2b} stimulation triggers jaw closure

To investigate the role of Sup5^{Phox2b} in vivo, we injected a Cre-dependent opsin (AAV1/2-Ef1a-DIO-stCoChR-P2A-mScarlet)(**Forli et al., 2021**) into the Sup5 of *Phox2b::Cre* mice and unilaterally implanted an optic fibre above this nucleus (**Fig 5a,b**). We then optogenetically stimulated these cells with short (200 ms) single pulses in head-fixed mice while video recording the face (**Fig 5c and Sup.video**). Optogenetic stimulation triggered an abrupt jaw adduction (of small amplitude since they occurred from the resting, essentially closed, position) in all mice (n=4), followed by return to the baseline position upon cessation of photostimulation (**Sup. Video**). Photostimulation of Sup5^{Phox2b} with 10ms pulses at 5Hz evoked repetitive jaw adduction from the resting position at the same frequency (**Fig 5d, e**), showing that Sup5^{Phox2b} can operate within this frequency range. Longer photostimulation (1s) prolonged the phase of adduction, but the jaw gradually returned to its resting position during the stimulation (**Sup. Video**). To determine if this evoked behavior recruits the jaw-closing muscles, we carried out acute EMG recordings of the masseter in lightly anesthetized head-fixed mice, while photostimulating Sup5^{Phox2b}. Optogenetic stimulation of Sup5^{Phox2b} resulted in contraction of the masseter concurrent with jaw adduction that were consistent across trials (n=9 trials)(**Fig 5c**), and that progressively waned despite sustained photostimulation, to reach baseline levels before the end of photostimulation, similar to what was observed in the video recordings of alert animals. This may be due to refractoriness at the neuromuscular junction attendant with supramaximal stimulation or Ib inhibition following an increase in tension in tendon organs (Hiraoka, 2004). Thus, Sup5^{Phox2b} can close the jaw by activating the masseter, which is coherent with its projections to masseter motoneurons in Mo5.

We then asked whether tonic photostimulation of Sup5^{Phox2b} could disrupt volitional ingestive sequences. We established an optogenetic stimulation protocol during licking in head-fixed mice, whereby 4 successive licks trigger prolonged (1s) optogenetic stimulation of Sup5^{Phox2b}(**Fig 5g**). During this protocol, all licking activity was abolished concurrent with jaw adduction as shown in **Fig 5 h,i**). Small vertical and horizontal jaw movements occurred immediately after optogenetic stimulation, although licking per se took longer to resume. This sequence was consistent across all tested animals (n=4) (**Sup. Fig**). Similarly, photostimulation of Sup5^{Phox2b} in freely moving animals during chewing of a food pellet consistently interrupted the chewing sequence (**Sup. Video**).

Sup5^{Phox2b} is active during ingestive orofacial movements

The disruptive effect of induced tonic Sup5^{Phox2b} activity on ingestive behaviors suggested that its spontaneous, patterned activity could play a role in them. We carried out in vivo bulk fluorescent calcium recordings of Sup5^{Phox2b} during spontaneous licking in head-fixed mice using fiber photometry (**G. Cui et al., 2013**). We injected a Cre-dependent GCaMP7s vector (**Dana et al., 2019**) into the Sup5 of *Phox2b::Cre* mice (**Fig 6a**) and an optical fiber was implanted unilaterally above this nucleus to measure changes in Ca²⁺ dynamics while tracking jaw movements with the DeepLabCut toolbox (**Mathis et al., 2018**). In all tested animals (n=4), the jaw-closing phase of licking bouts correlated with increases in fluorescence of Sup5^{Phox2b} (**Fig 6d, e**), indicating that Sup5^{Phox2b} is recruited during licking. To test whether Sup5^{Phox2b} participates in other types of ingestive behaviors, we recorded changes in bulk calcium fluorescence in head-fixed mice while they chewed a flake of almond. The calcium transient from Sup5^{Phox2b} was much larger than during licking and displayed a complex but regular pattern that was consistent within and across trials: a large rise in fluorescence occurred upon each biting event — when the animal, having brought the almond to the mouth, was breaking off a piece of it, with minimal vertical jaw movements. This was followed by a progressive decrease in fluorescence while the mouse began to rhythmically chew on the morsel it had bitten off. Superimposed on the descending slope, small calcium transients occurred at the same frequency as chewing (**Fig 6 f, g**). These two nested patterns (reproducible for n=3 animals, across n=3 chewing sequences) suggested the operation of two population dynamics within Sup5^{Phox2b}, possibly depending on the occlusal load (presumably higher during biting than chewing) or underlying phasic (singular) versus rhythmic movements. During the same trial, switching from almond to raw pasta (much tougher and less brittle than almond) only moderately increased the maximum amplitude of the calcium transients but changed the rhythmic pattern to a more chaotic one.

All in all, recording of *Sup5^{Phox2b}* revealed phasic activity during biting, and rhythmic activity during the occlusion phase of volitional lapping and chewing, with an intensity that parallels the load force (low in lapping and highest when biting hard material).

Fig. 1 : Markers and topology of $Sup5^{Phox2b}$. (a-c) coronal sections at P0 through the pons of a *Vglut2::Cre; Rosa^{nlsLacZ}* (a), wild type (b) and *Hoxa2::Cre; Rosa^{nlsLacZ}* (c), stained for the indicated markers. (d, e), parasagittal sections through the pons and medulla of a E13.5 *Hoxa2::Cre; Rosa^{nlsLacZ}* embryo (d) and an E12.5 wild type embryo (e), labeled for the indicated markers. The rhomboid shape of the medulla entails that a sagittal section will intersect the ventricular zone at several dorsoventral levels, the more dorsal, the more caudally); The $Phox2b^+$ domain dB2 is intersected at the red arrowhead. The r3/r4 boundary is indicated as the caudal limit of *Lmbx1* expression in the $Phox2b^+/Lbx1^+$ progeny of dB2 (white cells, triple labeled). More caudally, dB2 progeny is $Phox2b^+/Lbx1^+/Lmx1b^-$ (purple)(Sieber et al., 2007). (f) Hemi coronal section through the pontine curvature of a wild type E11.5 embryo labeled for the indicated markers. The dotted line indicates the recess of the 4th ventricle, above and below which, r1 and r3 are transversally sectioned, providing mirror images of the dB2 domain ($Phox2b^+$) and of the dB3 domain (unmarked but giving rise to *Lmx1b^+* neurons). The yellow arrowhead points to the onset of *Lmx1b* expression in the dB2 progeny, which was unnoticed so far(Di Bonito and Studer, 2017b; Storm et al., 2009b), and is restricted to r1-r3.

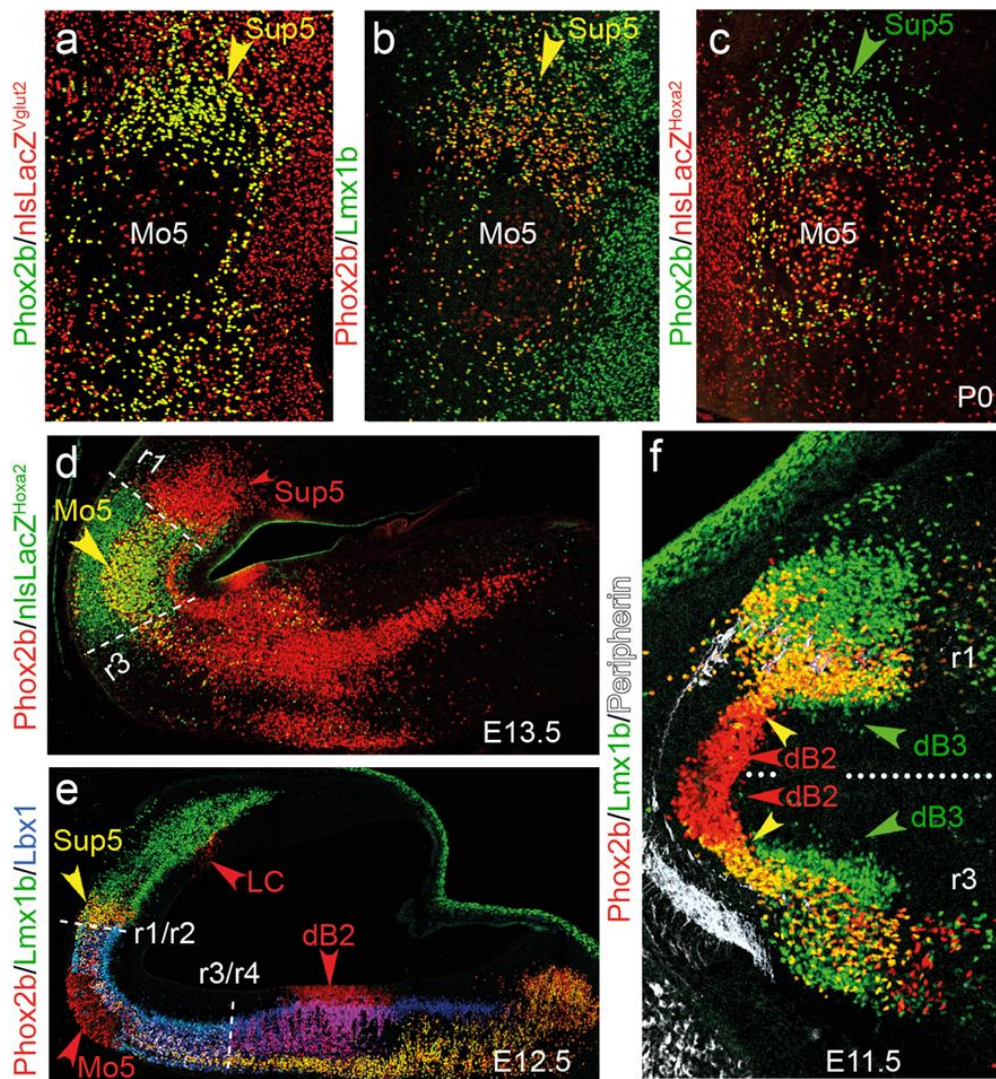


Fig. 2: Developmental dependencies of Sup5^{Phox2b}. (a) Hemi-coronal section through the pontine curvature of a *Phox2b* KO embryo at E11.5 labeled for the indicated markers (compare with wild type in Fig.1f). The dB2 domain is now made up of radial glia extending to the surface of the hindbrain and does not give off any progeny in r3 (yellow asterisk), and presumably not in r1 where it is separated by a gap from a persistent *Lmx1b*⁺/*Phox2b*⁺ population. (b, c) Coronal sections through the pons of a E12.5 and E10.5 wild type embryo showing the intimate association between the tract of Mes5 and *Lmx1b*⁺/*Phox2b*⁺ cells of the locus coeruleus and dB2. (d) Parasagittal section through the hindbrain at E12.5 showing association of the tract of Mes5 (blue arrowhead) with *Lmx1b*⁺/*Phox2b*⁺ cells throughout the pons and medulla. Double arrowheads indicate the forming spinal trigeminal tract. (e, f) Coronal section through the pons of E13.5 wild type (e) and *Onecut1/2* double mutant embryo (f). In the mutant the tract of Mes5 is absent and much fewer *Lmx1b*⁺/*Phox2b*⁺ are present in Sup5.

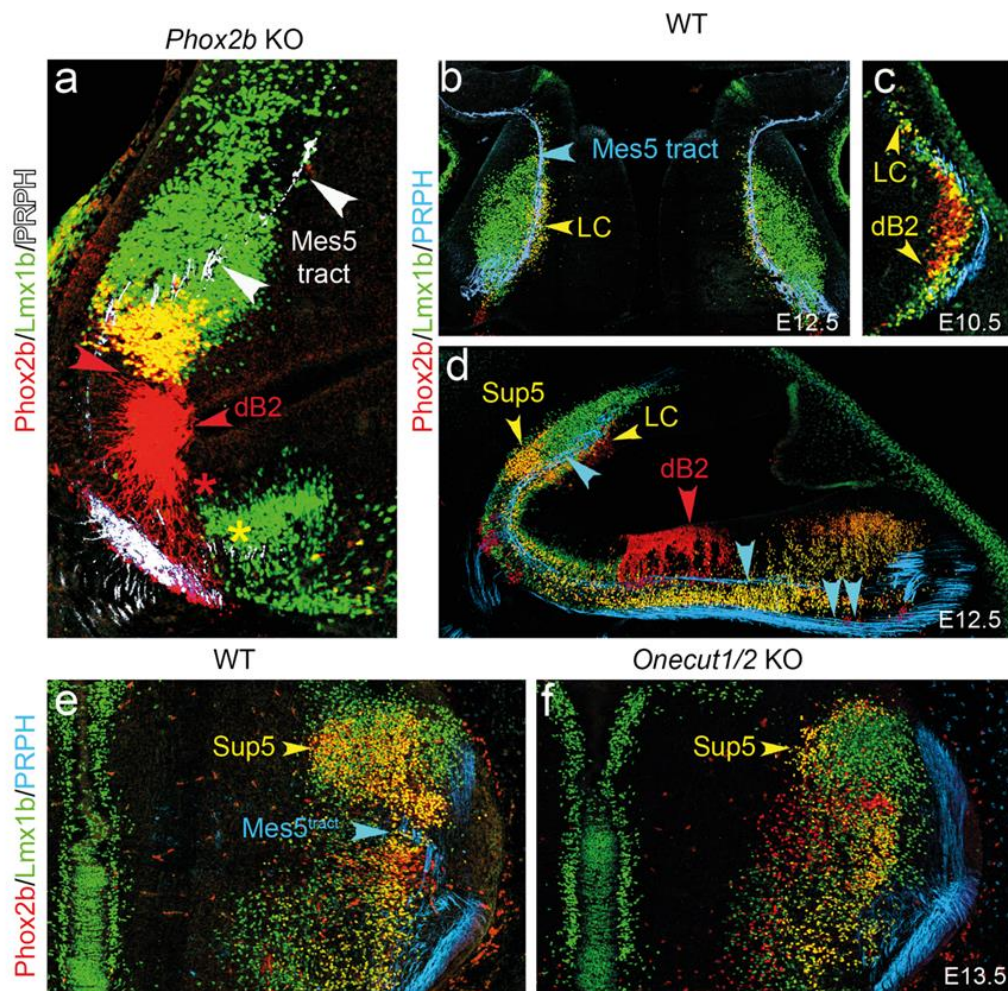


Fig. 3: Projections of Sup5^{Phox2b}. (a) Schematic of retrograde monosynaptic tracing from the masseter. (b) (and inset) Double labeled seed motoneurons in Mo5. (c) Transynaptically labeled Phox2b neurons in the ipsilateral Sup5. (d) Transynaptically labeled Phox2b neurons in the contralateral Sup5. (e) Schematic of strategy for anterograde labeling of Sup5^{Phox2b}. (f) Transfected mGFP+/syp-Ruby+ neurons in Sup5^{Phox2b}. (g-j) Coronal sections (left panels: low-magnification, right panels: high-magnification) through the brain of a P56 *Phox2b::cre* mouse after injection of the Sup5 with a mGFP/Syp-Ruby encoding AAV, showing the fibers and boutons (right panels) of Sup5^{Phox2b} covering Mo5 and contralateral Sup5 (g), IRT and intermediate Mo7(h), dorsal Mo12 (i) and ventral PAG(VPAG) as well as the deep mesencephalic nucleus(dpMe)(i).

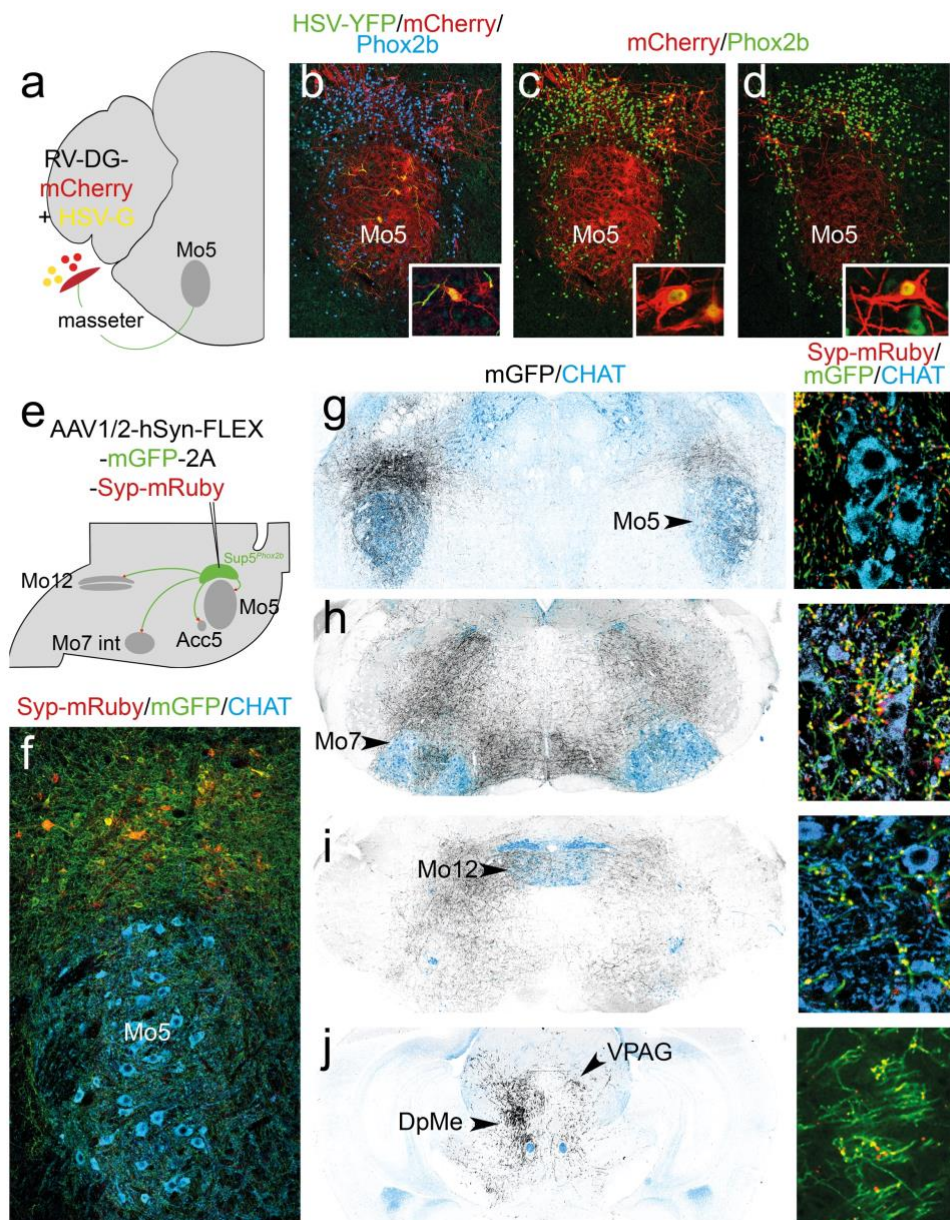


Fig. 4: Inputs to Sup5^{Phox2b} (a) Schematic of retrograde monosynaptic tracing strategy from Sup5^{Phox2b}, with major input sites depicted. (b) Images at low magnification (right panel) and high magnification (left panel) of seed cells in Sup5 co-expressing nlsGFP and mcherry. (c-h) Main sources of inputs to Sup5^{Phox2b} include the caudal reticular formation (IRt/PCrt), central amygdaloid nucleus (CeA), mesencephalic trigeminal nucleus (Mes5), contralateral superior colliculus (SC), contralateral medial dorsolateral cerebellar nucleus (MedDL), ipsilateral dorsolateral interposed cerebellar nucleus (IntDL) and M1 motor cortex.

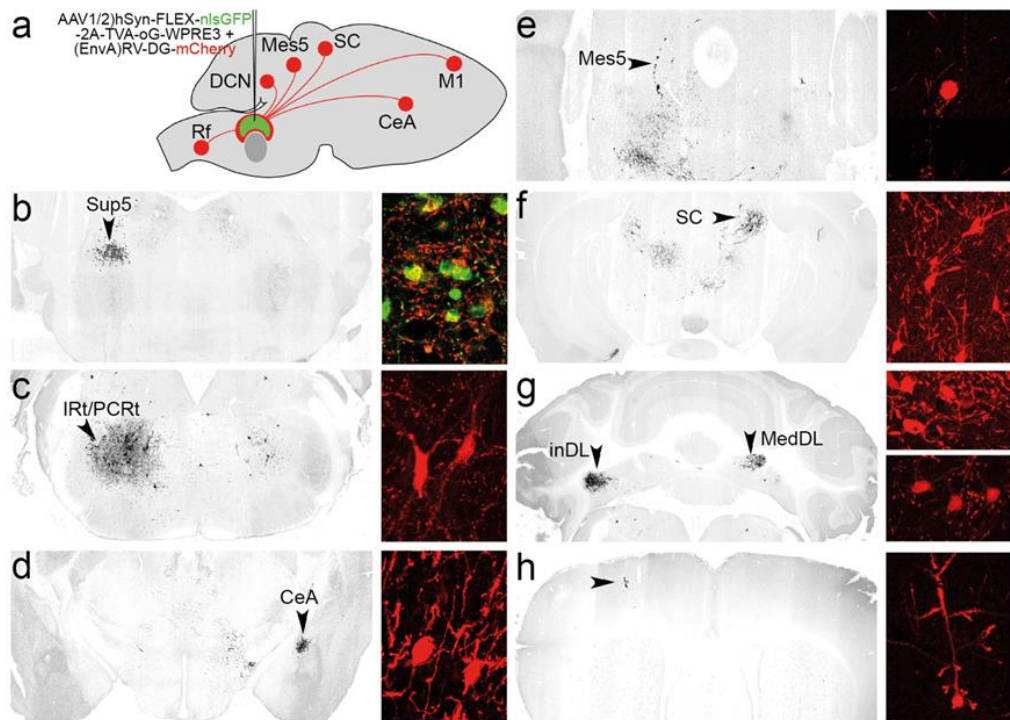


Fig. 5: Optogenetic activation of Sup5^{Phox2b} (see below) (a) Schematic of viral-mediated excitatory opsin transduction and fiber-optic implantation for in-vivo stimulation of Sup5^{Phox2b} and (b) coronal section through the rostral medulla at the level of Mo5(ChAT+), showing transduced Sup5^{Phox2b} neurons (mScarlet) and the fiber tract position with respect to this nucleus. (c) Schematic showing set-up for stimulating Sup5^{Phox2b} with blue light while video-recording jaw movements in head-fixed mice during licking. (d) Profile view of the jaw before (left panel) and after (right panel) Sup5^{Phox2b} photostimulation. Note the adduction of the lower jaw after photostimulation in the right panel. (e) Example trace of tracked jaw position during photostimulation of Sup5^{Phox2b} at 5Hz (10ms pulses). Lower jaw adduction faithfully follows the pattern of photostimulation. (f) Acute EMG recordings of the masseter in an anesthetized mouse during photostimulation of Sup5^{Phox2b}. (g,h) Protocol for triggering optogenetic stimulation of Sup5^{Phox2b} during licking. A pulse generator was programmed to deliver pulses of light of 1s duration 480ms after the first tongue contact with the lick port. In this way, optogenetic stimulation of Sup5^{Phox2b} was triggered after ≥ 4 consecutive licks. This resulted in robust interruption of volitional licking in all tested mice (n=4). (i) Representative portrait images of a mouse's face at rest (left), during lapping (middle) and after optogenetic stimulation of Sup5^{Phox2b} (right) during a licking bout. Note the enhanced adducted posture of the jaw compared to the 'rest state'.

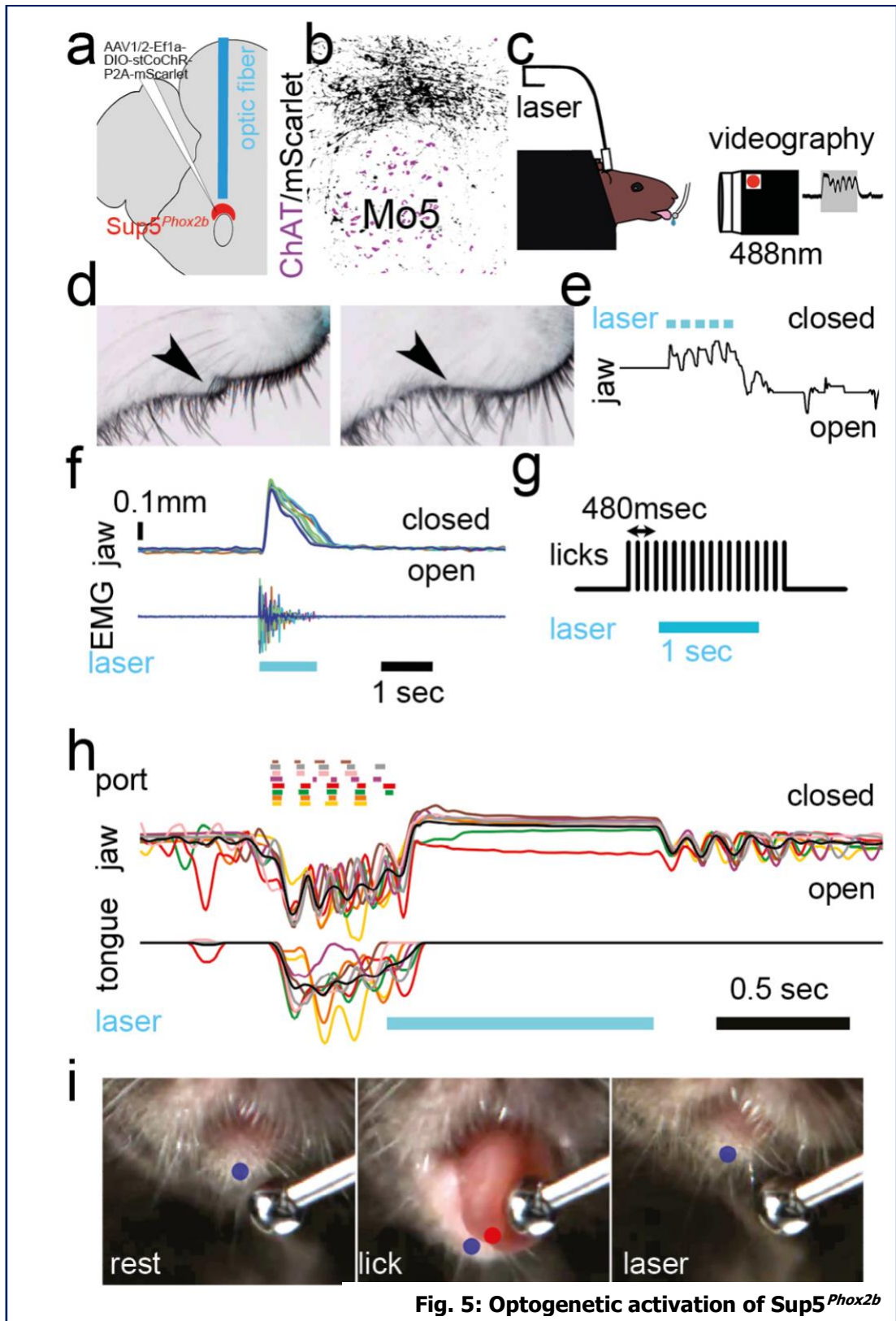


Fig. 5: Optogenetic activation of Sup5^{Phox2b}

Fig. 6: Spontaneous activity of Sup5^{Phox2b} (see below) (a) Schematic of virally-mediated transduction of a GCaMP7s actuator in Sup5^{Phox2b} and (b) coronal section through the hindbrain at the level of Mo5 showing GCaMP7s-expressing cells in this nucleus and post-hoc diagnosis of the optic fiber tract position. (c) Schematic illustrating the experimental set-up for fiber photometry recordings of Sup5^{Phox2b}. Sup5^{Phox2b} activity was monitored in behaving (spontaneously chewing or licking) head-fixed animals via GCaMP7s fluorescence excited by 465 nm light. Excitation at 405 nm (isosbestic point) provided a control for motion artefacts. (d, e) Example trace of normalized changes in bulk GCaMP7s fluorescence during spontaneous licking bouts in head-fixed mice. Contact events with the lick port and movements of the jaw and tongue on the Y-axis are also shown. Note that changes in bulk fluorescence in Sup5^{Phox2b} specifically tracked jaw movements and were independent of tongue protrusion during licking (d). Below (e) are example profile frames of a mouse's face during lapping, showing DeepLabCut-tracked positions of the jaw on the Y-axis during fiber photometry experiments. From left to right: jaw at rest, jaw in a partially-abducted position during the opening phase of lapping, jaw in fully abducted position while the tongue makes contact with the lick port and return of the jaw to baseline position. (f, g) Example trace of normalized calcium transient recorded during spontaneous chewing in head-fixed mice. A complex pattern of GCaMP7s fluorescence emerged during chewing: an initial large increase in bulk fluorescence that correlated with the biting phase preceded a chewing epoch, followed by small amplitude, higher frequency increases in fluorescence (black arrowheads) that occurred at the same frequency as rhythmic chewing (red arrowheads). Shown in (g), from left to right, are corresponding profile frames of a mouse's face before biting, during biting and during chewing, including the tracked positions of the jaw on the Y-axis during photometry recordings. (h) Example traces of bulk GCaMP7s fluorescence changes during licking bouts (left), chewing an almond (middle) and chewing pasta (right). Note the difference in amplitude of fluorescence changes between licking bouts and chewing hard foods.

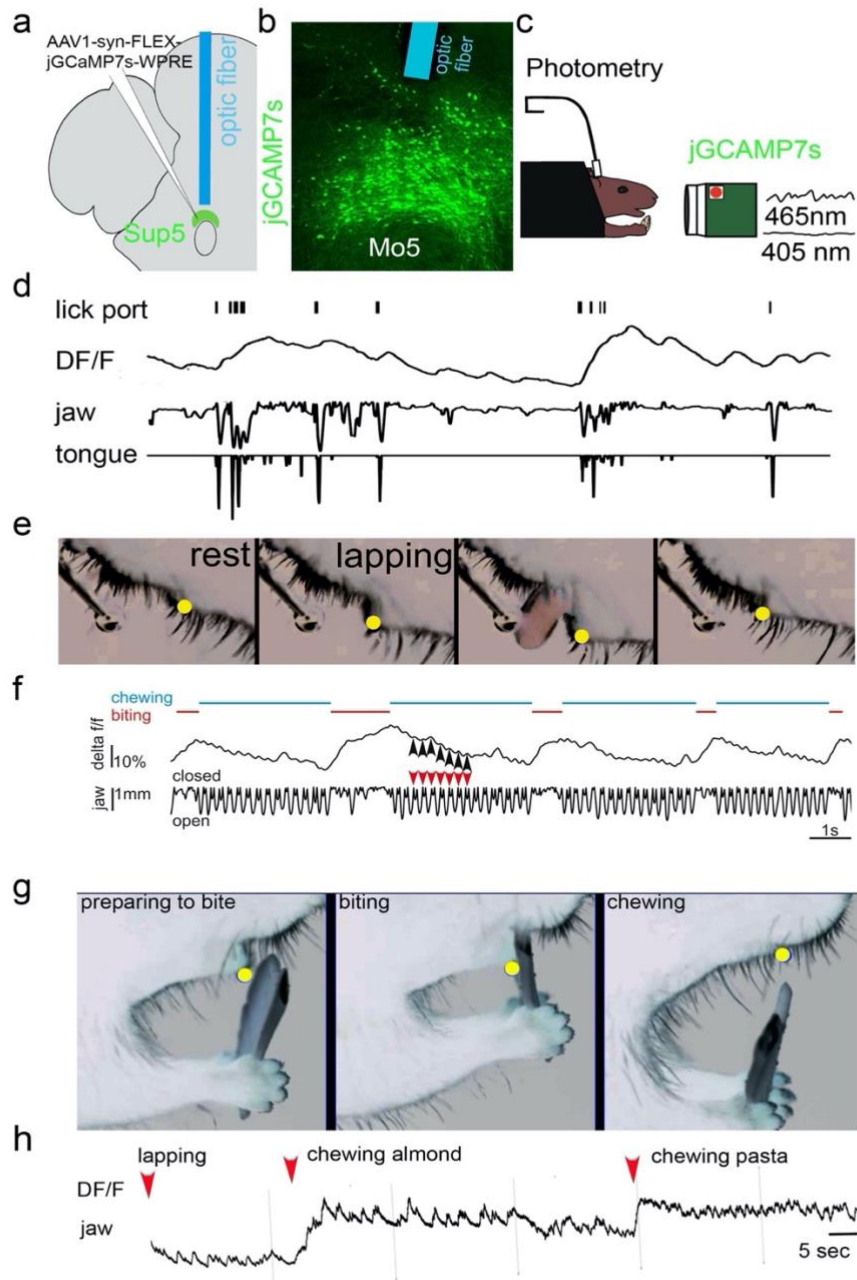


Fig. 6: Spontaneous activity of Sup5^{Phox2b}

METHODS

Mouse strain, sex, and age

The following transgenic mouse lines were used: Phox2b::Cre(**d'Autréaux et al., 2011**), VGlut2-ires::Cre(**Vong et al., 2011**), Tau::Syp-GFP, Rosa::nlsLacZ (also known as Tau^{mGFP}(**Pecho-Vrieseling et al., 2009**)), HoxA2::Cre (**Ren et al., 2002**), Phox2b:LacZ (**Pattyn et al., 1999**). For behavioral experiments, all mice were produced in a B6D2 background. Experiments were performed on embryos at embryonic (E) days E9.5–17.5, neonate pups at postnatal day 2–8 (P1–8), and adult (P30–56) animals of either sex. All experimental procedures and protocols were approved by the Ethical Committee CEEA-005 Charles Darwin (authorization 26763-2020022718161012) and conducted in accordance with EU Directive 2010/63/EU. All possible measures were taken to minimize the suffering and number of animals used.

Animal husbandry

Animals were group-housed under standard housing conditions: room temperature clamped at 21–22 °C, humidity between 40 and 50%, and *ad libitum* access to regular chow and water. They were maintained in a conventional 12-12-h light/dark cycle except for animals implanted for optogenetics and photometry experiments, which were subjected to a 12h reverse light/dark cycle and tested in the dark phase.

Viral vectors for tracing, optogenetic, and fiber photometry experiments

All viral injections were carried out unilaterally in phox2b::cre mice, except for masseter muscle injections, for which wild-type pups were used.

Anterograde tracing from Sup5^{Phox2b} was carried out by injecting 250 nl of a Cre-dependent AAV - pAAV-*hSyn-FLEX-mGFP-2A-Synaptophysin-mRuby* (Titer 7×10^{12} viral genomes (vg)/ml, Addgene #71760-AAV1)- which expresses membranous GFP in infected neurons and a red fluorescent reporter mRuby fused to the synaptophysin gene which accumulates in the synaptic boutons, enabling labeling of target neurons (**Beier et al., 2015**).

Retrograde transsynaptic tracing from the masseter muscle was carried out by injecting 50 to 100 nl of a 1:1 viral cocktail of G-deficient rabies (*RABV-*

SADB19-ΔG-mCherry; titer: 1.3×10^9 TU/ml, Viral Vector Core—Salk Institute for Biological Studies) and a G-complementing helper virus (*HSV-hCMV-YFP-TVA-B19G* (titer: 3×10^8 TU/ml, Viral Core MIT McGovern Institute).

Retrograde tracing to label inputs of *Sup5^{Phox2b}* was carried out by a two-step tracing strategy: First, 50 nl of a Cre-dependent AAV- *AAV1/2-Syn-flex-nGToG-WPRE3* (titer: 8.1×10^{11} vg/ml, Viral Core Facility Charité) - which packages genes for an EnvA-interacting receptor (TVA), a nuclear green fluorescent protein (NLS-GFP) as well as an optimized G protein (oG; Kim et al., 2016) was injected into the *Sup5*. Two weeks later, EnvA-pseudotyped rabies (EnvA-RABV-SADB19-ΔG-mCherry; titer: 3.1×10^8 vg/ml, Viral Vector Core, Salk Institute for Biological Studies) was injected at the same coordinates in the *Sup5*. This construct initiates retrograde transport to presynaptic neurons of *Sup5* by specifically infecting the GFP+/TVA+ neurons, which then express the red fluorescent reporter mCherry. After an additional 7 days, the brains were harvested and the presynaptic neurons were sorted by their location against the Paxinos Atlas.

For optogenetic and photometry experiments, 250 nl of an opsin-expressing AAV (*AAV1/2-Ef1a-DIO-stCoChR-P2A-mScarlet* (Forli et al., 2021); titer: 3×10^{13} vg/ml, kind gift from O. Yzhar) or 250 nl of a GCaMP-expressing AAV (*AAV1-syn-FLEX-jGCaMP7s-WPRE* (titer: 1×10^{12} vg/ml Addgene #104487-AAV1) were respectively injected into the *Sup5*.

Surgical procedures

• Stereotaxic injections and implants

Phox2b::Cre mice were anesthetized with an intraperitoneal injection of 50 mg/kg Zoletil (Zoletil 100, Virbac Sante Animale, France) and 10 mg/kg Xylazine (Rompun, 2%). 30 minutes before the start of surgery, buprenorphine ((0.3 mg/mL, 0.1mg per kg body weight, Buprecare)) was administered subcutaneously as analgesia. Mice's core temperature was maintained within the physiological range using a homeothermic pad (37.5-38°C). Briefly, anesthetized animals were placed in a stereotaxic frame (Kopf), and 100 μl of lidocaine (2%) was injected under the skin overlying the skull for local analgesia. Standard surgery was performed to expose the brain surface above the *Sup5* at the following stereotaxic coordinates: bregma -5.00mm, lateral +1.40mm, dura -2.80mm to target the *Sup5^{Phox2b}* neurons. For viral injections, 50-250 nL volumes were delivered at the rate of 75-100nL per minute via quartz glass capillaries (QF100-50-7,5, WPI) backfilled with

mineral oil with a 10 μ L Hamilton syringe (701 RN) connected to a pump (Legato 130, KD Scientific, Phymep, France). After infusion, the injection capillary was maintained in position for 5 min to reduce backflow of the virus during retraction of the capillary. For optogenetics experiments, 200 μ m core optic fibers (0.39NA, Smart Laser Co., Ltd) were placed at the same dorsoventral coordinates as the injections. For photometry experiments, optic fibers (0.57 NA, Smart Laser Co., Ltd) were implanted 200 μ m below the injection sites (Dura -3.00 mm). An anchor screw was then placed into the cranium on the contralateral side to the implant and injection site and the optic fibers were secured via a ceramic ferrule and the anchor screw to the skull by UV-cured dental adhesive cement (Tetric Evoflow, Ivoclar Vivadent). Head-fixation implants (Ymetry, Paris France) were positioned on the skull and similarly affixed with dental adhesive cement. Mice recovered from anesthesia on a heating pad for a day before being placed back in their home cages. Appropriate postsurgical care was provided, and animals were regularly monitored for signs of infection, pain, or lethargy until behavioral assays began.

- ***Intramuscular masseter injections***

All masseter muscle injections were performed at P3 neonatal stage. Pups were anesthetized by deep hypothermia: for induction, pups were placed in latex sleeves buried in crushed ice for 3–5 min, and anesthesia was maintained (up to 10 min) by placing pups on a cold pack (3–4 °C). A small incision was made in the skin and the viral cocktail was injected via a pneumatic dispenser (Picospritzer) connected to a glass pipette (tip diameter ca. 0.1 mm) that was guided into the masseter with a 3D micromanipulator. Muscular filling with the viral cocktail was typically achieved with 5–10 pressure pulses (100 ms, 3–5 bars) and was verified by the spreading of Fast-Green dye (0.025%) added to the viral solution. After injection, the pipette was withdrawn, and the incision irrigated with physiological saline and closed using a 10-0 gage suture (Ethilon). After recovery on a heating pad, pups were promptly returned to the mother, and the brains were harvested six days post-injection.

Histology

Depending on the stage, histology of the brain was carried out either on whole embryos dissected out of uterine horns (up to E16.5) or dissected out of the cranial vault of embryos (E17.5 to P0). Adults and postnatal animals were euthanized by an intraperitoneal injection of pentobarbital (Euthasol

Vet,140mg/kg), perfused with ice-cold PBS followed by 4% freshly prepared PFA. Brains or embryos were then postfixed in 4% PFA overnight at 4 °C, then rinsed 3 times for 30 minutes each in PBS followed by cryoprotection in 15% sucrose in PBS, overnight at 4 °C. Tissues were then embedded in gelatin-sucrose solution (7.5% gelatin in 15% sucrose in PBS) and frozen for cryo-sectioning at 30-60 µm on a CM3050s cryostat (Leica). Sections were washed for 1 h in PBS and incubated in blocking solution (5% calf serum in 0.5% Triton-X100 PBS) containing the primary antibody, applied to the surface of each slide (300 µl per slide) placed in a humidified chamber on a rotating platform. Incubation lasted 4–8 h at room temperature followed by 4 °C overnight. Sections were washed in PBS (3 × 10 min), then incubated with the secondary antibody in blocking solution for 2 h at room temperature. They were protected from light in aluminum-covered slide mailers during PBS washes (3 × 10 min), air-dried, and mounted under a coverslip with a fluorescence-mounting medium (Dako). Primary antibodies used were: goat anti-Phox2b (RD system AF4940, 1:100), rabbit anti-peripherin (Abcam ab4666, 1:1000), guinea pig anti-Lmx1b (Müller et al., 2002, 1:1000), goat anti-ChAT (Millipore AB144p), 1:100), chicken anti-βGal (Abcam, ab9361, 1:1000), chicken anti-GFP (Aves Labs, GFP-1020,1:1000), Rabbit anti-Lmx1b (Müller et al., 2002, 1:2000), guinea pig anti-Lbx1, 1: 10000) and Rabbit anti-DsRed(1:500).

All secondary antibodies were used at 1:500 dilution: donkey anti-chicken 488 (Jackson laboratories, 703-545-155), donkey anti-chicken Cy5 (Jackson laboratories, 703-176-155), donkey anti-goat Cy5 (Jackson laboratories, 705-606-147), donkey anti-rabbit 488 (Jackson laboratories, 711-545-152) donkey anti-rabbit Cy5 (Jackson laboratories, 712-165-153), donkey anti-rat Cy3 (Jackson laboratories, 711-495-152), and donkey anti-Guinea pig Cy3 (Jackson laboratories, 706-165-148). Epifluorescence images were acquired with a NanoZoomer S210 digital slide scanner (Hamamatsu Photonics) with NDPview2+; and confocal images with a Leica SP8 confocal microscope (Leica) with Leica Application suite X. Image formatting, including adjustments of brightness and contrast and pseudocoloring, was carried out in Adobe Photoshop and FIJI.

Behavioral experiments

- ***Habituation and training***

All behavioral experiments were carried out 3-4 weeks after viral injections and optic fiber implantation. Typically, habituation to handling, head

fixation and tethering to the patch cable began two weeks post-surgery and were initially implemented daily for 3-5min and gradually extended to a final duration of 10 min which corresponded to the length of a recording session. Mice were introduced into a plastic tube (4 cm diameter) that was mounted onto a small aluminium breadboard (450mm X 450mm X 12.7mm, ThorLabs; MB4545/M) and head fixed via custom-made head fixation implant to a fast fixation system (Ymetry, Paris France) with head protruding out and forepaws resting on the tube edge. Animals were systematically rewarded with a hazelnut after each habituation session. Animals were water-deprived for 12 h prior to optogenetics and photometry experiments to increase their motivation for fluids. During the trial sessions, mice were given 15% sucrose solution via a lick port to induce licking behavior. Mice were illuminated from below and from the sides with white LED lights to highlight the jaw silhouette during video acquisitions, which were carried out at 120 Hz.

- ***Head-fixed chewing assays***

Animals were food deprived for 12 hours and trained over several days to pick up food pieces (either an almond flake or a pasta) and chew while head-fixed and tethered to the fiber photometry patch cable. They were then video recorded during freely-initiated chewing epochs.

- ***Optogenetics***

For optogenetic excitation of Sup5^{Phox2b} neurons, a surgically implanted fiber-optic cannula was connected to a 473-nm DPSS laser (CNI, Changchun, China) through a patch cord (200 μ m, 0.37 NA) via a zirconia mating sleeve (Thorlabs). The pulse onset, frequency, and duration were controlled by a pulse generator (accupulser, WPI) connected to the laser system, and was programmed to deliver single continuous light pulses of 50–1000 ms or trains of 100 ms pulses at 5 Hz. The minimal laser output sufficient to elicit a response was used in all behavioral experiments and measured to be \sim 5 mW at the fiber tip using a digital power meter (PM100USB, Thorlabs). All laser stimuli were separated by minimal periods of 10 s. Laser output was digitized at 1 kHz by a NI USB-6008 card (National Instruments) and acquired using Spike 2 (CED Spike 2 Data Acquisition & Analysis Software).

- *Optogenetics during licking bouts*

Two weeks post-recovery from surgery, mice were habituated for several days (20-min/day) to being head-fixed inside a 5cm cylindrical tube and tethered via the optical implant. Mice were then filmed in 10 min trial sessions while they received pulses (1000 ms) of optical stimulation that were triggered 480ms after licking onset during a discrete licking bout (>6 successive licks). This duration was calculated from the average licking rate (7Hz, n= 4 mice) and corresponds to approximately 4 licks. We alternated the stimulation onset within a session such that a spontaneous licking bout(control trial) was followed by a bout during which the laser was triggered (laser trial). Thus, this protocol selectively initiates optical stimulation on average 4 licks after a spontaneously initiated bout every other bout.

- *Optogenetics during spontaneous feeding*

Mice were habituated to being tethered to the patch cable in their home cage for at least three days before the behavioral sessions began. During habituation, they were regularly given an almond to reduce neophobia towards this food prior to testing. Mice were then filmed in 5 min trial sessions in their home cage while they received pulses of optogenetic stimulation during spontaneous chewing epochs. Videos and spike data were analyzed offline to investigate the effect of laser stimulations on chewing behavior.

- *Acute electromyographic recordings*

Prior to the electromyography (EMG) recordings, mice were anaesthetized with an intraperitoneal injection of a mixture of 50 mg/kg Zoletil (Zoletil 100, Virbac Sante Animale, France) and 10 mg/kg Xylazine (Rompun, 2%). Bipolar electrodes were prepared from 30-cm-long stainless steel wire coated with Teflon (140 μ m; Phymep, s.a.r.l, France) as published (**Loeb & Gans, 1986**). The wire was exposed over 1mm at the tip by stripping the Teflon insulation and the bared region was threaded into a hypodermic needle(0.6 mm). After exposing the masseter via a small overlying incision, the needle was used to guide the electrode into the muscle. A ground electrode was similarly inserted into the neck skin. The electrodes were then connected via electrode cables to a Backyard Brains® Muscle Spiker Box Pro and the EMG signal was digitized by a NI USB-6008 card (National Instruments) and acquired using DORIC Neuroscience studio software. A TTL signal input from

the laser connected to the same acquisition board served as timestamp for optogenetic excitation.

- ***Fiber photometry***

A conventional fiber photometry system for behaving animals was employed (Doric Lenses Inc, Canada) to record GCaMP fluorescence excited by 405 nm light (isosbestic point), and its calcium-dependent fluorescence excited by 465 nm light using a single photodetector. The photometry hardware was controlled via Doric neuroscience studio software interface (Doric Lenses Inc, Canada) to acquire the photometry signal. In practice, 2-channel LED drivers sinusoidally modulated the 465 and 405 nm LED wavelengths at 208.616 and 572.205 Hz, respectively (to reduce sensitivity to electrical system harmonics at frequencies of 50/60, 100/120, and 200/240 Hz) at an intensity of 30 μ W. Modulated excitation light was directed by an optical assembly (iLFMC4, Doric Lenses Inc, Canada) onto an implanted fiber-optic cannula (diam. 200 μ m, 0.57 NA) via a low-autofluorescence optical patch cord of matching diameter and NA. The emitted signal was then returned via the same patch cord to a fluorescence detector head mounted on the optical assembly and amplified. The detected fluorescence signal was acquired at 12 kHz via a data acquisition unit (Doric fiber photometry console) and then demodulated in real time to reconstitute the excited isosbestic and calcium-dependent GCaMP signals. Tongue contacts with the lickport during spontaneous licking were detected by an SEN-1204 capacitance sensor (Sparkfun) that was connected to an Arduino Uno R3 microcontroller board (Arduino) and acquired at 12 kHz via the Doric fiber photometry console.

Automated markless pose estimation

Spontaneous and light-evoked jaw adduction sequences were filmed at portrait and profile angles with a CMOS camera (Jai GO-2400-C-USB) synchronized by a 5V TTL pulse. The acquired frames (800 \times 800 pixels, 120 fps,) were streamed to a hard disk using 2ndlook software (IO Industries) and compressed using a MPEG-4 codec. Portrait views were used for video tracking of optogenetically-evoked oromotor movements.

Using DeepLabCut (version 2.0.771), a 2 ResNet-50 based neural network was trained on either profile or portrait frames of a mouse's face (20 frames (800 \times 800 pixels each) per mouse, n=4 each) for >500,000 iterations

to identify the tip of the tongue and lower jaw during licking or chewing. Y-axis position cartesian estimates of the lower jaw and tongue were then generated by the network for experimental videos.

Data analysis

- ***Fiber photometry***

Behavioral and fiber photometry data were analyzed using custom-written Python scripts (Python version 3.7, Python Software Foundation). Fiber photometry and photostimulation data were resampled to 120 Hz to match the acquisition rate of video recordings. Photometry data were processed by applying a low-pass filter (Butterworth) to the calcium-dependent 465 nm and isosbestic 405 nm signals with a 20 Hz cut-off. The 465 nm signal was then normalized using the function $\Delta F/F = (F - F_0)/F_0$, in which F is the 465 nm signal, and F₀ is the least-squared mean fit of the 405 nm signal.

- ***Normalization of jaw and tongue pose estimation***

Cartesian pixel estimates of the jaw and tongue were corrected to a 5 mm scale bar within the video frame and smoothed using the Savitzky-Golay filter. For optogenetic photostimulation, the jaw position was normalized to its averaged location 50–100 ms prior to stimulation. For fiber photometry experiments, the jaw position was normalized to its average location during quiet periods between 1–3 s long.

DISCUSSION

In this work, we describe three hindbrain nuclei, IRt^{Phox2b} , $Peri5^{Atoh1}$ and $Sup5^{Phox2b}$, that drive qualitatively distinct orofacial behaviors related to the ingestion of food and liquids. Salient aspects of their function, connectivity, and ontogeny as well as directions for future studies are discussed below.

IS IRt^{Phox2b} REQUIRED FOR LAPPING?

We showed that optogenetic stimulation of IRt^{Phox2b} neurons drives a licking behavior in vivo, but did not establish their requirement for licking, which will require loss of function experiments. In vitro, depending on the mechanism of rhythm generation in IRt^{Phox2b} (see below), the network could either be pharmacologically silenced (e.g., by blocking chemical or electrical synaptic neurotransmission) in a slice preparation while monitoring motor output activity of the XIIth nerve, or by expressing an inhibitory opsin in IRt^{Phox2b} and monitoring the output of nXII. In vivo, we attempted (unpublished data) to acutely silence IRt^{Phox2b} by bilaterally expressing a light-gated chloride channel (eGTACR1) in this nucleus but licking appeared to be refractory to optogenetic silencing (although we did not quantify licking under those conditions and might have missed subtle changes in licking parameters). This may either reflect the inefficiency of short-term optogenetic silencing (Takato et al., 2022) or the fact that IRt^{Phox2b} is not necessary to induce licking and parallel pathways can also elicit this behavior. A more drastic inactivation approach such as permanently silencing IRt^{Phox2b} by expression of the tetanus light chain toxin (TeLC) should be investigated (**Schiavo et al., 1992**).

IS IRt^{Phox2b} A LAPPING CPG?

We showed that optogenetic stimulation of IRt^{Phox2b} neurons drives rhythmic jaw opening and tongue protrusion in vivo. This is consistent with the findings of (**J. B. Travers et al., 1997c**) who find that many IRt neurons are rhythmically active during licking in awake animals, although there was neither a genetic signature for the recorded neurons, nor a causal role. Our results suggest that IRt^{Phox2b} premotor neurons are sufficient to induce licking behavior in vivo and thus either constitute a CPG or form part of a wider CP(R)G network underlying rhythmic licking. The 'gold-standard' to prove the former hypothesis would be to demonstrate both the sufficiency and necessity

of IRt^{Phox2b} for fictive rhythmic licking in vitro (**Marder & Bucher, 2001**). In practice, due to uncertainty about the operational mode of CPGs in general, this would necessitate several lines of investigation that would collectively support or invalidate this hypothesis.

Rhythmicity could be the result of intrinsic pacemaker properties of IRt^{Phox2b} cells or a network property (**Marder & Bucher, 2001**). To test the intrinsic pacemaker hypothesis, whole-cell recordings of IRt^{Phox2b} in brainstem slices (see details of the preparation below) would be necessary to determine if there is a rhythmic oscillation of membrane potential in these neurons. Such a preparation should be done in $Phox2b::Cre^{+/-}; Rosa^{Tdt+/-}$ mice to visualize $Phox2b+$ cells (which are intermingled with $Phox2b^{-}$ ones) and treated with a cocktail of chemical (e.g., NBQX, APV, picrotoxin, and strychnine) or electrical (e.g., CBX, LTCC (nifedipine)) synaptic transmission blockers typically used to halt synaptic communication between neurons (**Wei et al., 2022b**). Persistent synchronous rhythmicity of IRt^{Phox2b} neurons under such conditions would support the 'intrinsic rhythmicity' hypothesis. It should be noted that robust intrinsically oscillatory neurons are seldomly present in circuits, probably as this would render them less flexible to external modulation (**Marder & Bucher, 2001**).

A further complication (since licking is a transient behavior — volitional or reflex — and the licking CPG likely conditional) is that the putative rhythmic activity in IRt^{Phox2b} is unlikely to be spontaneous in vitro and will require transient or tonic inputs to activate or gate it, for example by stimulating descending inputs, by directly adding exogenous neuromodulators (**Dickinson, 2006; Marder & Bucher, 2001**) or by elevating the extracellular $[K^{+}]$ (**Ballerini et al., 1999**). In line with this, glutamatergic transmission involving ionotropic glutamate receptors have been implicated in the genesis of ororhythmic behaviors in vitro. For example, both NMDA and non-NMDA receptor agonists drive rhythmical discharge of trigeminal motoneurons in a brainstem en bloc preparation (**Kogo et al., 1996**) and NMDA agonists induce alternating rhythmic activity in the trigeminal and hypoglossal nerves, which has been suggested to represent the neural correlate of suckling behavior (**Ihara et al., 2013**).

In practice, rhythmic activity in IRt^{Phox2b} neurons (monitored by whole cell recordings of by imaging GCaMP6f fluorescence expressed transgenically in $Phox2b::Cre; Ai95^{+/-}$ mice (**Madisen et al., 2015**)) in a minimal slice preparation that isolates this nucleus (i.e., extending from the caudal pole of the facial motor nucleus to the rostral pole of the Nucleus ambiguus (thus

excluding the preBötC and the attendant inspiratory drive on the nXII)) should correlate with rhythmic nXII output to the tongue (preserved in the slice and monitored by extracellular recordings with suction electrodes) during bath application of (empirically tested) glutamatergic excitatory agonist(s). Another strategy to access (and activate) this putative conditional pacemaker in vitro would involve emulating descending inputs onto IRt^{Phox2b} by electrical stimulation. Our retrograde tracing experiments revealed inputs from the NTS as well as longer-range inputs from the motor cortex that project to IRt^{Phox2b} neurons (**Fig 5b,g**). Therefore, the experiment described above could be reproduced using a thicker slice preparation in which the NTS or the pyramidal tract are stimulated to engage the CPG.

Even if a rhythm emerges in a network in vitro, its assignment to a particular behavior in vivo remains challenging in mammals (**Kogo et al., 1996; Marder & Bucher, 2001**), especially if the same networks participate in many different pattern or rhythm generating circuits (**Lieske et al., 2000**). Indeed, (**Chen et al., 2001**) has suggested that the same circuits in IRt may underlie licking and gaping responses. Furthermore, technical limitations associated with slice preparations in vitro imply the restriction of experimental manipulations to neonatal stages (which are more resistant to anoxia). For orofacial ingestive behaviors, the caveat is that neural activity in neonatal slices may not correspond to a behavior in the adult, from which most physiological and behavioral data are collected: licking emerges in the adult while pups suckle, and it is not known what changes in neural substrates (e.g., refinement of networks) and/or function (e.g., as a result of developmental differences in expression of neuronal ionic channels), underlie the transition between these behaviors — although evidence suggests that a maturation in the neural control of orofacial movements is not uncommon during development (**S. Nakamura et al., 2008; Takatoh et al., 2013b, 2021c**). In view of the above limitation, recording the in vivo activity of IRt^{Phox2b} during licking will be required to complement in vitro demonstrations of rhythmicity in this nucleus. To investigate whether IRt^{Phox2b} is rhythmic during licking in vivo, extracellular multielectrode recordings of ChR2-expressing IRt^{Phox2b} neurons could be carried out while tracking licking behavior in awake head-fixed mice implanted with an optetrode (**Anikeeva et al., 2012**). Delivering brief pulses of 473 nm light in IRt^{Phox2b} during spontaneous licking should result in short-latency, light-induced antidromic spikes in lick-active IRt^{Phox2b} units (opto-tagging). The activity of tagged units can then be analyzed to determine if they are rhythmic and if rhythmic bursting is time-locked to licking in vivo.

The second broad hypothesis is that rhythmicity is an emergent network property of IRt^{Phox2b} , i.e., rhythmicity arises in tonically firing IRt^{Phox2b} neurons

as a result of local excitatory or inhibitory feedbacks on them. An excitatory input could come from IRt^{Phox2b} neurons themselves (which are glutamatergic). Suggestive of this, we found that individual genioglossus premotor IRt^{Phox2b} neurons receive inputs from IRt^{Phox2b} neurons themselves (unpublished data). This hypothesis could be explored using a 'circuit optogenetics' approach, e.g., by coupling all-optical-interrogation approaches (**Emiliani et al., 2015**) with cellular specificity provided by a new transgenic line, Ai203(Bounds, n.d.), in which a red-shifted (to reduce optical crosstalk during imaging) excitatory opsin (ChroME) and a calcium actuator (GCaMP7s) are coexpressed in genetically defined cells. In this protocol, the activity of IRt^{Phox2b} cells in $Phox2bCre^{+/-}; Ai203^{+/-}$ slices can be monitored with two-photon (2P) calcium imaging, while the activity of individual IRt^{Phox2b} neurons (or microcircuits) is manipulated(e.g., subthreshold depolarization) with millisecond resolution by holographic optogenetics, such as the 2P-multiplexed temporally focused light shaping (MTF-LS) technique (**Accanto et al., 2019**). This approach would provide insight into the precise functional organization of IRt^{Phox2b} at the microcircuit level.

Alternatively, the rhythm generator could consist of $Phox2b^{-}$ neurons downstream of IRt^{Phox2b} , in the IRt or elsewhere, which would be the recipient of tonic drives from IRt^{Phox2b} neurons. For example, IRt^{Phox2b} neurons are largely intermingled with other cell-types, such as *Dbx1*-expressing neurons, some of which are premotor to the XIIth motor nucleus(Gray, 2008b)(Wu et al., 2017). One argument in favor of such a scenario is that IRt^{Phox2b} activity recorded with fiber photometry during lapping was not rhythmic (whereas with the same Ca²⁺ actuator (GCaMP7s) we detected a rhythmic activity in $Sup5^{Phox2b}$, see below). On the other hand, IRt^{Phox2b} neurons are themselves premotor to the rhythmically entrained motoneurons (**Fig 1b**), which would make counterintuitive or even paradoxical their relegation to some tonically active upper layer of the circuitry.

Finally, rhythmic licking requires an alternation between opposite movements (tongue protraction/jaw opening versus tongue retraction/jaw closing) which likely implies the rhythmic inhibition of antagonist interneurons, thus the involvement of $Phox2b^{-}$ neurons, since IRt^{Phox2b} neurons are exclusively glutamatergic. In support for this, both gabaergic and glutamatergic premotor neurons in the IRt/PCRT that project to Mo5 are recruited during rhythmic mastication (Y. Nakamura et al., 2017; Y. Nakamura & Katakura, 1995).

WIDER INTEGRATIVE ROLES FOR IRT^{Phox2b}

IRT^{Phox2b} receives converging inputs relevant for organizing ingestive motor behaviors in general: gustatory inputs from the overlying NTS and from parabrachial nucleus, oral somatosensory inputs from the mesencephalic nucleus of the trigeminal and descending inputs from the orofacial motor cortex and deep layers of the superior colliculus. This suggests that IRT^{Phox2b} could have a wider role than licking in ingestion. Interestingly, infusion of a GABA_A antagonist in the IRT is involved in switching oral motor responses from licking to gaping (Chen et al., 2001), suggesting that local interactions in IRT may underlie different oral ingestive behaviors in mice. (Stanek et al., 2014b) found premotors to the masseter in the dorsomedial IRT and (Han et al., 2017b) showed that inhibition of Gabaergic neurons in the PCRt induces chewing. In this vein, future studies could address whether these circuits interact with IRT^{Phox2b} to mediate chewing - which would thus participate in the control of different types of ingestive movements - or whether these neurons represent separate licking and chewing circuits. One could begin to address whether these neurons are also active during spontaneous chewing or gaping by performing fiber photometry of GCaMP7f fluorescence in IRT^{Phox2b}. Next, other photostimulation protocols to excite IRT^{Phox2b} may be tested (e.g., different pulse frequencies or laser power) to determine if other types of ingestive responses may be induced. In addition, manipulation of other excitatory and inhibitory cell types intermingled with IRT^{Phox2b} may help determine to what extent functionally distinct circuits are present in this region.

INTEGRATIVE ROLE OF Sup5^{Phox2b}

We found that Sup5^{Phox2b} provides a strong input to jaw closing muscles, is active during phasic jaw closure and rhythmic jaw movements and is capable of interrupting the latter when tonically activated. Sup5^{Phox2b} receives inputs relevant for modulating chewing behavior: spindle afferent proprioceptive inputs from Mes5 (Fig 4e) probably involved in prolonging jaw muscle resistance during biting via a disynaptic jaw stretch reflex (P. Luo et al., 2001), inputs from the motor cortex, cerebellum and superior colliculus involved in sensorimotor integration of jaw movements (Fig 4 f, h) (Benavidez et al., 2021; Ferreira et al., 2019; Goldberg, J.G., 1990; Liu et al., 1993). The functional relevance of monosynaptic CeA inputs to the Sup5^{Phox2b} is less obvious. It has been shown that gabaergic CeA inputs to gabaergic PCRt neurons that project to Mo5 promote biting via a disinhibitory mechanism (Han et al., 2017b). It is thus not clear how inhibitory inputs from the CeA might regulate biting and jaw closure via an exclusively glutamatergic

Sup5^{Phox2b}-Mo5 pathway. One role of the CeA-Sup5^{Phox2b} pathway may instead be to inhibit jaw closure to allow opening of the jaw characteristic of the first phase of rhythmic chewing (**Rioch, 1934**) or for the expression of aversive responses (e.g., gaping) (**Van Daele et al., 2011**). Altogether, Sup5^{Phox2b} appears to constitute an important premotor node for biting and mastication, whose requirement remains to be tested with the techniques outlined for IRt^{Phox2b} (see above). Unlike IRt^{Phox2b}, we could not elicit a rhythmic behavior from Sup5^{Phox2b}, despite its activity being detectably rhythmic during chewing. Thus, Sup5^{Phox2b} is either downstream of the masticatory CPG (which is indeed so far hypothesized to lie further caudally (**Lund, 1991**), or it is part of this CPG, but the stimulation protocol used to excite Sup5^{Phox2b} in our experiments was not physiologically salient for inducing rhythmic chewing in vivo. Indeed, studies suggest that 40-60 Hz stimulations of the cortex are required to induce rhythmic jaw movements in awake acute preparations (**Lund, 1991**). Ideally, injecting an opsin with faster kinetics, such as the soma-targeted ST-ChroMe (**Mardinly et al., 2018**) or ChRmine (**Marshall et al., 2019**) into Sup5^{Phox2b} would be determinant to evaluate the effect of higher frequency stimulations on jaw movement kinematics.

Two different calcium dynamics were observed during fiber photometry recordings of Sup5^{Phox2b} in head-fixed chewing mice: high frequency small-amplitude fluorescence changes and a slower fluorescence change of higher amplitude. It is conceivable that this output reflects the existence of two functionally specialized Sup5^{Phox2b} microcircuits: one that lies downstream of the masticatory CPG and relays the masticatory pattern to cranial motoneurons - including Mo5; and another that integrates orofacial sensory inputs from Mes5 to produce the appropriate discharge pattern in trigeminal motoneurons. Indeed, rhythmically active neurons were found in Sup5 during cortically-induced mastication (**Tomio et al., 1992**), and both periodontal and spindle inputs to Mo5 premotors (via fusimotor drive) have been implicated in the control of jaw-closing muscle activities and masticatory force through a positive feedback loop, particularly at the transition from the preparatory to the reduction series of chewing (**Lund, 1991; Tomio et al., 1992**). The qualitative difference in amplitude of fluorescence changes between chewing and licking might either reflect the additional recruitment of local premotor neurons, an increased firing of individual premotor neurons or an increased temporal coherence of firing of Sup5^{Phox2b} premotor neurons postsynaptic to Mes5 (**Fig 4e**) to produce higher forces contingent on occlusal loading during chewing of hard foods. In vivo functional imaging using a minimally invasive microendoscopy system such as Gradient-index (Grin) lenses (**Jung & Schnitzer, 2003**) might provide the cellular resolution necessary to elucidate putative microcircuit connectivity in Sup5^{Phox2b} during chewing.

(Takato et al., 2021c), in their monosynaptic tracing study in adults, found a large population of masseter premotor neurons in Sup5 (without genetic signature but in the location where we find many *Phox2b*⁺ neurons), whereas we observed much fewer Sup5 masseter premotor neurons in postnatal mice using the same tracing strategy (all of them expressing *Phox2b*). The difference possibly lies in the stage at which the tracing experiments were made and suggests that there is a further recruitment of Sup5 premotor neurons after P8 (the timepoint at which we terminated our tracing experiments), and which likely express *Phox2b* given that the majority of this nucleus comprises Vglut2-expressing neurons and all Vglut2⁺ neurons express *Phox2b*. This is pertinent given that mastication only arises at around P12 in mice (**Westneat & Hall, 1992**) concurrent with the eruption of teeth during weaning, suggesting that masticatory premotor recruitment might support this behavioral transition. This could easily be verified using the same three-step monosynaptic tracing technique to identify the adult premotor population in Sup5 that expresses *Phox2b*.

In the anterograde tracing experiments, in addition to Mo5, we found efferent inputs from Sup5^{*Phox2b*} to Acc5, Acc7 and the intermediate Mo7 bilaterally. The Acc5 and Acc7, which contain the motoneurons for the anterior and posterior bellies of the digastric, are involved in jaw opening. The intermediate Mo7 innervates the platysma involved in depressing the jaw. Together, these targets appear incoherent given the role of Sup5 in jaw closure. A plausible explanation is that these inputs represent projections from the dorsal segment of Peri5^{*Phox2b*}, a functionally distinct subnucleus yet contiguous with Sup5^{*Phox2b*} neurons, and which we could not avoid tracing from in *Phox2b::Cre* mice. Indeed, the efferent projectome of Peri5^{*Phox2b*}, using an intersectional genetic strategy to avoid tracing from the larger Sup5^{*Phox2b*} population, includes the Acc5 and Acc7 as well as the platysma. Thus it is likely that the Sup5^{*Phox2b*} nucleus is a heterogeneous population, which has implications for the interpretation of the functional manipulations of this nucleus. This work provides a first genetic signature for manipulating a subpopulation of glutamatergic neurons in the reticular formation dorsal to Mo5 neurons. A more refined molecular dissection of this nucleus will be required to be able to better understand its functions during orofacial behaviors. In addition to the *Atoh1* marker, we found that the dorsolateral part of Sup5^{*Phox2b*} expresses the gene *Cited1* (data not shown), which might be a candidate marker to further functionally parcellate this nucleus.

***Phox2b* AS A MASTER GENE FOR INGESTIVE BEHAVIORS**

My Ph.D. work reveals that large populations of pontine and medullary interneurons that are in a position to coordinate oropharyngeal movements for feeding and drinking express the homeodomain TF *Phox2b*. *Phox2b* is also expressed in the main downstream synaptic partners of these interneurons, branchiomotor neurons (**Pattyn et al., 2000b**). In addition, the NTS, made of second-order visceral sensory neurons that also express *Phox2b*⁺ (**Dauger et al., 2003**) and are indeed sister cells to IRT^{*Phox2b*} (**Dempsey et al., 2021**) also subserves a premotor role to branchiomotor neurons (e.g. in MoA, (**Hernandez-Miranda et al., 2017**)), and is pre-premotor to jaw openers and tongue protractors via IRT^{*Phox2b*} (**Dempsey et al., 2021**). Thus, *Phox2b* emerges as a circuit-wide determinant of the motor control of ingestive behaviors.

The other, previously described, and equally striking, physiological correlate of *Phox2b* expression is with the sensorimotor circuits of the visceral nervous system (with the exception of sympathetic premotor neurons) (**Brunet & Pattyn, 2002; Dufour et al., 2006b**). Even though oropharyngeal motor neurons (let alone premotor neurons) are not classically included in the autonomic nervous system, they have affinities with it that were recognized long ago. Branchiomotor neurons are developmentally close to preganglionic parasympathetic neurons. Even before any embryological data was available, their dorso-lateral position had inspired their grouping into the same “visceral” category (“general visceral” for preganglionic neurons, “special visceral” for branchiomotor neurons) (**Herrick, 1918**). We now know that they arise from the same progenitors (the pMNv neuroepithelial domain of the hindbrain) and share their transcriptional code (*Phox2a*⁺, *Phox2b*⁺, *Tbx20*⁺, *Hb9*⁻, *Lhx3/4*⁻), and indeed, are so far indistinguishable. The visceral anatomic and ontogenetic classification was paralleled by that of the muscles that they command, which are derived from the branchial or, “visceral arches” that surround the oral end of the digestive tube, not from the somites. From the start, the “visceral” category, concerning muscles as well as nerves, has encapsulated a combination of developmental and physiological arguments: visceral or somatic nerves and muscles were seen as having both different developmental pathways and different roles: in behaviors that subserve homeostasis and locomotion, respectively (**Romer, 1972**). Indeed, in the vertebrate ancestors, branchiomeric muscles and their neurons are devoted to feeding and breathing exclusively, thus directly relevant to homeostasis (even though they were recruited for additional roles in terrestrial vertebrate, such as facial expression or vocalization).

Thus, branchiomotor neurons could be included in a visceral nervous system *sensu lato* that would control not only homeostasis, but the ingestion of required fluids and calories. They could even represent its ancestral form: before the advent of the neural crest and epibranchial placodes, which are the source of much of the visceral (or “autonomic”) circuits in vertebrates, *Phox2b* was employed in motoneurons for ingestive and respiratory structures as in tunicates (**Dufour et al., 2006a**) or even mollusks (**Nomaksteinsky et al., 2013b**). The findings of my Ph.D. extend the boundary of this visceral nervous system *sensu lato* to include the layer of premotor neurons, that can coordinate oropharyngeal movements for feeding and drinking, including rhythmic ones. Thus, entire sensorimotor reflex circuits for food-related orofacial behaviors are made of *Phox2b*⁺ neurons. For example, taste aversive or appetitive motions (gaping, or lapping and biting) involve an afferent pathway made of *Phox2b*⁺ taste neurons in the geniculate, petrosal and nodose ganglia, and their target, the *Phox2b*⁺ NTS; and an efferent pathway, made of orofacial pre-motoneurons and motoneurons, most of which are *Phox2b*⁺. Moreover, in some cases at least, the NTS has a direct input on premotor neurons (**J. B. Travers et al., 1997a**)(**Dempsey et al., 2021**). Taste-induced salivation involves a similar circuitry, in which the efferent pathway is made of preganglionic neurons in the medulla (the salivary nuclei) and parasympathetic ganglia of salivary glands, all *Phox2b*⁺. Further processing of food and liquids is also under the control of *Phox2b*⁺ neurons: motor neurons for the esophagus (in MoA) and all enteric neurons, intrinsic and extrinsic (**Pattyn et al., 1997**).

From a developmental viewpoint, this remarkable correlation between *Phox2b* expression and physiological circuits suggests that *Phox2b* is developmentally key to the connectivity of *Phox2b* neurons. Recently a similar case was described in *C. elegans* (**Berghoff et al., 2021**), whereby another homeodomain transcription factor, *Prop1*, was found to be preferentially expressed in pharyngeal circuits.

As discussed at length in the introduction, ingestive movements also involve somatic muscles (tongue and hypobranchial muscles) derived from somites, and their somatic motoneurons. Thus, at the oropharyngeal border between the inside and outside of the body, the somatic and the visceral bodies meet and cooperate. The premotor centers Sup5^{*Phox2b*}, IRt^{*Phox2b*} and Peri5^{*Atoh1*}, which extend their axons beyond the world of *Phox2b* neurons towards the somatic motoneurons of Mo12, are a site of this integration.

Mes5 AS ORGANIZING CENTER FOR Sup5^{Phox2b}

An intriguing, although preliminary observation is that the development of Sup5^{Phox2b} seems to require the axons of Mes5, one of its main inputs. This would represent one of the rare observations, so far, of an input structure that organizes one of its main targets. A precedent are cranial nerves that transport the precursors of parasympathetic ganglionic neurons (the targets of their preganglionic fibers) to the site of ganglion formation (**Espinosa-Medina et al., 2014**). The influence of Mes5 could consist in attracting Sup5^{Phox2b} cells, or to specify them by inducing expression of *Lmx1b* in the *Phox2b*⁺ progeny of dB2 or *Phox2b* in the *Lmx1b*⁺ progeny of dB3 (since Sup5^{Phox2b} seems to have a dual origin in dB2 and dB3), or to insure their survival. Analysis of Sup5^{Phox2b} at earlier and later time points should help in sorting out these effects.

A caveat to my observation is that *Onecut1/2* (whose knock out entails the disappearance of the Mes5 tract) has a relatively broad and transient expression domain in the CNS, and could thus impact the development of Sup5^{Phox2b} in a cell-autonomous fashion. I am in the process of verifying the expression of *Onecut1/2* from E9.5 to E12.5. I also plan to examine the integrity of Sup5^{Phox2b} in another mutant in which the Mes5 tract might be deleted early on: *Brn3a* mutants, in collaboration with the laboratory of Tudor Badea.

REFERENCES

- Accanto, N., Chen, I.-W., Ronzitti, E., Molinier, C., Tourain, C., Papagiakoumou, E., & Emiliani, V. (2019). Multiplexed temporally focused light shaping through a gradient index lens for precise in-depth optogenetic photostimulation. *Scientific Reports*, *9*(1), Article 1. <https://doi.org/10.1038/s41598-019-43933-w>
- Amiel, J., Laudier, B., Attié-Bitach, T., Trang, H., de Pontual, L., Gener, B., Trochet, D., Etchevers, H., Ray, P., Simonneau, M., Vekemans, M., Munnich, A., Gaultier, C., & Lyonnet, S. (2003). Polyalanine expansion and frameshift mutations of the paired-like homeobox gene PHOX2B in congenital central hypoventilation syndrome. *Nature Genetics*, *33*(4), 459–461.
- Amri, M., Car, A., & Roman, C. (1990). Axonal branching of medullary swallowing neurons projecting on the trigeminal and hypoglossal motor nuclei: Demonstration by electrophysiological and fluorescent double labeling techniques. *Experimental Brain Research*, *81*(2), Article 2. <https://doi.org/10.1007/BF00228130>
- Anikeeva, P., Andalman, A. S., Witten, I., Warden, M., Goshen, I., Grosenick, L., Gunaydin, L. A., Frank, L. M., & Deisseroth, K. (2012). Optetrode: A multichannel readout for optogenetic control in freely moving mice. *Nature Neuroscience*, *15*(1), 163–170. <https://doi.org/10.1038/nn.2992>
- Arber, S., Ladle, D. R., Lin, J. H., Frank, E., & Jessell, T. M. (2000). ETS Gene Er81 Controls the Formation of Functional Connections between Group Ia Sensory Afferents and Motor Neurons. *Cell*, *101*(5), 485–498. [https://doi.org/10.1016/S0092-8674\(00\)80859-4](https://doi.org/10.1016/S0092-8674(00)80859-4)
- Arendt, D., Bertucci, P. Y., Achim, K., & Musser, J. M. (2019). Evolution of neuronal types and families. *Current Opinion in Neurobiology*, *56*, 144–152. <https://doi.org/10.1016/j.conb.2019.01.022>
- Ashwell, K. W. (1982). The adult mouse facial nerve nucleus: Morphology and musculotopic organization. *J Anat.*, *135*(Pt 3), 531–538.
- Auclair, F., Valdès, N., & Marchand, R. (1996). Rhombomere-specific origin of branchial and visceral motoneurons of the facial nerve in the rat embryo. *The Journal of Comparative Neurology*, *369*(3), 451–461.
- Avivi-Arber, L., Martin, R., Lee, J.-C., & Sessle, B. J. (2011a). Face sensorimotor cortex and its neuroplasticity related to orofacial sensorimotor functions. *Archives of Oral Biology*, *56*(12), 1440–1465. <https://doi.org/10.1016/j.archoralbio.2011.04.005>
- Avivi-Arber, L., Martin, R., Lee, J.-C., & Sessle, B. J. (2011b). Face sensorimotor cortex and its neuroplasticity related to orofacial sensorimotor functions. *Archives of Oral Biology*, *56*(12), Article 12. <https://doi.org/10.1016/j.archoralbio.2011.04.005>

- Baertsch, N. A., Severs, L. J., Anderson, T. M., & Ramirez, J.-M. (2019). A spatially dynamic network underlies the generation of inspiratory behaviors. *Proceedings of the National Academy of Sciences*, *116*(15), 7493–7502. <https://doi.org/10.1073/pnas.1900523116>
- Ballerini, L., Galante, M., Grandolfo, M., & Nistri, A. (1999). Generation of rhythmic patterns of activity by ventral interneurons in rat organotypic spinal slice culture. *The Journal of Physiology*, *517*(2), 459–475. <https://doi.org/10.1111/j.1469-7793.1999.0459t.x>
- Barlow, S. M., Radder, J. P. L., Radder, M. E., & Radder, A. K. (2010). Central pattern generators for orofacial movements and speech. In *Handbook of Behavioral Neuroscience* (Vol. 19, pp. 351–369). Elsevier. <https://doi.org/10.1016/B978-0-12-374593-4.00033-4>
- Beier, K. T., Steinberg, E. E., DeLoach, K. E., Xie, S., Miyamichi, K., Schwarz, L., Gao, X. J., Kremer, E. J., Malenka, R. C., & Luo, L. (2015). Circuit Architecture of VTA Dopamine Neurons Revealed by Systematic Input-Output Mapping. *Cell*, *162*(3), Article 3. <https://doi.org/10.1016/j.cell.2015.07.015>
- Benavidez, N. L., Bienkowski, M. S., Zhu, M., Garcia, L. H., Fayzullina, M., Gao, L., Bowman, I., Gou, L., Khanjani, N., Cotter, K. R., Korobkova, L., Becerra, M., Cao, C., Song, M. Y., Zhang, B., Yamashita, S., Tugangui, A. J., Zingg, B., Rose, K., ... Dong, H.-W. (2021). Organization of the inputs and outputs of the mouse superior colliculus. *Nature Communications*, *12*(1), Article 1. <https://doi.org/10.1038/s41467-021-24241-2>
- Berg, R. W., & Kleinfeld, D. (2003). Rhythmic Whisking by Rat: Retraction as Well as Protraction of the Vibrissae Is Under Active Muscular Control. *Journal of Neurophysiology*, *89*(1), 104–117. <https://doi.org/10.1152/jn.00600.2002>
- Berghoff, E. G., Glenwinkel, L., Bhattacharya, A., Sun, H., Varol, E., Mohammadi, N., Antone, A., Feng, Y., Nguyen, K., Cook, S. J., Wood, J. F., Masoudi, N., Cros, C. C., Ramadan, Y. H., Ferkey, D. M., Hall, D. H., & Hobert, O. (2021). The Prop1-like homeobox gene *unc-42* specifies the identity of synaptically connected neurons. *ELife*, *10*, e64903. <https://doi.org/10.7554/eLife.64903>
- Blessing, W. W. (1997a). *The lower brainstem and bodily homeostasis*. Oxford University Press, USA.
- Blessing, W. W. (1997b). Inadequate frameworks for understanding bodily homeostasis. *Trends Neurosci*, *20*(6), 235–239.
- Bosman, L. W. J., Koekkoek, S. K. E., Shapiro, J., Rijken, B. F. M., Zandstra, F., van der Ende, B., Owens, C. B., Potters, J.-W., de Gruijl, J. R., Ruigrok, T. J. H., & De Zeeuw, C. I. (2010). Encoding of whisker input by cerebellar Purkinje cells. *The Journal of Physiology*, *588*(Pt 19), 3757–3783. <https://doi.org/10.1113/jphysiol.2010.195180>
- Bounds, H. (n.d.). *Multifunctional Cre-dependent transgenic mice for high-precision all-optical interrogation of neural circuits*. 28.
- Bouvier, J., Caggiano, V., Leiras, R., Caldeira, V., Bellardita, C., Balueva, K., Fuchs, A., & Kiehn, O. (2015). Descending Command Neurons in the Brainstem that Halt Locomotion. *Cell*, *163*(5), 1191–1203. <https://doi.org/10.1016/j.cell.2015.10.074>

- Bouvier, J., Thoby-Brisson, M., Renier, N., Dubreuil, V., Ericson, J., Champagnat, J., Pierani, A., Chedotal, A., & Fortin, G. (2010). Hindbrain interneurons and axon guidance signaling critical for breathing. *Nature Neuroscience*, *13*(9), Article 9.
- Bowman, J. P., & Aldes, L. D. (1980). Organization of the cerebellar tongue representation in the monkey. *Experimental Brain Research*, *39*(3). <https://doi.org/10.1007/BF00237114>
- Bretzner, F., & Brownstone, R. M. (2013). Lhx3-Chx10 reticulospinal neurons in locomotor circuits. *The Journal of Neuroscience: The Official Journal of the Society for Neuroscience*, *33*(37), 14681–14692. <https://doi.org/10.1523/JNEUROSCI.5231-12.2013>
- Brown, T. G., & Sherrington, C. S. (1911). The intrinsic factors in the act of progression in the mammal. *Proceedings of the Royal Society of London. Series B, Containing Papers of a Biological Character*, *84*(572), 308–319. <https://doi.org/10.1098/rspb.1911.0077>
- Brunet, J.-F., & Pattyn, A. (2002). Phox2 genes—From patterning to connectivity. *Current Opinion in Genetics & Development*, *12*(4), Article 4.
- Bryant, J. L., Boughter, J. D., Gong, S., LeDoux, M. S., & Heck, D. H. (2010). Cerebellar cortical output encodes temporal aspects of rhythmic licking movements and is necessary for normal licking frequency. *The European Journal of Neuroscience*, *32*(1), 41–52. <https://doi.org/10.1111/j.1460-9568.2010.07244.x>
- Cao, Y., Maran, S. K., Dhamala, M., Jaeger, D., & Heck, D. H. (2012). Behavior-Related Pauses in Simple-Spike Activity of Mouse Purkinje Cells Are Linked to Spike Rate Modulation. *The Journal of Neuroscience*, *32*(25), 8678–8685. <https://doi.org/10.1523/JNEUROSCI.4969-11.2012>
- Chédotal, A., Pourquié, O., & Sotelo, C. (1995). Initial Tract Formation in the Brain of the Chick Embryo: Selective Expression of the BEN/SC1/DM-GRASP Cell Adhesion Molecule. *European Journal of Neuroscience*, *7*(2), 198–212. <https://doi.org/10.1111/j.1460-9568.1995.tb01056.x>
- Chen, Z., Travers, S. P., & Travers, J. B. (2001). Muscimol infusions in the brain stem reticular formation reversibly block ingestion in the awake rat. *American Journal of Physiology-Regulatory, Integrative and Comparative Physiology*, *280*(4), R1085–R1094. <https://doi.org/10.1152/ajpregu.2001.280.4.R1085>
- Chopek, J. W., Zhang, Y., & Brownstone, R. M. (2021). Intrinsic brainstem circuits comprised of Chx10-expressing neurons contribute to reticulospinal output in mice. *Journal of Neurophysiology*, *126*(6), 1978–1990. <https://doi.org/10.1152/jn.00322.2021>
- Chul Bae, Y., Nakagawa, S., Yasuda, K., Yabuta, N. H., Yoshida, A., Pil, P. K., Moritani, M., Chen, K., Nagase, Y., Takemura, M., & Shigenaga, Y. (1996). Electron microscopic observation of synaptic connections of jaw-muscle spindle and periodontal afferent terminals in the trigeminal motor and supratrigeminal nuclei in the cat. *The Journal of Comparative Neurology*, *374*(3), 421–435. [https://doi.org/10.1002/\(SICI\)1096-9861\(19961021\)374:3<421::AID-CNE7>3.0.CO;2-3](https://doi.org/10.1002/(SICI)1096-9861(19961021)374:3<421::AID-CNE7>3.0.CO;2-3)
- Connors, B. W., & Ahmed, O. J. (2011). Integration and autonomy in axons. *Nature Neuroscience*, *14*(2), 128–130. <https://doi.org/10.1038/nn0211-128>

- Coppola, E., d'Autréaux, F., Nomaksteinsky, M., & Brunet, J.-F. (2012). Phox2b expression in the taste centers of fish. *The Journal of Comparative Neurology*, *520*(16), 3633–3649.
- Corbin, K. B. (1940). Observations on the peripheral distribution of fibers arising in the mesencephalic nucleus of the fifth cranial nerve. *The Journal of Comparative Neurology*, *73*(1), 153–177. <https://doi.org/10.1002/cne.900730110>
- Cregg, J. M., Leiras, R., Montalant, A., Wanken, P., Wickersham, I. R., & Kiehn, O. (2020). Brainstem neurons that command mammalian locomotor asymmetries. *Nature Neuroscience*, *23*(6), 730–740. <https://doi.org/10.1038/s41593-020-0633-7>
- Cui, G., Jun, S. B., Jin, X., Pham, M. D., Vogel, S. S., Lovinger, D. M., & Costa, R. M. (2013). Concurrent activation of striatal direct and indirect pathways during action initiation. *Nature*, *494*(7436), Article 7436. <https://doi.org/10.1038/nature11846>
- Cui, Y., Kam, K., Sherman, D., Janczewski, W. A., Zheng, Y., & Feldman, J. L. (2016). Defining preBötzing Complex Rhythm- and Pattern-Generating Neural Microcircuits In Vivo. *Neuron*, *91*(3), Article 3.
- d'Autréaux, F., Coppola, E., Hirsch, M.-R., Birchmeier, C., & Brunet, J.-F. (2011). Homeoprotein Phox2b commands a somatic-to-visceral switch in cranial sensory pathways. *Proceedings of the National Academy of Sciences of the United States of America*, *108*(50), Article 50.
- Dana, H., Sun, Y., Mohar, B., Hulse, B. K., Kerlin, A. M., Hasseman, J. P., Tsegaye, G., Tsang, A., Wong, A., Patel, R., Macklin, J. J., Chen, Y., Konnerth, A., Jayaraman, V., Looger, L. L., Schreier, E. R., Svoboda, K., & Kim, D. S. (2019). High-performance calcium sensors for imaging activity in neuronal populations and microcompartments. *Nature Methods*, *16*(7), Article 7. <https://doi.org/10.1038/s41592-019-0435-6>
- Dauger, S., Pattyn, A., Lofaso, F., Gaultier, C., Goridis, C., Gallego, J., & Brunet, J.-F. (2003). Phox2b controls the development of peripheral chemoreceptors and afferent visceral pathways. *Development*, *130*(26), Article 26.
- Dellow, P. G., & Lund, J. P. (1971). Evidence for central timing of rhythmical mastication. *The Journal of Physiology*, *215*(1), 1–13. <https://doi.org/10.1113/jphysiol.1971.sp009454>
- Dempsey, B., Sungeelee, S., Bokinić, P., Chettouh, Z., Diem, S., Autran, S., Harrell, E. R., Poulet, J. F. A., Birchmeier, C., Carey, H., Genovesio, A., McMullan, S., Goridis, C., Fortin, G., & Brunet, J.-F. (2021). A medullary centre for lapping in mice. *Nature Communications*, *12*(1), 6307. <https://doi.org/10.1038/s41467-021-26275-y>
- Deschênes, M., Takatoh, J., Kurnikova, A., Moore, J. D., Demers, M., Elbaz, M., Furuta, T., Wang, F., & Kleinfeld, D. (2016). Inhibition, not excitation, drives rhythmic whisking. *Neuron*, *90*(2), 374–387. <https://doi.org/10.1016/j.neuron.2016.03.007>
- Dessem, D., & Taylor, A. (1989). Morphology of jaw-muscle spindle afferents in the rat. *The Journal of Comparative Neurology*, *282*(3), 389–403. <https://doi.org/10.1002/cne.902820306>

Di Bonito, M., & Studer, M. (2017). Cellular and Molecular Underpinnings of Neuronal Assembly in the Central Auditory System during Mouse Development. *Frontiers in Neural Circuits*, *11*, 18. <https://doi.org/10.3389/fncir.2017.00018>

Dickinson, P. S. (2006). Neuromodulation of central pattern generators in invertebrates and vertebrates. *Current Opinion in Neurobiology*, *16*(6), 604–614. <https://doi.org/10.1016/j.conb.2006.10.007>

Dimitriou, M. (2022). Human muscle spindles are wired to function as controllable signal-processing devices. *ELife*, *11*, e78091. <https://doi.org/10.7554/eLife.78091>

Dong, H. W. (2008). *The Allen reference atlas: A digital color brain atlas of the C57Bl/6J male mouse* (pp. ix, 366). John Wiley & Sons Inc.

Dong, Y., Li, J., Zhang, F., & Li, Y. (2011). Nociceptive Afferents to the Premotor Neurons That Send Axons Simultaneously to the Facial and Hypoglossal Motoneurons by Means of Axon Collaterals. *PLOS ONE*, *6*(9), e25615. <https://doi.org/10.1371/journal.pone.0025615>

Donga, R., & Lund, J. P. (1991). Discharge patterns of trigeminal commissural last-order interneurons during fictive mastication in the rabbit. *Journal of Neurophysiology*, *66*(5), Article 5. <https://doi.org/10.1152/jn.1991.66.5.1564>

Dörfl, J. (1982). The musculature of the mystacial vibrissae of the white mouse. *Journal of Anatomy*, *135*(Pt 1), 147–154.

Drew, T., Dubuc, R., & Rossignol, S. (1986). Discharge patterns of reticulospinal and other reticular neurons in chronic, unrestrained cats walking on a treadmill. *Journal of Neurophysiology*, *55*(2), 375–401. <https://doi.org/10.1152/jn.1986.55.2.375>

Dufour, H. D., Chettouh, Z., Deyts, C., de Rosa, R., Goridis, C., Joly, J.-S., & Brunet, J.-F. (2006a). Precranial origin of cranial motoneurons. *Proceedings of the National Academy of Sciences of the United States of America*, *103*(23), Article 23.

Dufour, H. D., Chettouh, Z., Deyts, C., de Rosa, R., Goridis, C., Joly, J.-S., & Brunet, J.-F. (2006b). Precranial origin of cranial motoneurons. *Proceedings of the National Academy of Sciences of the United States of America*, *103*(23), 8727–8732.

Economo, M. N., Viswanathan, S., Tasic, B., Bas, E., Winnubst, J., Menon, V., Graybiel, L. T., Nguyen, T. N., Smith, K. A., Yao, Z., Wang, L., Gerfen, C. R., Chandrashekar, J., Zeng, H., Looger, L. L., & Svoboda, K. (2018). Distinct descending motor cortex pathways and their roles in movement. *Nature*, *563*(7729), Article 7729. <https://doi.org/10.1038/s41586-018-0642-9>

Emiliani, V., Cohen, A. E., Deisseroth, K., & Häusser, M. (2015). All-Optical Interrogation of Neural Circuits. *Journal of Neuroscience*, *35*(41), 13917–13926. <https://doi.org/10.1523/JNEUROSCI.2916-15.2015>

Eng, S. R., Gratwick, K., Rhee, J. M., Fedtsova, N., Gan, L., & Turner, E. E. (2001). Defects in Sensory Axon Growth Precede Neuronal Death in Brn3a-Deficient Mice. *The Journal of Neuroscience*, *21*(2), 541–549. <https://doi.org/10.1523/JNEUROSCI.21-02-00541.2001>

Erzurumlu, R. S., Murakami, Y., & Rijli, F. M. (2010). Mapping the face in the somatosensory brainstem. *Nature Reviews. Neuroscience*, *11*(4), Article 4. <https://doi.org/10.1038/nrn2804>

Espana, A., & Clotman, F. (2012). Onecut factors control development of the Locus Coeruleus and of the mesencephalic trigeminal nucleus. *Molecular and Cellular Neuroscience*, *50*(1), 93–102. <https://doi.org/10.1016/j.mcn.2012.04.002>

Espinosa-Medina, I., Outin, E., Picard, C. A., Chettouh, Z., Dymecki, S., Consalez, G. G., Coppola, E., & Brunet, J. F. (2014). Neurodevelopment. Parasympathetic ganglia derive from Schwann cell precursors. *Science*, *345*(6192), Article 6192.

Fay, R. A., & Norgren, R. (1997). Identification of rat brainstem multisynaptic connections to the oral motor nuclei in the rat using pseudorabies virus. *Brain Research Reviews*, *25*(3), 276–290. [https://doi.org/10.1016/S0165-0173\(97\)00027-1](https://doi.org/10.1016/S0165-0173(97)00027-1)

Fedtsova, N. G., & Turner, E. E. (1995). Brn-3.0 expression identifies early post-mitotic CNS neurons and sensory neural precursors. *Mechanisms of Development*, *53*(3), 291–304. [https://doi.org/10.1016/0925-4773\(95\)00435-1](https://doi.org/10.1016/0925-4773(95)00435-1)

Feldman, J. L., & Kam, K. (2015). Facing the challenge of mammalian neural microcircuits: Taking a few breaths may help. *The Journal of Physiology*, *593*(1), 3–23. <https://doi.org/10.1113/jphysiol.2014.277632>

Ferreira, B., Palinkas, M., Gonçalves, L., da Silva, G., Arnoni, V., Regalo, I., Vasconcelos, P., Júnior, W.-M., Hallak, J., Regalo, S., & Siéssere, S. (2019). Spinocerebellar ataxia: Functional analysis of the stomatognathic system. *Medicina Oral, Patología Oral y Cirugía Bucal*, *24*(2), e165–e171. <https://doi.org/10.4317/medoral.22839>

Ferreira-Pinto, M. J., Kanodia, H., Falasconi, A., Sigrist, M., Esposito, M. S., & Arber, S. (2021). Functional diversity for body actions in the mesencephalic locomotor region. *Cell*, *184*(17), 4564–4578.e18. <https://doi.org/10.1016/j.cell.2021.07.002>

Forli, A., Pisoni, M., Printz, Y., Yizhar, O., & Fellin, T. (2021). Optogenetic strategies for high-efficiency all-optical interrogation using blue-light-sensitive opsins. *eLife*, *10*, e63359. <https://doi.org/10.7554/eLife.63359>

Fregosi, R. F., & Ludlow, C. L. (2014). Activation of upper airway muscles during breathing and swallowing. *J Appl Physiol*, *116*(3), 291–301.

Gasser, R. F. (1967). The development of facial muscles in man. *The American Journal of Anatomy*, *120*, 357–376.

Gavalas, A., Davenne, M., Lumsden, A., Chambon, P., & Rijli, F. M. (1997). Role of Hoxa-2 in axon pathfinding and rostral hindbrain patterning. *Development*, *124*(19), 3693–3702. <https://doi.org/10.1242/dev.124.19.3693>

Goldberg, J.G., C., S. H. (1990). Rhythmic Trigeminal Activity. In *Neurophysiology of the jaws and teeth* (Taylor A, pp. 268–293). Macmillan Press.

- Goldberg, L. J., & Tal, M. (1978). Intracellular recording in trigeminal motoneurons of the anesthetized guinea pig during rhythmic jaw movements. *Experimental Neurology*, *58*(1), 102–110. [https://doi.org/10.1016/0014-4886\(78\)90125-5](https://doi.org/10.1016/0014-4886(78)90125-5)
- Gray, P. A. (2008a). Transcription factors and the genetic organization of brain stem respiratory neurons. *Journal of Applied Physiology*, *104*(5), 1513–1521. <https://doi.org/10.1152/jappphysiol.01383.2007>
- Gray, P. A. (2008b). Transcription factors and the genetic organization of brain stem respiratory neurons. *Journal of Applied Physiology*, *104*(5), Article 5. <https://doi.org/10.1152/jappphysiol.01383.2007>
- Gray, P. A. (2013). Transcription factors define the neuroanatomical organization of the medullary reticular formation. *Frontiers in Neuroanatomy*, *7*, 7.
- Gray, P. A., Janczewski, W. A., Mellen, N., McCrimmon, D. R., & Feldman, J. L. (2001). Normal breathing requires preBötzing complex neurokinin-1 receptor-expressing neurons. *Nature Neuroscience*, *4*(9), Article 9. <https://doi.org/10.1038/nn0901-927>
- Grill, H. J., & Norgren, R. (1978). The taste reactivity test. II. Mimetic responses to gustatory stimuli in chronic thalamic and chronic decerebrate rats. *Brain Research*, *143*(2), 281–297. [https://doi.org/10.1016/0006-8993\(78\)90569-3](https://doi.org/10.1016/0006-8993(78)90569-3)
- Grillner, S., Cangiano, L., Hu, G.-Y., Thompson, R., Hill, R., & Wallén, P. (2000). The intrinsic function of a motor system—From ion channels to networks and behavior11Published on the World Wide Web on 22 November 2000. *Brain Research*, *886*(1–2), Article 1–2. [https://doi.org/10.1016/S0006-8993\(00\)03088-2](https://doi.org/10.1016/S0006-8993(00)03088-2)
- Grinevich, V., Brecht, M., & Osten, P. (2005). Monosynaptic Pathway from Rat Vibrissa Motor Cortex to Facial Motor Neurons Revealed by Lentivirus-Based Axonal Tracing. *The Journal of Neuroscience*, *25*(36), 8250–8258. <https://doi.org/10.1523/JNEUROSCI.2235-05.2005>
- Gross, R. D., Atwood, C. W., Ross, S. B., Eichhorn, K. A., Olszewski, J. W., & Doyle, P. J. (2008). The coordination of breathing and swallowing in Parkinson's disease. *Dysphagia*, *23*(2), 136–145.
- Guyenet, P. G., & Bayliss, D. A. (2015). Neural Control of Breathing and CO₂ Homeostasis. *Neuron*, *87*(5), 946–961.
- Guyenet, P. G., Stornetta, R. L., Abbott, S. B. G., Depuy, S. D., & Kanbar, R. (2012). The Retrotrapezoid Nucleus and Breathing. In *Advances in Experimental Medicine and Biology* (pp. 115–122). Springer Netherlands. https://doi.org/10.1007/978-94-007-4584-1_16
- Han, W., Tellez, L. A., Rangel, M. J., Motta, S. C., Zhang, X., Perez, I. O., Canteras, N. S., Shammah-Lagnado, S. J., Pol, A. N. van den, & Araujo, I. E. de. (2017a). Integrated Control of Predatory Hunting by the Central Nucleus of the Amygdala. *Cell*, *168*(1), 311-324.e18. <https://doi.org/10.1016/j.cell.2016.12.027>
- Han, W., Tellez, L. A., Rangel, M. J., Motta, S. C., Zhang, X., Perez, I. O., Canteras, N. S., Shammah-Lagnado, S. J., Pol, A. N. van den, & Araujo, I. E. de. (2017b). Integrated Control

of Predatory Hunting by the Central Nucleus of the Amygdala. *Cell*, 168(1), 311-324.e18. <https://doi.org/10.1016/j.cell.2016.12.027>

Hernandez-Miranda, L. R., Ruffault, P.-L., Bouvier, J. C., Murray, A. J., Morin-Surun, M.-P., Zampieri, N., Cholewa-Waclaw, J. B., Ey, E., Brunet, J.-F., Champagnat, J., Fortin, G., & Birchmeier, C. (2017). Genetic identification of a hindbrain nucleus essential for innate vocalization. *Proceedings of the National Academy of Sciences of the United States of America*, 114(30), Article 30.

Herrick, C. J. (1918). *An Introduction to Neurology*.

Herrick, C. J. (1948). *The brain of the tiger salamander, Ambystoma tigrinum*.

Hill, D. N., Bermejo, R., Zeigler, H. P., & Kleinfeld, D. (2008). Biomechanics of the Vibrissa Motor Plant in Rat: Rhythmic Whisking Consists of Triphasic Neuromuscular Activity. *The Journal of Neuroscience*, 28(13), 3438–3455. <https://doi.org/10.1523/JNEUROSCI.5008-07.2008>

Hiraoka, K. (2004). Changes in masseter muscle activity associated with swallowing. *Journal of Oral Rehabilitation*, 31(10), 963–967. <https://doi.org/10.1111/j.1365-2842.2004.01325.x>

Hobert, O. (2021). Homeobox genes and the specification of neuronal identity. *Nature Reviews Neuroscience*, 22(10), 627–636. <https://doi.org/10.1038/s41583-021-00497-x>

Holstege, G., & Kuypers, H. G. (1977). Propriobulbar fibre connections to the trigeminal, facial and hypoglossal motor nuclei. I. An anterograde degeneration study in the cat. *Brain*, 100(2), 239–264.

Hunter, E., Begbie, J., Mason, I., & Graham, A. (2001). Early development of the mesencephalic trigeminal nucleus. *Developmental Dynamics*, 222(3), 484–493. <https://doi.org/10.1002/dvdy.1197>

Ichikawa, H., Qiu, F., Xiang, M., & Sugimoto, T. (2005). Brn-3a is required for the generation of proprioceptors in the mesencephalic trigeminal tract nucleus. *Brain Research*, 1053(1–2), 203–206. <https://doi.org/10.1016/j.brainres.2005.06.026>

Ihara, Y., Nakayama, K., Nakamura, S., Mochizuki, A., Takahashi, K., & Inoue, T. (2013). Coordination of NMDA-induced rhythmic activity in the trigeminal and hypoglossal nerves of neonatal mice in vitro. *Neuroscience Research*, 75(2), Article 2.

Jacquin, M. F., & Zeigler, H. P. (1982). Trigeminal orosensory deafferentation disrupts feeding and drinking mechanisms in the rat. *Brain Research*, 238(1), 198–204. [https://doi.org/10.1016/0006-8993\(82\)90783-1](https://doi.org/10.1016/0006-8993(82)90783-1)

Jean, A. (2001). Brain Stem Control of Swallowing: Neuronal Network and Cellular Mechanisms. *Physiological Reviews*, 81(2), Article 2. <https://doi.org/10.1152/physrev.2001.81.2.929>

Jessell, T. M. (2000). Neuronal specification in the spinal cord: Inductive signals and transcriptional codes. *Nature Reviews Genetics*, 1(1), Article 1. <https://doi.org/10.1038/35049541>

- Jones, B. (Ed.). (2003). *Normal and Abnormal Swallowing: Imaging in Diagnosis and Therapy*. Springer New York. <https://doi.org/10.1007/978-0-387-22434-3>
- Jung, J. C., & Schnitzer, M. J. (2003). Multiphoton endoscopy. *Optics Letters*, *28*(11), 902–904. <https://doi.org/10.1364/OL.28.000902>
- Kam, K., Worrell, J. W., Janczewski, W. A., Cui, Y., & Feldman, J. L. (2013). Distinct Inspiratory Rhythm and Pattern Generating Mechanisms in the preBötzing Complex. *The Journal of Neuroscience*, *33*(22), 9235–9245. <https://doi.org/10.1523/JNEUROSCI.4143-12.2013>
- Kaneshige, M., Shibata, K., Matsubayashi, J., Mitani, A., & Furuta, T. (2018). A Descending Circuit Derived From the Superior Colliculus Modulates Vibrissal Movements. *Frontiers in Neural Circuits*, *12*. <https://www.frontiersin.org/articles/10.3389/fncir.2018.00100>
- Kawai, K., Koizumi, M., Honma, S., Tokiyoshi, A., & Kodama, K. (2003). Derivation of the anterior belly of the digastric muscle receiving twigs from the mylohyoid and facial nerves. *Annals of Anatomy = Anatomischer Anzeiger: Official Organ of the Anatomische Gesellschaft*, *185*(1), 85–90.
- Kidokoro, Y., Kubota, K., Shuto, S., & Sumino, R. (1968). Possible interneurons responsible for reflex inhibition of motoneurons of jaw-closing muscles from the inferior dental nerve. *Journal of Neurophysiology*, *31*(5), 709–716. <https://doi.org/10.1152/jn.1968.31.5.709>
- Kim, E. J., Jacobs, M. W., Ito-Cole, T., & Callaway, E. M. (2016). Improved Monosynaptic Neural Circuit Tracing Using Engineered Rabies Virus Glycoproteins. *Cell Reports*, *15*(4), Article 4.
- Kitamura, S., Nishiguchi, T., Okubo, J., Chen, K. L., & Sakai, A. (1986). An HRP study of the motoneurons supplying the rat hypobranchial muscles: Central localization, peripheral axon course and soma size. *The Anatomical Record*, *216*(1), 73–81.
- Kogo, M., Funk, G. D., & Chandler, S. H. (1996). Rhythmical Oral-Motor Activity Recorded in an In Vitro Brainstem Preparation. *Somatosensory & Motor Research*, *13*(1), 39–48. <https://doi.org/10.3109/08990229609028910>
- Kolta, A., Westberg, K.-G., & Lund, J. P. (2000). Identification of brainstem interneurons projecting to the trigeminal motor nucleus and adjacent structures in the rabbit. *Journal of Chemical Neuroanatomy*, *19*(3), 175–195. [https://doi.org/10.1016/S0891-0618\(00\)00061-2](https://doi.org/10.1016/S0891-0618(00)00061-2)
- Krumlauf, R., Marshall, H., Studer, M., Nonchev, S., Sham, M. H., & Lumsden, A. (1993). Hox homeobox genes and regionalisation of the nervous system. *Journal of Neurobiology*, *24*(10), 1328–1340. <https://doi.org/10.1002/neu.480241006>
- Kurnikova, A., Moore, J. D., Liao, S.-M., Deschênes, M., & Kleinfeld, D. (2017). Coordination of Orofacial Motor Actions into Exploratory Behavior by Rat. *Current Biology: CB*, *27*(5), 688–696. <https://doi.org/10.1016/j.cub.2017.01.013>
- Latarjet, A., & Testut, L. (1948). *Traité d'anatomie humaine*. G. Doin.
- Lemon, R. N. (2008). Descending Pathways in Motor Control. *Annual Review of Neuroscience*, *31*(1), 195–218. <https://doi.org/10.1146/annurev.neuro.31.060407.125547>

- Li, N., Chen, T.-W., Guo, Z. V., Gerfen, C. R., & Svoboda, K. (2015). A motor cortex circuit for motor planning and movement. *Nature*, *519*(7541), 51–56. <https://doi.org/10.1038/nature14178>
- Li, Y.-Q., Takada, M., & Mizuno, N. (1993). Premotor neurons projecting simultaneously to two orofacial motor nuclei by sending their branched axons. A study with a fluorescent retrograde double-labeling technique in the rat. *Neuroscience Letters*, *152*(1–2), 29–32. [https://doi.org/10.1016/0304-3940\(93\)90475-Z](https://doi.org/10.1016/0304-3940(93)90475-Z)
- Lieske, S. P., Thoby-Brisson, M., Telgkamp, P., & Ramirez, J. M. (2000). Reconfiguration of the neural network controlling multiple breathing patterns: Eupnea, sighs and gasps. *Nature Neuroscience*, *3*(6), 600–607. <https://doi.org/10.1038/75776>
- Lindsay, N. M., Knutsen, P. M., Lozada, A. F., Gibbs, D., Karten, H. J., & Kleinfeld, D. (2019). Orofacial movements involve parallel corticobulbar projections from motor cortex to trigeminal premotor nuclei. *Neuron*, *104*(4), 765–780.e3. <https://doi.org/10.1016/j.neuron.2019.08.032>
- Liu, Z. J., Masuda, Y., Inoue, T., Fuchihata, H., Sumida, A., Takada, K., & Morimoto, T. (1993). Coordination of cortically induced rhythmic jaw and tongue movements in the rabbit. *Journal of Neurophysiology*, *69*(2), Article 2. <https://doi.org/10.1152/jn.1993.69.2.569>
- Loeb, G. E., & Gans, C. (1986). *Electromyography for Experimentalists*. University of Chicago Press. <https://press.uchicago.edu/ucp/books/book/chicago/E/bo5960315.html>
- Lorente De No, R. (1922). Contribucion al conocimiento del nervio trigemino. In *Libro en honor de DS Ramon y Cajal; trabajos originales de sus admiradores y discipulos extranjeros y nacionales*. (Vol. 2, pp. 13–30).
- Louvi, A., Yoshida, M., & Grove, E. A. (2007). The derivatives of theWnt3a lineage in the central nervous system. *The Journal of Comparative Neurology*, *504*(5), Article 5. <https://doi.org/10.1002/cne.21461>
- Lu, L., Cao, Y., Tokita, K., Heck, D. H., & Jr., J. D. B. (2013). Medial cerebellar nuclear projections and activity patterns link cerebellar output to orofacial and respiratory behavior. *Frontiers in Neural Circuits*, *7*, 56. <https://doi.org/10.3389/fncir.2013.00056>
- Lumsden, A., & Keynes, R. (1989). Segmental patterns of neuronal development in the chick hindbrain. *Nature*, *337*(6206), 424–428. <https://doi.org/10.1038/337424a0>
- Lumsden, A., & Krumlauf, R. (1996). Patterning the vertebrate neuraxis. *Science (New York, N.Y.)*, *274*(5290), 1109–1115. <https://doi.org/10.1126/science.274.5290.1109>
- Lund, J. P. (1991). Mastication and its Control by the Brain Stem. *Critical Reviews in Oral Biology & Medicine*, *2*(1), 33–64. <https://doi.org/10.1177/10454411910020010401>
- Luo, P. F., Wang, B. R., Peng, Z. Z., & Li, J. S. (1991). Morphological characteristics and terminating patterns of masseteric neurons of the mesencephalic trigeminal nucleus in the rat: An intracellular horseradish peroxidase labeling study. *The Journal of Comparative Neurology*, *303*(2), 286–299. <https://doi.org/10.1002/cne.903030210>

- Luo, P., Moritani, M., & Dessem, D. (2001). Jaw-muscle spindle afferent pathways to the trigeminal motor nucleus in the rat. *Journal of Comparative Neurology*, *435*(3), 341–353. <https://doi.org/10.1002/cne.1034>
- Madisen, L., Garner, A. R., Shimaoka, D., Chuong, A. S., Klapoetke, N. C., Li, L., van der Bourg, A., Niino, Y., Egnor, L., Monetti, C., Gu, H., Mills, M., Cheng, A., Tasic, B., Nguyen, T. N., Sunkin, S. M., Benucci, A., Nagy, A., Miyawaki, A., ... Zeng, H. (2015). Transgenic Mice for Intersectional Targeting of Neural Sensors and Effectors with High Specificity and Performance. *Neuron*, *85*(5), 942–958. <https://doi.org/10.1016/j.neuron.2015.02.022>
- Maeda, N., Kobashi, M., Mitoh, Y., Fujita, M., Minagi, S., & Matsuo, R. (2014). Differential involvement of two cortical masticatory areas in submandibular salivary secretion in rats. *Brain Research*, *1543*, 200–208. <https://doi.org/10.1016/j.brainres.2013.11.024>
- Marder, E., & Bucher, D. (2001). Central pattern generators and the control of rhythmic movements. *Current Biology*, *11*(23), R986–R996. [https://doi.org/10.1016/S0960-9822\(01\)00581-4](https://doi.org/10.1016/S0960-9822(01)00581-4)
- Mardinly, A. R., Oldenburg, I. A., Pégard, N. C., Sridharan, S., Lyall, E. H., Chesnov, K., Brohawn, S. G., Waller, L., & Adesnik, H. (2018). Precise multimodal optical control of neural ensemble activity. *Nature Neuroscience*, *21*(6), 881–893. <https://doi.org/10.1038/s41593-018-0139-8>
- Marshall, J. H., Kim, Y. S., Machado, T. A., Quirin, S., Benson, B., Kadmon, J., Raja, C., Chibukhchyan, A., Ramakrishnan, C., Inoue, M., Shane, J. C., McKnight, D. J., Yoshizawa, S., Kato, H. E., Ganguli, S., & Deisseroth, K. (2019). Cortical layer-specific critical dynamics triggering perception. *Science (New York, N.Y.)*, *365*(6453), eaaw5202. <https://doi.org/10.1126/science.aaw5202>
- Matesz, C. (1981). Peripheral and central distribution of fibres of the mesencephalic trigeminal root in the rat. *Neuroscience Letters*, *27*(1), 13–17. [https://doi.org/10.1016/0304-3940\(81\)90198-1](https://doi.org/10.1016/0304-3940(81)90198-1)
- Mathis, A., Mamidanna, P., Cury, K. M., Abe, T., Murthy, V. N., Mathis, M. W., & Bethge, M. (2018). DeepLabCut: Markerless pose estimation of user-defined body parts with deep learning. *Nature Neuroscience*, *21*(9), Article 9. <https://doi.org/10.1038/s41593-018-0209-y>
- McClung, J. R., & Goldberg, S. J. (2002). Organization of the hypoglossal motoneurons that innervate the horizontal and oblique components of the genioglossus muscle in the rat. *Brain Res*, *950*(1–2), 321–324.
- McCrea, D. A., & Rybak, I. A. (2008). Organization of mammalian locomotor rhythm and pattern generation. *Brain Research Reviews*, *57*(1), 134–146. <https://doi.org/10.1016/j.brainresrev.2007.08.006>
- McEvelly, R. J., Erkman, L., Luo, L., Sawchenko, P. E., Ryan, A. F., & Rosenfeld, M. G. (1996). Requirement for Brn-3.0 in differentiation and survival of sensory and motor neurons. , *Published Online: 12 December 1996; | Doi:10.1038/384574a0*, *384*(6609), 574–577.
- Meessen, H., & Olszewski, J. (1949). *Cytoarchitectonic Atlas of the Rhombencephalon of the Rabbit*. Karger.

- Miller, F. R., & Sherrington, C. S. (1915a). SOME OBSERVATIONS ON THE BUCCO-PHARYNGEAL STAGE OF REFLEX DEGLUTITION IN THE CAT. *Quarterly Journal of Experimental Physiology*, *9*(2), 147–186. <https://doi.org/10.1113/expphysiol.1915.sp000201>
- Miller, F. R., & Sherrington, C. S. (1915b). SOME OBSERVATIONS ON THE BUCCO-PHARYNGEAL STAGE OF REFLEX DEGLUTITION IN THE CAT. *Quarterly Journal of Experimental Physiology*, *9*(2), Article 2. <https://doi.org/10.1113/expphysiol.1915.sp000201>
- Mizuno, N., Konishi, A., & Sato, M. (1975). Localization of masticatory motoneurons in the cat and rat by means of retrograde axonal transport of horseradish peroxidase. *The Journal of Comparative Neurology*, *164*(1), 105–115.
- Mizuno, N., Yasui, Y., Nomura, S., Itoh, K., Konishi, A., Takada, M., & Kudo, M. (1983). A light and electron microscopic study of premotor neurons for the trigeminal motor nucleus. *The Journal of Comparative Neurology*, *215*(3), 290–298. <https://doi.org/10.1002/cne.902150305>
- Moore, J. D., Kleinfeld, D., & Wang, F. (2014a). How the brainstem controls orofacial behaviors comprised of rhythmic actions. *Trends in Neurosciences*, *37*(7), 370–380. <https://doi.org/10.1016/j.tins.2014.05.001>
- Moore, J. D., Kleinfeld, D., & Wang, F. (2014b). How the brainstem controls orofacial behaviors comprised of rhythmic actions. *Trends Neurosci*, *37*(7), 370–380.
- Morquette, P., Lavoie, R., Fhima, M.-D., Lamoureux, X., Verdier, D., & Kolta, A. (2012). Generation of the masticatory central pattern and its modulation by sensory feedback. *Progress in Neurobiology*, *96*(3), 340–355.
- Nagoya, K., Nakamura, S., Ikeda, K., Onimaru, H., Yoshida, A., Nakayama, K., Mochizuki, A., Kiyomoto, M., Sato, F., Kawakami, K., Takahashi, K., & Inoue, T. (2017). Distinctive features of Phox2b-expressing neurons in the rat reticular formation dorsal to the trigeminal motor nucleus. *Neuroscience*, *358*, 211–226. <https://doi.org/10.1016/j.neuroscience.2017.06.035>
- Nakamura, S., Inoue, T., Nakajima, K., Moritani, M., Nakayama, K., Tokita, K., Yoshida, A., & Maki, K. (2008). Synaptic transmission from the supratrigeminal region to jaw-closing and jaw-opening motoneurons in developing rats. *J Neurophysiol*, *100*(4), Article 4.
- Nakamura, Y., & Katakura, N. (1995). Generation of masticatory rhythm in the brainstem. *Neuroscience Research*, *23*(1), Article 1. [https://doi.org/10.1016/0168-0102\(95\)90003-9](https://doi.org/10.1016/0168-0102(95)90003-9)
- Nakamura, Y., Yanagawa, Y., Morrison, S. F., & Nakamura, K. (2017). Medullary Reticular Neurons Mediate Neuropeptide Y-Induced Metabolic Inhibition and Mastication. *Cell Metabolism*, *25*(2), 322–334. <https://doi.org/10.1016/j.cmet.2016.12.002>
- Narayanan, C. H., & Narayanan, Y. (1978). Determination of the embryonic origin of the mesencephalic nucleus of the trigeminal nerve in birds. *Journal of Embryology and Experimental Morphology*, *43*, 85–105.
- Nattie, E. E., & Li, A. (2002). Substance P–saporin lesion of neurons with NK1 receptors in one chemoreceptor site in rats decreases ventilation and chemosensitivity. *The Journal of Physiology*, *544*(Pt 2), Article Pt 2. <https://doi.org/10.1113/jphysiol.2002.020032>

- Nomaksteinsky, M., Kassabov, S., Chettouh, Z., Stoeklé, H.-C., Bonnaud, L., Fortin, G., Kandel, E. R., & Brunet, J.-F. (2013a). Ancient origin of somatic and visceral neurons. *BMC Biology*, *11*(1), 53.
- Nomaksteinsky, M., Kassabov, S., Chettouh, Z., Stoeklé, H.-C., Bonnaud, L., Fortin, G., Kandel, E. R., & Brunet, J.-F. (2013b). Ancient origin of somatic and visceral neurons. *BMC Biology*, *11*(1), Article 1.
- Nomura, S., & Mizuno, N. (1983). Axonal trajectories of masticatory motoneurons: A genu formation of axons of jaw-opening motoneurons in the cat. *Neurosci Lett*, *37*(1), Article 1.
- Nomura, S., & Mizuno, N. (1985). Differential distribution of cell bodies and central axons of mesencephalic trigeminal nucleus neurons supplying the jaw-closing muscles and periodontal tissue: A transganglionic tracer study in the cat. *Brain Research*, *359*(1–2), 311–319. [https://doi.org/10.1016/0006-8993\(85\)91442-8](https://doi.org/10.1016/0006-8993(85)91442-8)
- Novitsch, B. G., Chen, A. I., & Jessell, T. M. (2001). Coordinate regulation of motor neuron subtype identity and pan-neuronal properties by the bHLH repressor Olig2. *Neuron*, *31*(5), Article 5.
- Olszewski, J. (1950). On the anatomical and functional organization of the spinal trigeminal nucleus. *Journal of Comparative Neurology*, *92*(3), 401–413. <https://doi.org/10.1002/cne.900920305>
- Pattyn, A., Hirsch, M., Golidis, C., & Brunet, J. F. (2000a). Control of hindbrain motor neuron differentiation by the homeobox gene Phox2b. *Development*, *127*(7), Article 7.
- Pattyn, A., Hirsch, M., Golidis, C., & Brunet, J. F. (2000b). Control of hindbrain motor neuron differentiation by the homeobox gene Phox2b. *Development*, *127*(7), 1349–1358.
- Pattyn, A., Morin, X., Cremer, H., Golidis, C., & Brunet, J. F. (1997). Expression and interactions of the two closely related homeobox genes Phox2a and Phox2b during neurogenesis. *Development*, *124*(20), Article 20.
- Pattyn, A., Morin, X., Cremer, H., Golidis, C., & Brunet, J. F. (1999). The homeobox gene Phox2b is essential for the development of autonomic neural crest derivatives. *Nature*, *399*(6734), Article 6734.
- Pattyn, A., Vallstedt, A., Dias, J. M., Samad, O. A., Krumlauf, R., Rijli, F. M., Brunet, J.-F., & Ericson, J. (2003). Coordinated temporal and spatial control of motor neuron and serotonergic neuron generation from a common pool of CNS progenitors. *Genes & Development*, *17*(6), Article 6.
- Paxinos, G., & Franklin, K. B. J. (2004). *The mouse brain in stereotaxic coordinates* (Compact 2. ed). Elsevier Acad. Press.
- Pecho-Vrieseling, E., Sigrist, M., Yoshida, Y., Jessell, T. M., & Arber, S. (2009). Specificity of sensory–motor connections encoded by Sema3e–Plxnd1 recognition. *Nature*, *459*(7248), Article 7248. <https://doi.org/10.1038/nature08000>

Price, S., & Daly, D. T. (2022). Neuroanatomy, Trigeminal Nucleus. In *StatPearls*. StatPearls Publishing. <http://www.ncbi.nlm.nih.gov/books/NBK539823/>

Puelles, L., & Ferran, J. L. (2012). Concept of neural genoarchitecture and its genomic fundament. *Frontiers in Neuroanatomy*, *6*. <https://doi.org/10.3389/fnana.2012.00047>

Pujol, N., Torregrossa, P., Ewbank, J. J., & Brunet, J. F. (2000). The homeodomain protein CePHOX2/CEH-17 controls antero-posterior axonal growth in *C. elegans*. *Development*, *127*(15), 3361–3371.

Raappana, P., & Arvidsson, J. (1993). Location, morphology, and central projections of mesencephalic trigeminal neurons innervating rat masticatory muscles studied by axonal transport of cholera toxin B subunit. *The Journal of Comparative Neurology*, *328*(1), 103–114. <https://doi.org/10.1002/cne.903280108>

Ren, S.-Y., Pasqualetti, M., Dierich, A., Le Meur, M., & Rijli, F. M. (2002). A *Hoxa2* mutant conditional allele generated by Flp- and Cre-mediated recombination. *Genesis*, *32*(2), 105–108. <https://doi.org/10.1002/gene.10052>

Revoll, A. L., Vann, N. C., Akins, V. T., Kottick, A., Gray, P. A., Del Negro, C. A., & Funk, G. D. (2015). *Dbx1* precursor cells are a source of inspiratory XII premotoneurons. *eLife*, *4*, e12301. <https://doi.org/10.7554/eLife.12301>

Rioch, J. McK. (1934). THE NEURAL MECHANISM OF MASTICATION. *American Journal of Physiology-Legacy Content*, *108*(1), 168–176. <https://doi.org/10.1152/ajplegacy.1934.108.1.168>

Robinson, M. J. F., Warlow, S. M., & Berridge, K. C. (2014). Optogenetic Excitation of Central Amygdala Amplifies and Narrows Incentive Motivation to Pursue One Reward Above Another. *The Journal of Neuroscience*, *34*(50), 16567–16580. <https://doi.org/10.1523/JNEUROSCI.2013-14.2014>

Rokx, J. T. M., Jüch, P. J. W., & van Willigen, J. D. (1986). Arrangement and Connections of Mesencephalic Trigeminal Neurons in the Rat. *Cells Tissues Organs*, *127*(1), 7–15. <https://doi.org/10.1159/000146233>

Romer, A. S. (1972). The Vertebrate as a Dual Animal—Somatic and Visceral. *Evolutionary Biology*, *6*, 121–156.

Ruder, L., Schina, R., Kanodia, H., Valencia-Garcia, S., Pivetta, C., & Arber, S. (2021). A functional map for diverse forelimb actions within brainstem circuitry. *Nature*, *590*(7846), Article 7846. <https://doi.org/10.1038/s41586-020-03080-z>

Ruffault, P.-L., d'Autréaux, F., Hayes, J. A., Nomaksteinsky, M., Autran, S., Fujiyama, T., Hoshino, M., Häggglund, M., Kiehn, O., Brunet, J.-F., Fortin, G., & Goridis, C. (2015a). The retrotrapezoid nucleus neurons expressing *Atoh1* and *Phox2b* are essential for the respiratory response to CO₂. *eLife*, *4*.

Ruffault, P.-L., d'Autréaux, F., Hayes, J. A., Nomaksteinsky, M., Autran, S., Fujiyama, T., Hoshino, M., Häggglund, M., Kiehn, O., Brunet, J.-F., Fortin, G., & Goridis, C. (2015b). The

retrotrapezoid nucleus neurons expressing Atoh1 and Phox2b are essential for the respiratory response to CO₂. *ELife*, 4.

Sambasivan, R., Gayraud-Morel, B., Dumas, G., Cimper, C., Paisant, S., Kelly, R. G., & Tajbakhsh, S. (2009). Distinct Regulatory Cascades Govern Extraocular and Pharyngeal Arch Muscle Progenitor Cell Fates. *Developmental Cell*, 16(6), 810–821. <https://doi.org/10.1016/j.devcel.2009.05.008>

Sasamoto, K. (1979). Motor Nuclear Representation of Masticatory Muscles in the Rat. *The Japanese Journal of Physiology*, 29(6), 739–747. <https://doi.org/10.2170/jjphysiol.29.739>

Schiavo, G. G., Benfenati, F., Poulain, B., Rossetto, O., de Laureto, P. P., DasGupta, B. R., & Montecucco, C. (1992). Tetanus and botulinum-B neurotoxins block neurotransmitter release by proteolytic cleavage of synaptobrevin. *Nature*, 359(6398), 832–835. <https://doi.org/10.1038/359832a0>

Schindler, M., Sellers, L. A., Humphrey, P. P. A., & Emson, P. C. (1996). Immunohistochemical localization of the somatostatin sst2(a) receptor in the rat brain and spinal cord. *Neuroscience*, 76(1), 225–240. [https://doi.org/10.1016/S0306-4522\(96\)00388-0](https://doi.org/10.1016/S0306-4522(96)00388-0)

Schubert, F. R., Dietrich, S., Mootosamy, R. C., Chapman, S. C., & Lumsden, A. (2001). Lbx1 marks a subset of interneurons in chick hindbrain and spinal cord. *Mechanisms of Development*, 101(1–2), 181–185. [https://doi.org/10.1016/S0925-4773\(00\)00537-2](https://doi.org/10.1016/S0925-4773(00)00537-2)

Selverston, A. I., & Miller, J. P. (1980). Mechanisms underlying pattern generation in lobster stomatogastric ganglion as determined by selective inactivation of identified neurons. I. Pyloric system. *Journal of Neurophysiology*, 44(6), 1102–1121. <https://doi.org/10.1152/jn.1980.44.6.1102>

Sessle, B. J. (2009). Orofacial Motor Control. In *Encyclopedia of Neuroscience* (pp. 303–308). Elsevier. <https://doi.org/10.1016/B978-008045046-9.01331-0>

Sherrington, C. S. (1917). Reflexes elicitable in the cat from pinna vibrissae and jaws. *The Journal of Physiology*, 51(6), 404–431. <https://doi.org/10.1113/jphysiol.1917.sp001809>

Shigenaga, Y., Doe, K., Suemune, S., Mitsuhiro, Y., Tsuru, K., Otani, K., Shirana, Y., Hosoi, M., Yoshida, A., & Kagawa, K. (1989). Physiological and morphological characteristics of periodontal mesencephalic trigeminal neurons in the cat—Intra-axonal staining with HRP. *Brain Research*, 505(1), 91–110. [https://doi.org/10.1016/0006-8993\(89\)90119-4](https://doi.org/10.1016/0006-8993(89)90119-4)

Sieber, M. A., Storm, R., Martinez-de-la-Torre, M., Müller, T., Wende, H., Reuter, K., Vasyutina, E., & Birchmeier, C. (2007). Lbx1 acts as a selector gene in the fate determination of somatosensory and viscerosensory relay neurons in the hindbrain. *The Journal of Neuroscience: The Official Journal of the Society for Neuroscience*, 27(18), 4902–4909.

Stanek, E., Cheng, S., Takatoh, J., Han, B.-X., & Wang, F. (2014a). Monosynaptic premotor circuit tracing reveals neural substrates for oro-motor coordination. *ELife*, 3, e02511.

Stanek, E., Cheng, S., Takatoh, J., Han, B.-X., & Wang, F. (2014b). Monosynaptic premotor circuit tracing reveals neural substrates for oro-motor coordination. *ELife*, 3, e02511.

Stanek, E., Rodriguez, E., Zhao, S., Han, B.-X., & Wang, F. (2016a). Supratrigeminal Bilaterally Projecting Neurons Maintain Basal Tone and Enable Bilateral Phasic Activation of Jaw-Closing Muscles. *The Journal of Neuroscience*, *36*(29), Article 29. <https://doi.org/10.1523/JNEUROSCI.0839-16.2016>

Stanek, E., Rodriguez, E., Zhao, S., Han, B.-X., & Wang, F. (2016b). Supratrigeminal Bilaterally Projecting Neurons Maintain Basal Tone and Enable Bilateral Phasic Activation of Jaw-Closing Muscles. *Journal of Neuroscience*, *36*(29), 7663–7675. <https://doi.org/10.1523/JNEUROSCI.0839-16.2016>

Steinberg, E. E., Gore, F., Heifets, B. D., Taylor, M. D., Norville, Z. C., Beier, K. T., Földy, C., Lerner, T. N., Luo, L., Deisseroth, K., & Malenka, R. C. (2020). Amygdala-Midbrain Connections Modulate Appetitive and Aversive Learning. *Neuron*, *106*(6), 1026-1043.e9. <https://doi.org/10.1016/j.neuron.2020.03.016>

Storm, R., Cholewa-Waclaw, J., Reuter, K., Bröhl, D., Sieber, M., Treier, M., Müller, T., & Birchmeier, C. (2009). The bHLH transcription factor Olig3 marks the dorsal neuroepithelium of the hindbrain and is essential for the development of brainstem nuclei. *Development*, *136*(2), Article 2. <https://doi.org/10.1242/dev.027193>

Stornetta, R. L., Moreira, T. S., Takakura, A. C., Kang, B. J., Chang, D. A., West, G. H., Brunet, J.-F., Mulkey, D. K., Bayliss, D. A., & Guyenet, P. G. (2006). Expression of Phox2b by brainstem neurons involved in chemosensory integration in the adult rat. *The Journal of Neuroscience: The Official Journal of the Society for Neuroscience*, *26*(40), 10305–10314.

Székely, G., & Matesz, C. (1982). The accessory motor nuclei of the trigeminal, facial, and abducens nerves in the rat. *The Journal of Comparative Neurology*, *210*(3), Article 3.

Takato, J., Nelson, A., Zhou, X., Bolton, M. M., Ehlers, M. D., Arenkiel, B. R., Mooney, R., & Wang, F. (2013a). New modules are added to vibrissal premotor circuitry with the emergence of exploratory whisking. *Neuron*, *77*(2), 346–360.

Takato, J., Nelson, A., Zhou, X., Bolton, M. M., Ehlers, M. D., Arenkiel, B. R., Mooney, R., & Wang, F. (2013b). New modules are added to vibrissal premotor circuitry with the emergence of exploratory whisking. *Neuron*, *77*(2), Article 2.

Takato, J., Park, J. H., Lu, J., Li, S., Thompson, P., Han, B.-X., Zhao, S., Kleinfeld, D., Friedman, B., & Wang, F. (2021a). Constructing an adult orofacial premotor atlas in Allen mouse CCF. *ELife*, *10*, e67291. <https://doi.org/10.7554/eLife.67291>

Takato, J., Park, J. H., Lu, J., Li, S., Thompson, P., Han, B.-X., Zhao, S., Kleinfeld, D., Friedman, B., & Wang, F. (2021b). Constructing an adult orofacial premotor atlas in Allen mouse CCF. *ELife*, *10*, e67291. <https://doi.org/10.7554/eLife.67291>

Takato, J., Park, J. H., Lu, J., Li, S., Thompson, P., Han, B.-X., Zhao, S., Kleinfeld, D., Friedman, B., & Wang, F. (2021c). Constructing an adult orofacial premotor atlas in Allen mouse CCF. *ELife*, *10*, e67291. <https://doi.org/10.7554/eLife.67291>

Takato, J., Prevosto, V., Thompson, P. M., Lu, J., Chung, L., Harrahill, A., Li, S., Zhao, S., He, Z., Golomb, D., Kleinfeld, D., & Wang, F. (2022). The whisking oscillator circuit. *Nature*, 1–9. <https://doi.org/10.1038/s41586-022-05144-8>

- Talikka, M., Stefani, G., Brivanlou, A. H., & Zimmerman, K. (2004). Characterization of *Xenopus* Phox2a and Phox2b defines expression domains within the embryonic nervous system and early heart field. *Gene Expression Patterns*, 4(5), 601–607. <https://doi.org/10.1016/j.modgep.2004.01.012>
- Tan, W., Janczewski, W. A., Yang, P., Shao, X. M., Callaway, E. M., & Feldman, J. L. (2008). Silencing preBötzing complex somatostatin-expressing neurons induces persistent apnea in awake rat. *Nature Neuroscience*, 11(5), 538–540. <https://doi.org/10.1038/nn.2104>
- Taylor, A., & Appenteng, K. (1981). Distinctive modes of static and dynamic fusimotor drive in jaw muscles. In A. Taylor & A. Prochazka (Eds.), *Muscle Receptors and Movement* (pp. 179–192). Palgrave Macmillan UK. https://doi.org/10.1007/978-1-349-06022-1_18
- Taylor, N. E., Pei, J., Zhang, J., Vlasov, K. Y., Davis, T., Taylor, E., Weng, F.-J., Dort, C. J. V., Solt, K., & Brown, E. N. (2019). The Role of Glutamatergic and Dopaminergic Neurons in the Periaqueductal Gray/Dorsal Raphe: Separating Analgesia and Anxiety. *ENeuro*, 6(1). <https://doi.org/10.1523/ENEURO.0018-18.2019>
- Terashima, T., Kishimoto, Y., & Ochiishi, T. (1993). Musculotopic organization of the facial nucleus of the reeler mutant mouse. *Brain Res*, 617(1), Article 1.
- Terashima, T., Kishimoto, Y., & Ochiishi, T. (1994). Musculotopic organization in the motor trigeminal nucleus of the reeler mutant mouse. *Brain Res*, 666(1), Article 1.
- Tokuno, H., Takada, M., Nambu, A., & Inase, M. (1995). Direct projections from the orofacial region of the primary motor cortex to the superior colliculus in the macaque monkey. *Brain Research*, 703(1–2), 217–222. [https://doi.org/10.1016/0006-8993\(95\)01079-3](https://doi.org/10.1016/0006-8993(95)01079-3)
- Tomio, I., Masuda, Y., Nagashima, T., Yoshikawa, K., & Morimoto, T. (1992). Properties of rhythmically active reticular neurons around the trigeminal motor nucleus during fictive mastication in the rat. *Neuroscience Research*, 14(4), 275–294. [https://doi.org/10.1016/0168-0102\(92\)90072-K](https://doi.org/10.1016/0168-0102(92)90072-K)
- Toporikova, N., Chevalier, M., & Thoby-Brisson, M. (2015). Sigh and Eupnea Rhythmogenesis Involve Distinct Interconnected Subpopulations: A Combined Computational and Experimental Study. *ENeuro*, 2(2), ENEURO.0074-14.2015. <https://doi.org/10.1523/ENEURO.0074-14.2015>
- Tovote, P., Esposito, M. S., Botta, P., Chaudun, F., Fadok, J. P., Markovic, M., Wolff, S. B. E., Ramakrishnan, C., Fenno, L., Deisseroth, K., Herry, C., Arber, S., & Lüthi, A. (2016). Midbrain circuits for defensive behaviour. *Nature*, 534(7606), 206–212. <https://doi.org/10.1038/nature17996>
- Travers, J. B., Dinardo, L. A., & Karimnamazi, H. (1997a). Motor and Premotor Mechanisms of Licking. *Neuroscience & Biobehavioral Reviews*, 21(5), 631–647. [https://doi.org/10.1016/S0149-7634\(96\)00045-0](https://doi.org/10.1016/S0149-7634(96)00045-0)
- Travers, J. B., Dinardo, L. A., & Karimnamazi, H. (1997b). Motor and Premotor Mechanisms of Licking. *Neuroscience & Biobehavioral Reviews*, 21(5), Article 5. [https://doi.org/10.1016/S0149-7634\(96\)00045-0](https://doi.org/10.1016/S0149-7634(96)00045-0)

- Travers, J. B., Dinardo, L. A., & Karimnamazi, H. (1997c). Motor and Premotor Mechanisms of Licking. *Neuroscience & Biobehavioral Reviews*, *21*(5), 631–647. [https://doi.org/10.1016/S0149-7634\(96\)00045-0](https://doi.org/10.1016/S0149-7634(96)00045-0)
- Travers, J. B., & Norgren, R. (1983). Afferent projections to the oral motor nuclei in the rat. *The Journal of Comparative Neurology*, *220*(3), 280–298.
- Travers, J. B., Yoo, J.-E., Chandran, R., Herman, K., & Travers, S. P. (2005). Neurotransmitter phenotypes of intermediate zone reticular formation projections to the motor trigeminal and hypoglossal nuclei in the rat. *The Journal of Comparative Neurology*, *488*(1), 28–47. <https://doi.org/10.1002/cne.20604>
- Travers, J., DiNardo, L., & Karimnamazi, H. (2000). Medullary reticular formation activity during ingestion and rejection in the awake rat. *Experimental Brain Research*, *130*(1), 78–92. <https://doi.org/10.1007/s002219900223>
- Troche, M. S., Huebner, I., Rosenbek, J. C., Okun, M. S., & Sapienza, C. M. (2011). Respiratory-swallowing coordination and swallowing safety in patients with Parkinson's disease. *Dysphagia*, *26*(3), 218–224.
- Umeda, T., Isa, T., & Nishimura, Y. (2019). The somatosensory cortex receives information about motor output. *Science Advances*, *5*(7), eaaw5388. <https://doi.org/10.1126/sciadv.aaw5388>
- Urbain, N., & Deschênes, M. (2007). Motor Cortex Gates Vibrissal Responses in a Thalamocortical Projection Pathway. *Neuron*, *56*(4), 714–725. <https://doi.org/10.1016/j.neuron.2007.10.023>
- Usseglio, G., Gatier, E., Heuzé, A., Hérent, C., & Bouvier, J. (2020). Control of Orienting Movements and Locomotion by Projection-Defined Subsets of Brainstem V2a Neurons. *Current Biology*, *30*(23), 4665–4681.e6. <https://doi.org/10.1016/j.cub.2020.09.014>
- Van Daele, D. J., Fazan, V. P. S., Agassandian, K., & Cassell, M. D. (2011). Amygdala connections with jaw, tongue and laryngo-pharyngeal premotor neurons. *Neuroscience*, *177*, 93–113. <https://doi.org/10.1016/j.neuroscience.2010.12.063>
- Vong, L., Ye, C., Yang, Z., Choi, B., Chua, S., & Lowell, B. B. (2011). Leptin Action on GABAergic Neurons Prevents Obesity and Reduces Inhibitory Tone to POMC Neurons. *Neuron*, *71*(1), Article 1. <https://doi.org/10.1016/j.neuron.2011.05.028>
- Walker, H. K. (1990). Cranial Nerve V: The Trigeminal Nerve. In H. K. Walker, W. D. Hall, & J. W. Hurst (Eds.), *Clinical Methods: The History, Physical, and Laboratory Examinations* (3rd ed.). Butterworths. <http://www.ncbi.nlm.nih.gov/books/NBK384/>
- Wang, C.-Z., Shi, M., Yang, L.-L., Yang, R.-Q., Luo, Z.-G., Jacquin, M. F., Chen, Z.-F., & Ding, Y.-Q. (2007). Development of the mesencephalic trigeminal nucleus requires a paired homeodomain transcription factor, Drg11. *Molecular and Cellular Neuroscience*, *35*(2), 368–376. <https://doi.org/10.1016/j.mcn.2007.03.011>

- Wei, X. P., Collie, M., Dempsey, B., Fortin, G., & Yackle, K. (2022a). A novel reticular node in the brainstem synchronizes neonatal mouse crying with breathing. *Neuron*, *110*(4), 644-657.e6. <https://doi.org/10.1016/j.neuron.2021.12.014>
- Wei, X. P., Collie, M., Dempsey, B., Fortin, G., & Yackle, K. (2022b). A novel reticular node in the brainstem synchronizes neonatal mouse crying with breathing. *Neuron*, *110*(4), 644-657.e6. <https://doi.org/10.1016/j.neuron.2021.12.014>
- Westberg, K.-G., Kolta, A., Clavelou, P., Sandström, G., & Lund, J. P. (2000). Evidence for functional compartmentalization of trigeminal muscle spindle afferents during fictive mastication in the rabbit: Functional compartmentalization of muscle spindle afferents. *European Journal of Neuroscience*, *12*(4), 1145–1154. <https://doi.org/10.1046/j.1460-9568.2000.00001.x>
- Westneat, M. W., & Hal, W. G. (1992). Ontogeny of feeding motor patterns in infant rats: An electromyographic analysis of suckling and chewing. *Behavioral Neuroscience*, *106*(3), Article 3. <https://doi.org/10.1037/0735-7044.106.3.539>
- Westneat, M. W., & Hall, W. G. (1992). Ontogeny of feeding motor patterns in infant rats: An electromyographic analysis of suckling and chewing. *Behavioral Neuroscience*, *106*(3), Article 3.
- WILSON, D. M. (1961). The Central Nervous Control of Flight in a Locust. *Journal of Experimental Biology*, *38*(2), 471–490. <https://doi.org/10.1242/jeb.38.2.471>
- Wilson, E. M., Green, J. R., Yunusova, Y. Y., & Moore, C. A. (2008). Task Specificity in Early Oral Motor Development. *Seminars in Speech and Language*, *29*(4), Article 4. <https://doi.org/10.1055/s-0028-1103389>
- Woods, J. W. (1964a). BEHAVIOR OF CHRONIC DECEREBRATE RATS. *Journal of Neurophysiology*, *27*(4), 635–644. <https://doi.org/10.1152/jn.1964.27.4.635>
- Woods, J. W. (1964b). BEHAVIOR OF CHRONIC DECEREBRATE RATS. *Journal of Neurophysiology*, *27*(4), Article 4. <https://doi.org/10.1152/jn.1964.27.4.635>
- Wu, J., Capelli, P., Bouvier, J., Goulding, M., Arber, S., & Fortin, G. (2017). A V0 core neuronal circuit for inspiration. *Nature Communications*, *8*(1), Article 1.
- Xiang, M., Gan, L., Zhou, L., Klein, W. H., & Nathans, J. (1996). Targeted deletion of the mouse POU domain gene *Brn-3a* causes selective loss of neurons in the brainstem and trigeminal ganglion, uncoordinated limb movement, and impaired suckling. *Proceedings of the National Academy of Sciences*, *93*(21), Article 21. <https://doi.org/10.1073/pnas.93.21.11950>
- Xie, Z., Wang, M., Liu, Z., Shang, C., Zhang, C., Sun, L., Gu, H., Ran, G., Pei, Q., Ma, Q., Huang, M., Zhang, J., Lin, R., Zhou, Y., Zhang, J., Zhao, M., Luo, M., Wu, Q., Cao, P., & Wang, X. (2021). Transcriptomic encoding of sensorimotor transformation in the midbrain. *ELife*, *10*, e69825. <https://doi.org/10.7554/eLife.69825>
- Yackle, K., Schwarz, L. A., Kam, K., Sorokin, J. M., Huguenard, J. R., Feldman, J. L., Luo, L., & Krasnow, M. A. (2017). Breathing control center neurons that promote arousal in mice. *Science*, *355*(6332), Article 6332.

- Yasui, Y., Nakano, K., Nakagawa, Y., Kayahara, T., Shiroyama, T., & Mizuno, N. (1992). Non-dopaminergic neurons in the substantia nigra project to the reticular formation around the trigeminal motor nucleus in the rat. *Brain Research*, *585*(1–2), 361–366. [https://doi.org/10.1016/0006-8993\(92\)91237-9](https://doi.org/10.1016/0006-8993(92)91237-9)
- Yasui, Y., Tsumori, T., Ando, A., & Domoto, T. (1995). Demonstration of axon collateral projections from the substantia nigra pars reticulata to the superior colliculus and the parvocellular reticular formation in the rat. *Brain Research*, *674*(1), 122–126. [https://doi.org/10.1016/0006-8993\(94\)01459-U](https://doi.org/10.1016/0006-8993(94)01459-U)
- Yasui, Y., Tsumori, T., Ando, A., Domoto, T., Kayahara, T., & Nakano, K. (1994). Descending projections from the superior colliculus to the reticular formation around the motor trigeminal nucleus and the parvocellular reticular formation of the medulla oblongata in the rat. *Brain Research*, *656*(2), 420–426. [https://doi.org/10.1016/0006-8993\(94\)91489-3](https://doi.org/10.1016/0006-8993(94)91489-3)
- Zeng, H., & Sanes, J. R. (2017). Neuronal cell-type classification: Challenges, opportunities and the path forward. *Nature Reviews Neuroscience*, *18*(9), 530–546. <https://doi.org/10.1038/nrn.2017.85>
- Zhang, J., Luo, P., & Pendlebury, W. W. (2001). Light and electron microscopic observations of a direct projection from mesencephalic trigeminal nucleus neurons to hypoglossal motoneurons in the rat. *Brain Research*, *917*(1), 67–80. [https://doi.org/10.1016/S0006-8993\(01\)02911-0](https://doi.org/10.1016/S0006-8993(01)02911-0)
- Zhang, J., Yang, R., Pendlebury, W., & Luo, P. (2005). Monosynaptic circuitry of trigeminal proprioceptive afferents coordinating jaw movement with visceral and laryngeal activities in rats. *Neuroscience*, *135*(2), 497–505. <https://doi.org/10.1016/j.neuroscience.2005.05.065>
- Zhou, Q., Choi, G., & Anderson, D. J. (2001). The bHLH Transcription Factor Olig2 Promotes Oligodendrocyte Differentiation in Collaboration with Nkx2.2. *Neuron*, *31*(5), 791–807. [https://doi.org/10.1016/S0896-6273\(01\)00414-7](https://doi.org/10.1016/S0896-6273(01)00414-7)

PUBLIC SUMMARY

Résumé de la thèse en français:

Le tronc cérébral (rhombencéphale) est capable de générer et d'organiser divers mouvements orofaciaux, qu'ils soient discrets ou rythmiques, liés à la respiration, à la mastication, au léchage, à la déglutition et, aussi à l'exploration de l'environnement (mouvements des vibrisses tactiles chez les rongeurs), et ce, sans intervention des centres cérébraux supérieurs (**Woods, 1964**). En effet, plusieurs études ont démontré que des générateurs de rythme et de *pattern* (ou CPRG pour Central Pattern and Rhythm Generator) situés dans le tronc cérébral sont à l'origine de plusieurs mouvements rythmiques de la face. Ces derniers sont des réseaux neuronaux qui, par leurs propriétés cellulaires et synaptiques, sont capables de générer des décharges rythmiques. Ces générateurs de rythme entraînent les motoneurones via des neurones prémoteurs, mais ils peuvent eux-mêmes contenir des neurones prémoteurs (**Kam et al. 2013**). Récemment, des neurones prémoteurs à certains noyaux moteurs des nerfs crâniens ont été cartographiés dans de nombreuses régions de la formation réticulée du bulbe et du pont par traçage rétrograde monosynaptique (**Stanek et al. 2014, 2016 ; Takatoh et al. 2021, 2022**). Cependant, peu de choses sont connues sur l'identité ou la connectivité des neurones sous-jacents, tout particulièrement parce que la formation réticulée est une région mal caractérisée du tronc cérébral (**Blessing, 1997**). Même en ce qui concerne les circuits les mieux étudiés dans cette région, comme ceux de la respiration, ce n'est que récemment qu'ils ont commencé à être documentés en termes d'identités neuronales et de connectivité, et de telles précisions sont toujours manquantes pour la majorité des circuits du bulbe et du pont - y compris ceux qui participent à la genèse des mouvements orofaciaux chez les mammifères.

Au cours du développement du système nerveux, une régionalisation génique et anatomique intervient- d'abord selon l'axe antéropostérieur, segmentant le rhombencéphale en 7 à 8 compartiments distincts appelés 'rhombomères'. Ce processus est gouverné par plusieurs facteurs qui interagissent pour induire, *in fine*, l'expression de gènes d'identité segmentaire du complexe *Hox*, qui partagent des limites antérieures franches avec les rhombomères. L'expression des gènes *Hox* encode et maintiennent une identité de position des neurones au sein de chacun des rhombomères, déterminant ainsi leur intégration précise au sein de circuits neuronaux au cours du développement. Dans un second temps, une régionalisation génique - mise en place par des signaux antagonistes (morphogènes) issus de la plaque

du plancher et de la notochorde d'une part, et de la plaque du toit d'autre part-intervient pour spécifier des identités dorso-ventrales au sein du tube neural, grâce à l'expression d'une combinatoire de facteurs de transcription qui définissent des domaines de progéniteurs neuronaux distincts. Des programmes de différenciation neuronaux mis en place par d'autres facteurs de transcription au sein de chacun de ces domaines de progéniteurs affineront davantage leur destin. Les données actuelles démontrent que ces combinaisons de facteurs de transcription constituent les marqueurs les plus précis de l'identité neuronale chez les vertébrés comme chez les invertébrés **(Arendt et al. 2019; Hobert, 2021; Jessell, 2000)**, permettant, grâce à l'emploi de stratégies de dissection génétique, d'explorer le rôle fonctionnel précis de certains circuits neuronaux, particulièrement dans la formation réticulée.

Le gène à homéoboîte *Phox2b* (Paired mesoderm homeobox protein 2b) exprime un facteur de transcription possédant un patron d'expression discret dans le rhombencéphale. Il est exprimé dans certains progéniteurs dorso-ventraux et/ou dans leurs neurones post-mitotiques et a été précédemment impliqué, grâce aux travaux menés au sein de mon laboratoire, dans le développement du système nerveux autonome et celui de nombreux motoneurones innervant les muscles oropharyngés **(Dauger et al, 2003 ; Pattyn et al. 1999 ; Pattyn et al. 2000)**. Ces derniers, appartenant à la classe des "motoneurones viscéraux spéciaux", peuvent être assimilés à une version plus étendue du système nerveux viscéral, en accord avec leurs fonctions physiologiques ancestrales, qui étaient purement homéostatiques : ils servaient notamment à l'alimentation et à la respiration. Pendant mon doctorat, j'ai étudié trois nouvelles populations de neurones de la formation réticulée chez la souris - nommées IRt^{Phox2b} , $Peri5^{Atoh1}$ et $Sup5^{Phox2b}$ - dotées d'une signature génétique qui inclut le facteur de transcription *Phox2b*. Nous démontrons que les neurones de l' IRt^{Phox2b} sont issus d'un domaine de progéniteurs d'identité dorsale appelé pA3, qui se caractérise par l'expression du facteur de transcription Olig3. Les neurones précurseurs de l' IRt^{Phox2b} n'expriment *Phox2b* qu'une fois sortis du cycle cellulaire (c.-à-d. à l'état post-mitotique). Les neurones du $Peri5^{Atoh1}$ comme ceux du $Sup5^{Phox2b}$ sont, quant à eux, issus de progéniteurs exprimant *Phox2b* au sein d'un domaine d'identité dorsale appelé Pb2, dont les neurones postmitotiques maintiennent l'expression de *Phox2b*.

Un traçage rétrograde à partir de l' IRt^{Phox2b} a permis d'identifier les centres supra-bulbaires projetant vers ce noyau: ceux-ci sont impliqués dans le contrôle sensorimoteur des mouvements orofaciaux et de leur intégration, ainsi que dans l'homéostasie énergétique, suggérant une implication de

l'IRt^{Phox2b} dans l'ingestion. Le traçage rétrograde à partir du Sup5^{Phox2b} a quant à lui démontré que ce noyau reçoit des projections de centres supra-bulbaires susceptibles d'être impliqués dans le contrôle sensorimoteur de la mastication. Afin de déterminer les cibles en aval de l'IRt^{Phox2b} ou du Peri5^{Atoh1}, nous avons procédé à un traçage antérograde à partir de ces noyaux, qui a permis de les identifier comme étant pré-moteurs (qui innervent les noyaux moteurs) aux muscles ouvrant la mâchoire (dans le cas de l'IRt et du Peri5) et qui élèvent (dans le cas de l'IRt) ou rétractent (dans le cas du Peri5) la langue. Ces données ont été confirmées grâce à un traçage rétrograde à partir de muscles spécifiques (notamment les abducteurs de la mâchoire et les éleveurs de la langue). Afin d'explorer le rôle fonctionnel de ces deux noyaux chez l'animal vigile, nous avons ciblé ces neurones pour leur faire exprimer soit un canal ionique (une opsine) qui provoque leur dépolarisation en présence de photons ou une sonde calcique (la GCaMP) qui mesure l'activité neuronale. La stimulation de l'IRt^{Phox2b} ou celle du Peri5^{Atoh1} avec un pulse de lumière bref chez l'animal vigile déclenche l'ouverture de la mâchoire, tandis que celle de l'IRt^{Phox2b} provoque aussi la protrusion de la langue, ce qui est cohérent avec leurs projections cibles. De façon inattendue, la stimulation non-rythmique de l'IRt^{Phox2b} induit une alternance rythmique de protraction et de rétraction de la langue, en synchronisme avec l'ouverture et la fermeture de la mâchoire qui s'apparentent à un comportement de léchage. La même stratégie de traçage citée plus haut a démontré que le Sup5^{Phox2b} contient des neurones pré-moteurs aux adducteurs de la mâchoire. La stimulation de ce noyau induit la fermeture de la mâchoire. Enfin, des enregistrements calciques par photométrie montrent que l'IRt^{Phox2b} et le Sup5^{Phox2b} sont actifs pendant le léchage et la mastication respectivement, et représentent ainsi des substrats sous-corticaux génétiquement définis qui sous-tendent deux comportements alimentaires stéréotypés.

Ainsi, de façon intéressante, les trois nouvelles classes d'interneurones que j'ai étudiées appartiennent à la version étendue du système nerveux viscéral, non seulement par leur ontogenèse (l'expression de *Phox2b*), mais aussi par leur rôle physiologique : ils sont prémoteurs aux motoneurones oropharyngés et impliqués dans la phase ingestive de l'alimentation.